TECHNICAL UNIVERSITY OF LIBEREC
Faculty of Textile Engineering

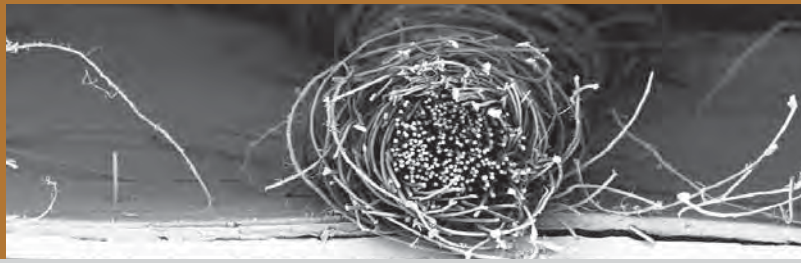

Book of Extended Abstracts

22nd International Conference STRUTEX

International Ph.D. Students Day

December 3, 2018
Building B, 2nd floor
Liberec, Czech Republic

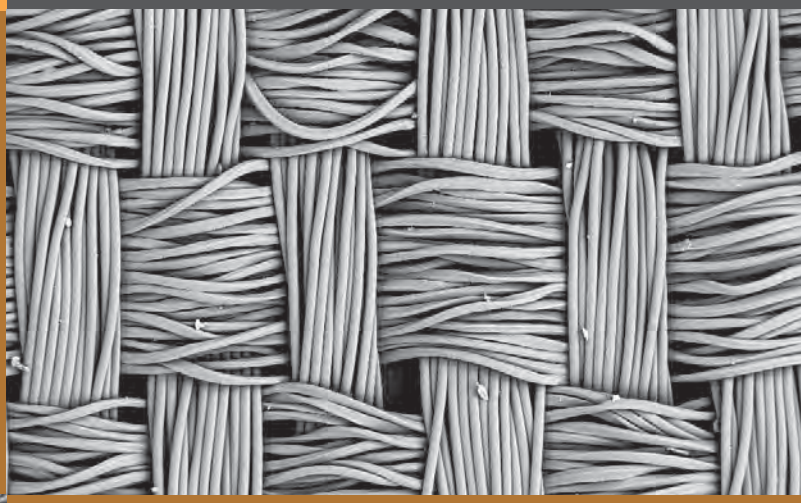

strutex.ft.tul.cz

Partners / Sponsors

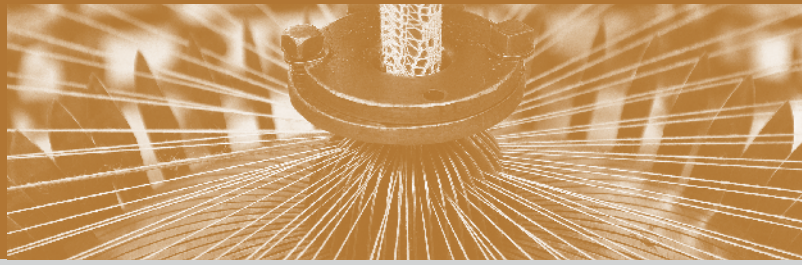

VLÁKNA a TEXTIL FIBRES AND TEXTILES
ISSN: 1335-0617

Liberec

Liberecký kraj

Lohmann & Rauscher

KORDÁRNA
KORDÁRNA PLUS A.S.

TORAY
Innovation by Chemistry

FESTO

RIETER

schoeller
Křešice

Caledon
Textile factory

Stap

ADFORS
SAINT-GOBAIN

International Ph.D. Students Day 2018

Content:

MEASUREMENT OF THERMAL RESISTANCE ON THERMAL FOOT MODEL COMPARED TO ALAMBETA

Abdelhamid R. R. Aboalasaad[1], Z. Skenderi[2], Brigita Kolčavová S.[1], Tariq Mansoor[3]

[1] *Technical University of Liberec, Department of Textile Technologies, Liberec 46117, Czechia*

[2] *University of Zagreb, Faculty of Textile Technology, 10000 Zagreb, Croatia*

[3] *Technical University of Liberec, Department of Textile Evaluation, Liberec 46117, Czechia*

Abdelhamid R. R. Aboalasaad, eabdo6@gmail.com

Abstract

Thermal Manikins are designed to simulate the human body's heat exchange and its interaction with the surrounding environment. There are two types of testing on Thermal Manikin (i.e. nude and clothed manikin). Initial thermal resistance (R_{ct0}) is measured on both nude and clothed Thermal Foot Model (TFM). Clothed TFM by using four types of woven compression bandages (WCBs). Thermal resistance (R_{ct}) is evaluated for the same types of WCBs. All bandage types were applied at extension ranges 10 to 80%, using both two and three layers bandaging. Obtained results of thermal resistance confirmed that clothed TFM is more accurate for measuring R_{ct0} due to more stabilization and less effect of air convection. Measured R_{ct} values were compared to the Alambeta instrument results. There is little deviation between R_{ct} values on TFM and Alambeta. Results by Alambeta are higher for all types of WCBs in both two and three layers techniques, this may be due to the variation of the testing methods and principles.

Keywords

Thermal resistance, Nude and clothed Thermal Foot Model, Alambeta, Woven compression bandages.

1. INTRODUCTION

Thermal manikins are devices by means of which it is possible to simulate heat exchange between the human and the environment [4]. The thermal resistance of fabrics is a primary determinant of body heat loss in cold environments. Generally, high thermal resistance values of the clothing are required to maintain the body under thermal equilibrium conditions. In hot environments or at high activity levels, evaporation of sweat becomes an important avenue of body heat loss and fabrics must allow water vapor to escape in time to maintain the relative humidity between the skin and the first layer of clothing about 50% [2-5]. There are six primary factors that must be approach when defining conditions for thermal comfort. These factors can be classified in two classes: measurable factors and personal factors. The measurable factors include: the air temperature, air velocity, radiant temperature and relative humidity. The personal factors include: activity level and clothing insulation [6].

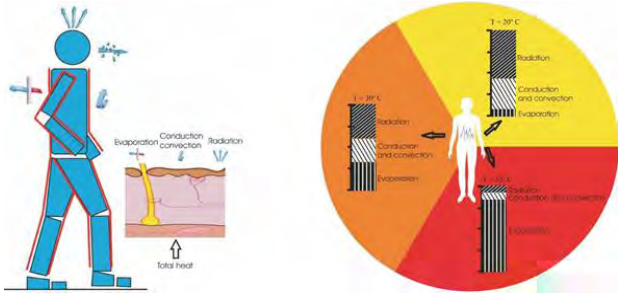

Figure 1. Heat transfer over the body [7]

2. EXPERIMENTAL WORK

2.1. *Materials*

Experimental samples consist of four WCBs as following: bleached cotton, Cotton/Polyamide/Polyurethane (CO-PA-PU), Viscose/Polyamide (VI-PA), and Viscose/Lycra (VI-LY) bandages, as shown in Figure 1:

a) Cotton bandage	**b) CO-PA-PU**	**c) VI-PA**	**d) VI-LY**
Fabric weight: 210.25 g/m^2 Fabric thickness: 1.06 mm	Weight: 236.48 g/m^2 Thickness: 1.09 mm	Weight: 83.34 g/m^2 Thickness: 0.91 mm	Weight: 219.54 g/m^2 Thickness: 1.01 mm
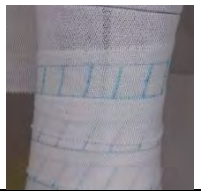	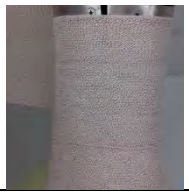		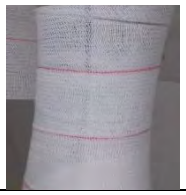

Figure 1. Experimental samples on TFM and its parameters

2.2. *Testing procedure*

Initial thermal resistance is measured on both nude and clothed TFM before each measurement of thermal resistance (R_{ct}) [8]. Moreover all samples were measured on three levels of ambient conditions (T: 20±2 °C, RH: 65±5%), (T: 22±2 °C, RH: 65±5%), (T: 20±2 °C, RH: 50±5%). The obtained results of R_{ct} were compared to Alambeta instrument values [9]. Clothed manikin using cotton socks as under layer is better to measure Rct0 for all measured samples to ensure more stabilization and steady conditions before measuring Rct as shown in Figure 2. The stabilization process continues till the device reads the standard ambient conditions (T: 20±2 °C, RH: 50±5 %), after that measurement of R_{ct0}, then stabilization (waiting for 20 min) while wearing CB sample over socks. Finally R_{ct} values can be measured using the measured R_{ct0} as a reference value, see Figure 3 and Equation (1) [5].

$$R_{ct} = \frac{A.\ (T_s - T_a)}{H} - R_{ct0} \quad (1)$$

Where: R_{ct}: dry resistance of sample only (m^2°C/W), T_s: hot plate surface temperature (°C), T_a: ambient temperature (°C), H/A: zone heat flux (W/m^2), R_{ct0}: clothed TFM dry resistance (m^2°C/W).

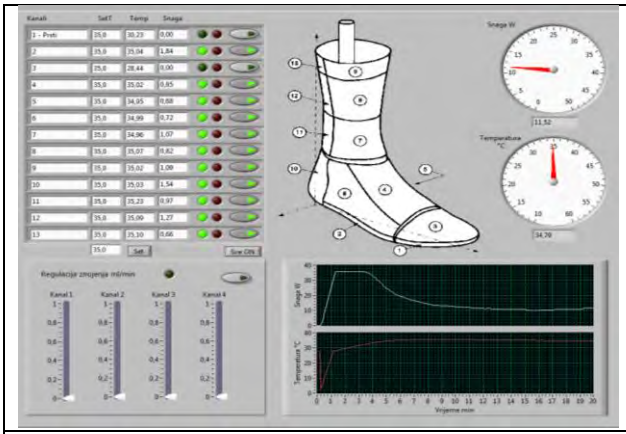

Figure 2. Reaching steady state condition for all segments of TFM

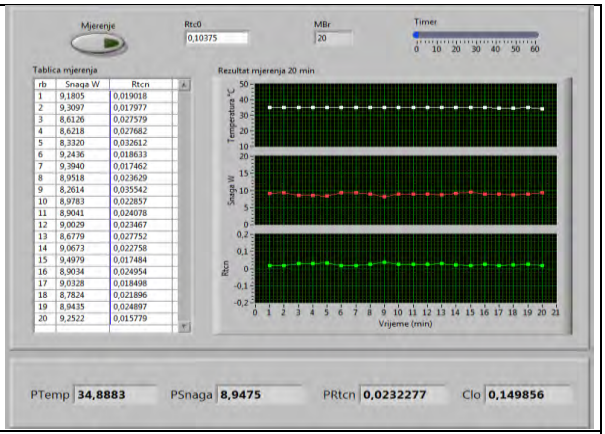

Figure 3. Measuring R_{ct} while wearing CB over socks

3. RESULTS AND DISCUSSIONS

3.1. *Effect of bandage extension and R_{ct0} on corresponding R_{ct} values*

As there are many factors can affect the thermal resistance measurements; it was necessary to measure R_{ct0} before each measurement of R_{ct} then calculate the relative change in thermal resistance (R_{ct}/R_{ct0}) to give accurate comparison between different bandage samples as shown in Figure 4 for two layers bandaging. The effect of yarns material is summarized as well; the Cotton bandage has the lowest thermal resistance then VI-PA then VI-LY then CO-PA-PU due to the higher moisture regain of Cotton and VI compared to PA and PU (8.5, 12, 4.5, and 0.3 respectively) [10, 11].

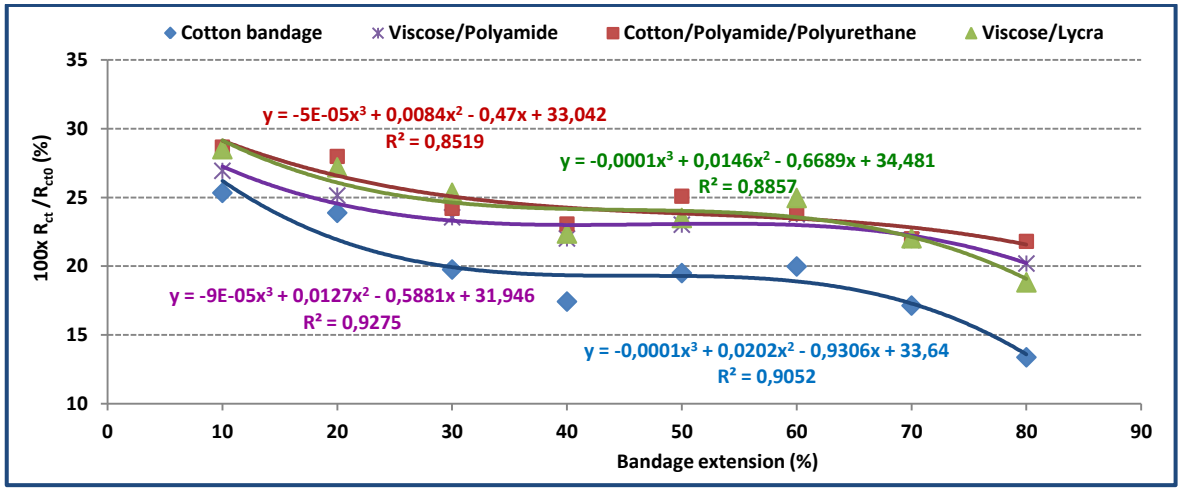

Figure 4. Effect of extension on relative thermal resistance of two layers CB

3.2. *Comparison between thermal resistance on TFM and Alambeta*

The average R_{ct} values on TFM are 0.0208, 0.02641, 0.02485, and 0.02572 (m^2°C W^{-1}) for cotton, CO-PA-PU, VI-PA, and VI-LY for two layers. These results are lower than Alambeta testing results which are 0.03057, 0.03735, 0.03478, and 0.0339 (m^2 °K W^{-1}) respectively. As for three layers, the average R_{ct} values on TFM are 0.02446, 0.02915, 0.02645, and 0.02892 (m^2 °C W^{-1}) and Alambeta testing results are 0.04197, 0.05325, 0.05007, and 0.04595 (m^2 °K W^{-1}) respectively. These results confirmed that the compression effect is more effective on TFM which simulates the real condition of CBs, in which case the higher applied pressure decreases the trapped air, as a result the R_{ct} values are lower compared to Alambeta, see Figure 5.

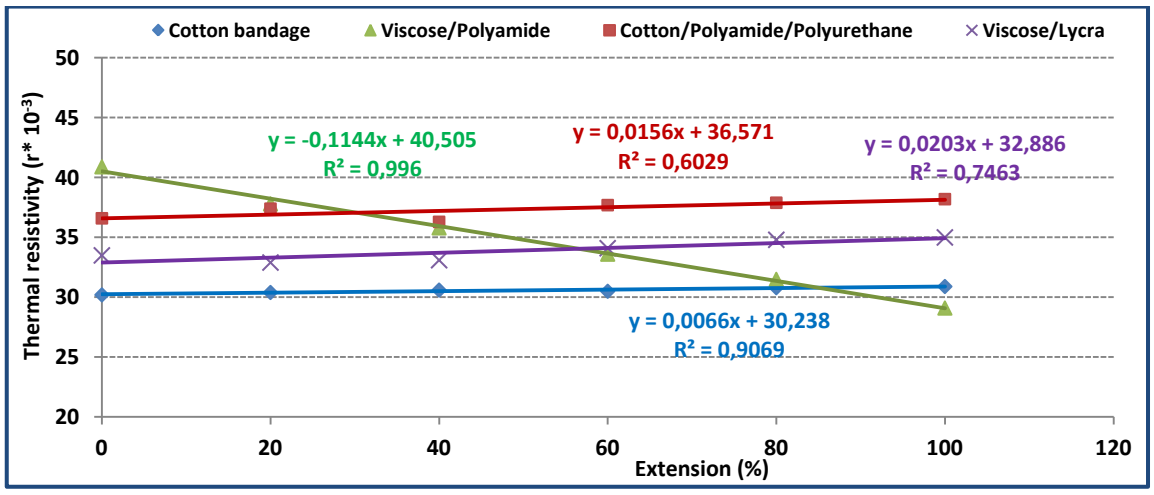

Figure 5. Thermal resistance on Alambeta instrument, two layers

4. CONCLUSIONS

According to TFM, relative thermal resistance of clothed manikin is significantly decreases by increasing bandage extension from 10 to 40 % then it is increases from 40 to 60% extension that may be due to the higher porosity of bandages (i.e. 0.364, 0.306, 0.471, and 0,325 for cotton, CO-PA-PU, VI-PA, and VI-LY bandages respectively) and optimum bandage thickness. After that R_{ct} is decreasing, especially at 80% extension due to lower bandage thickness and higher applied tension. The experimental results concluded that average R_{ct} values on TFM are 0.0208, 0.02641, 0.02485, and 0.02572 m^2 °C W^{-1} for cotton, CO-PA-PU, VI-PA, and VI-LY, lower than Alambeta testing results which are 0.03057, 0.03735, 0.03478, and 0.0339 m^2 °C W^{-1} respectively for two layers. The deviation ranges are 31.96, 29.29, 28.55, and 24.1% for two layers whereas the deviations for three layers are 41.42, 50.33, 41.79, and 37.06% respectively.

ACKNOWLEDGMENT

This work is supported by SGS 21249, Technical University of Liberec, Czech Republic.

References

[1] Mohamad G. A. (2015). The Role of Tests and Manikin in Defining Fabrics Thermal Characteristics. International Design Journal, Volume 5, Issue 3, pp 995-1001

[2] Huang, J. (2016). Review of heat and water vapor transfer through multilayer fabrics. Textile Research Journal, 86(3), 325-336

[3] Ghosh, A., Mal, P., Majumdar, A., Banerjee, D. (2017). An investigation on air and thermal transmission through knitted fabric structures using the Taguchi method. Autex Research Journal, 17(2), 152-163. DOI: 10.1515/aut-2016-0009

[4] Qian, X., Fan, J. (2009). A quasi-physical model for predicting the thermal insulation and moisture vapour resistance of clothing. Applied ergonomics, 40(4), 577-590.

[5] Salopek, Č. I., Skenderi, Z. (2010). Approach to the Prediction of Thermophysiological Comfort, Chapter 09 in DAAAM International Scientific Book 2010, pp. 081-088, B. Katalinic (Ed.). DOI: 10.2507/daaam.scibook.2010.09

[6] Simion M., Socaciu L., Unguresan P. (2016). Factors which Influence the Thermal Comfort Inside of Vehicles. Energy Procedia 85, pp: 472 – 480

[7] Mijović, B., SALOPEK, Č. I., & Skenderi, Z. (2010). Measurement of thermal parameters of skin-fabric environment. Periodicum biologorum, 112(1), 69-73.

[8] Mekjavic I., Lenart B., Vrhovec M., et al. (2005). Static and Dynamic Evaluation of Biophysical Properties of Footwear: The Jozef Stefan Institute Sweating Thermal Foot Manikin System. In Prevention of Cold Injuries (pp. 6-1 – 6-8). Meeting Proceedings RTO-MP-HFM-126, Paper 6.

[9] SENSORA INSTRUMENTS & CONSULTING, REG. No. 183 306 81, VAT No. CZ440128092 Na Výbezku 312, 460 15 LIBEREC, Czech Republic. http://www.sensora.eu/PermetestManual09.pdf

[10] Designation: D 1909 – 04, March 2004. Standard Table of Commercial Moisture Regains for Textile Fibers1.

[11] October 8, 2018. http://textilefashionstudy.com/polyamide-fiber-physical-and-chemical-properties-of-nylon-6/

METALIZED TEXTILE WITH COPPER AND SILVER PARTICLES

Azam Ali, Vijay Baheti, Jiří Militký, Asif Javed
Department of Material Engineering, Faculty of Textile Engineering, Technical University of Liberec, Studentská 2, Liberec 46117, Czech Republic
Corresponding author Email: - mehr_azam91@yahoo.com

Abstract

In this study, we make the electrically conductive multifunctional and durable fabrics by silver and copper nanoparticles. The fabric structure was pretreated with citric acid then nanoparticles were directly grown on fabric structure. The effect of pretreatment was analyzed by FTIR. The dynamic light scattering, SEM and XRD techniques were employed to study the morphology of deposited silver and copper particles. The utility of conductive fabrics was analyzed for electromagnetic shielding ability over frequency range of 30 MHz to 1.5 GHz. Furthermore, the role of deposited particles on antibacterial properties was examined against pathogenic bacteria such as Staphylococcus aureus and Escherichia coli. At the end, the durability of coated fabrics for comfort and electrical properties were examined against several washing cycles. The fabrics showed good retention of the particles, proved by SEM microstructures and small loss in the conductivity of the material after washing.

Key words

Conductive fabric, Silver and copper particles, Antibacterial, Electromagnetic shielding

1. INTRODUCTION

The demand for metalized fabrics is continuously increasing day by day and gaining attention in technical, high-tech and commercial applications. The most in applications are electromagnetic shielding, energy harvesting, anti-static, anti-bacterial properties, radar reflectivity, UV radiation screen and some important medical applications like the development of electrodes for TENs, ECG and EMG machine etc[1][2]. In this case selection of natural fiber based textile is more suitable. Because now a days, a major challenge is concern with the production and post-disposal processes of synthetic fibres regarding environmental pollution. So to overcome this issue researchers are fully conscious to develop the technical and smart textiles with natural fiber sources [3] [4]. Cotton fabric is well known for its environmental friendly properties like biodegradable and sustainability. It is well known that virgin cotton fabric is not intrinsically conductive. Generally, different types of conductive material imparts to insulator to make it conductive [5]. Textile surface metallization is done by various methods. However, metallic fabric produced in such traditional manners consists of defects, such as stiffness, poor air permeability and heavy in weight. The present work deals with the development of electrically conductive and multifunctional cotton fabrics by in-situ deposition of copper and silver particles.

2. EXPERIMENTAL

2.1. Materials and Methods

Cotton fabric with plain weave structure (GSM 150) was used. The fabric was purchased from Licolor,A,S. The chemicals used for metallization were of reagent grade. Before the deposition of copper and silver particles substrate was pre-treated. For pre-treatment, a solution of 20 g/L citric acid was made and fabric was dipped in it at 90°C for 2 hours. At first, different concentration of copper sulphate from 6g/200ml, 4g/200ml and 2g/200ml was dissolved in distilled water. Then, the cotton fabric was dipped in the solution and dried at 100 °C for 3 minutes. This procedure of dipping and drying was continuously carried out for 15 cycles. Subsequently, the treated fabrics were transferred to the 6g/200ml sodium hydrosulphite solution. The reduction was continued for the duration of 20 minutes. Likewise, for the deposition of silver particles, different concentration of silver nitrate (AgNO3)

from 0.30 M, 0.20 M and 0.10 M was dissolved in distilled water. The aqua ammonia (28wt %) was added drop wise into aqueous solution of AgNO3, and stirred continuously until a transparent solution of [Ag (NH3)2] + was obtained. Alkali treated cotton fabric was dipped in this solution for 3 minutes and dried at 100°C for 3 minutes. The dip and dry process was repeated a number of times to deposit the maximum concentration of [Ag (NH3)2] + on the fabric. This procedure of dipping and drying was continuously carried out for 15 cycles. Subsequently, the treated fabrics were transferred to 0.1M glucose stock solution. The reaction was allowed to proceed for 15 min. Finally, the fabrics were rinsed with water and dried in air. The microstructure of silver coated fabrics was observed on scanning electron microscope at accelerated voltage of 15 kV. Electrical resistivity was observed according to ASTM D257-07, Electromagnetic shielding ability was tested according to ASTM D4935-10 over frequency range of 30 MHz to 1.5 GHz. Antibacterial properties were tested by zone of inhibition (ZOI). The durability of fabrics were checked by using ISO 105-C01 washing test.

3. RESULTS AND DISCUSSION

3.1 Electrical conductivity of coated cotton fabrics

The effect of Silver nitrate and copper sulfate concentration and number of dipping cycles for increase in the conductivity of the fabrics was investigated. The resistivity of the samples were the mean values of three measurements as shown in Figure 1

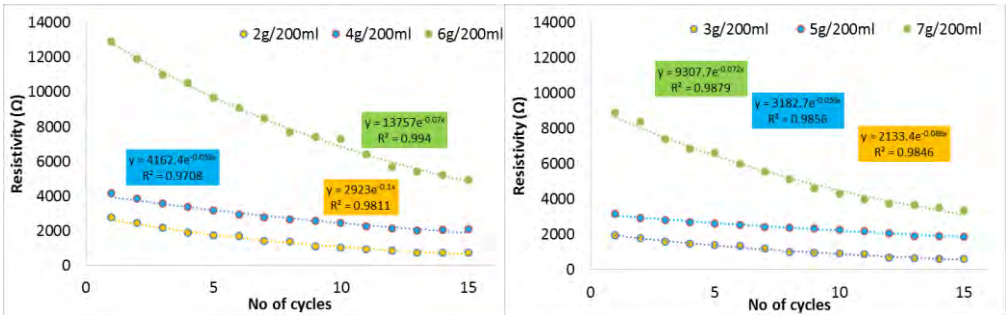

Figure 1: Electrical resistivity behavior of copper and silver coated fabric

The results showed the clear decrease in resistivity (increase in electrical conductivity). This behavior can be attributed to the formation of big sized copper particles at higher concentration of copper and silver salts solution. The lower concentration salts produced more conductive fabrics due to formation of percolated network by creation of continuous connectivity between the small metal particles.

3.2 Morphology of fabric surfaces

3.2.1 FTIR Spectra of pretreated cotton

The FTIR spectra of the cotton treated and u treated are shown in Figure 2. We observed a broad peak centered 3300 cmK1 corresponding to O–H stretching. Also we observed broad peak at 3000–2800 cm-1 region for C–H stretching. A peak around 1640 cm-1 is due to the adsorbed water molecules. It is due to the C=C stretching that can be attributed to the presence of aromatic rings. For the citric acid-grafted cotton, the carboxylic group absorption band clearly appears at 1732 cm-1 [1].

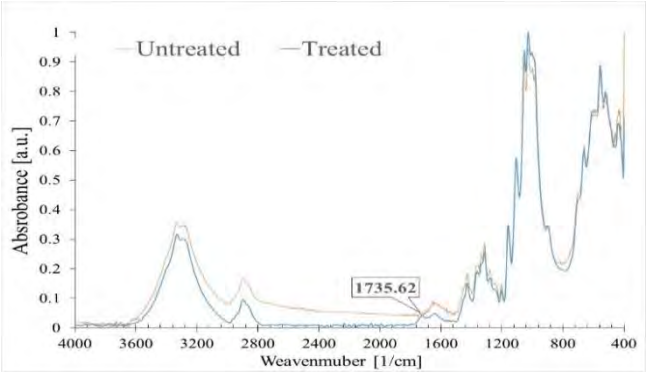

Figure 2: FT-IR spectra of treated and untreated cotton fabric

3.2.2 SEM Structures

The scanning electron microscopy was employed to observe the deposition of particles on fabric surface. The SEM images shown in Figure 3 & 4 revealed the nanometer scale of copper and silver particles deposited on fabric surface. With increase in number of dips, the deposition of particles was found more uniform and dense. This further indicated the higher tendency of formation of percolated network of particles when number of dipping cycles increased. It clearly showed the increase in contents of silver and copper metals with higher number of dips.

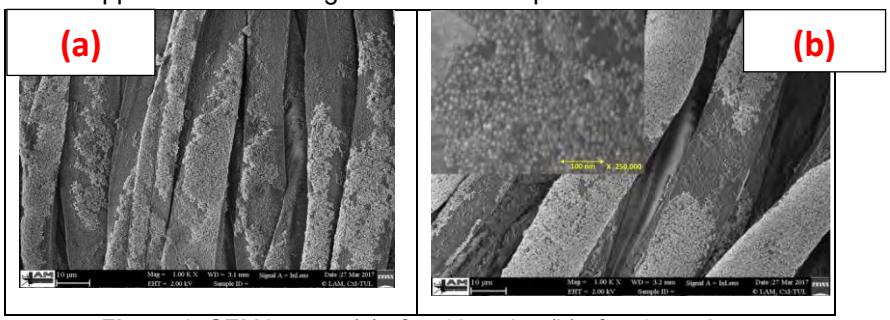

Figure 3: SEM images (a) after 10 cycles (b) after 15 cycles

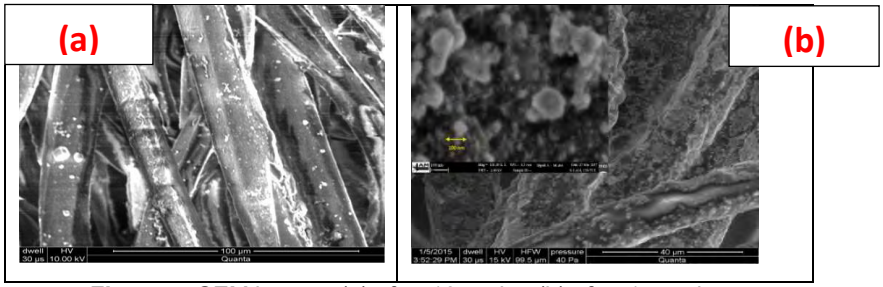

Figure 4: SEM images (a) after 10 cycles (b) after 15 cycles

3.2.3 XRD Analysis

Figure 5(a) shows the XRD patterns of samples for the 2θ range of 20 to 80 degrees with a step of 0.02 degree. The phase purity of the prepared silver particles can be clearly seen from perfect indexing of all the diffraction peaks to the silver structure. Compared to the untreated cotton fabric, four new peaks at 2θ values of 38.1°, 44.3°, 64.5° and 77.5° were detected for silver coated fabrics, which were respectively attributed to the diffraction peaks of the (1 1 1), (2 0 0), (2 2 0) and (3 1 1) planes of silver. Figure 5(b) shows the XRD patterns of samples for copper particles. The diffraction peaks appeared at 2θ of 43.3 °, 50.5 °, and 74.2 ° represented (1 1 1),(2 0 0) and (2 2 0) planes of copper, respectively [3]. The crystalline nature of copper particles was confirmed from the sharp peak, As such no characteristic peaks of impurities were detected, except the peak of copper oxide Cu_2O phase at 2θ of 38°[4].

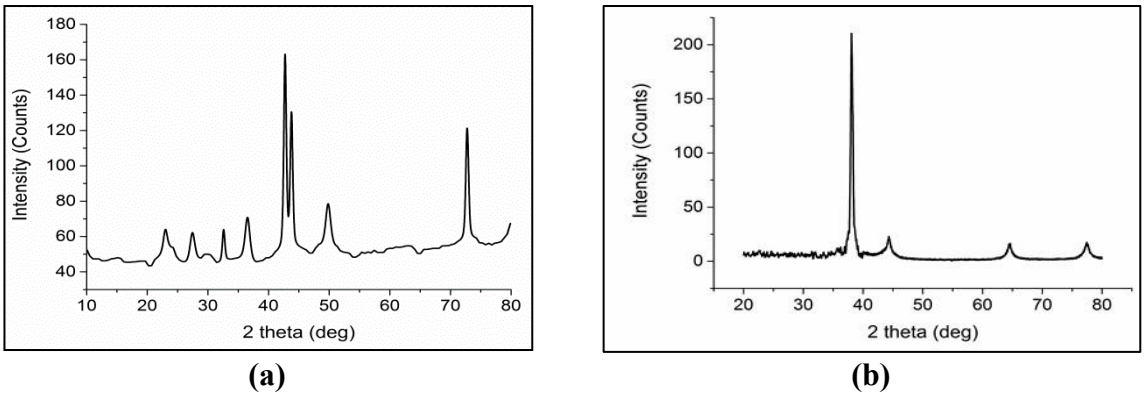

Figure 5: XRD patterns for (a) silver (b) copper coated fabrics

3.3 Electromagnetic Shielding

Electromagnetic shielding (EMI SE) effect as a function of frequency for fabric samples is showing in Figure 6. The high EMI SE was investigated coupled with good electrical properties. The results showed considerable changes in EMI SE occurs with decrease in resistivity (that is increase in electrical conductivity), which leads us to conclude that in addition to conductivity, the close packing of conducting networks controls the EMI SE. The maximum EMI SH values at 5, 10 and 15 cycles for silver coated fabric were 9.55, 15.04 and 18.54, while for copper coated fabric were recorded as 5.8, 9.5, 14.96 and 12.65 dB respectively. It is also clear from the figure that sudden increase in EMI SE of fabric samples occurred up to the frequency range between 300 to 400 MG Hz and then it is stable. It means that fabric samples are able to achieve high EMI at low frequency range, additionally EMI values are so stable till 1500 MG Hz. Furthermore the samples developed at 15 number of cycles has the highest value of EMI shielding because of highest electrical conductivity (low resistivity) among all samples.

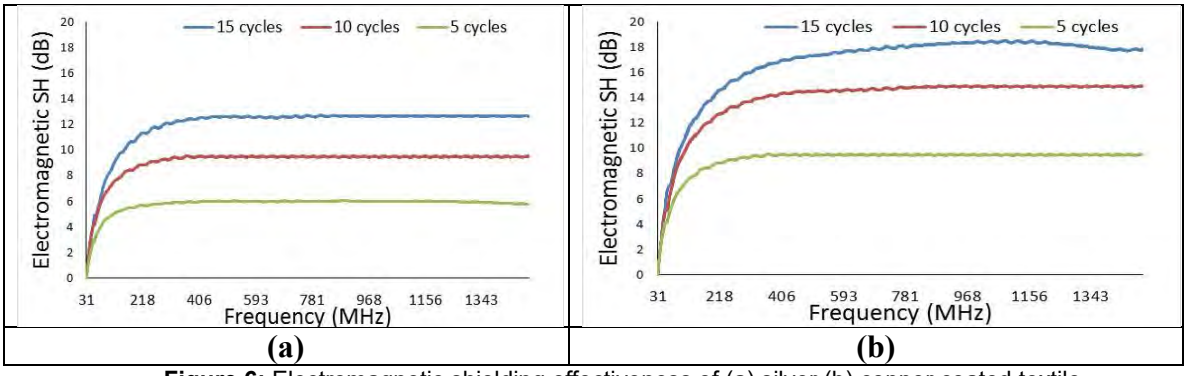

Figure 6: Electromagnetic shielding effectiveness of (a) silver (b) copper coated textile

3.4 Antibacterial Properties

The antibacterial activity of silver and copper coated fabrics was tested against Gram-negative *E.coli* and Gram-positive *S. aureus*. Samples shows the zones of inhibition around fabric samples after 24 h of incubation in dark at 37 °C. The test was repeated three times and the average value of zone of inhibition are presented. The virgin fabric sample without silver and copper coating showed no antibacterial activity. However, the zone of inhibitions was evidenced against both type of bacteria Staphylococcus aureus and Escherichia coli after the silver and copper coating. Further, Staphylococcus aureus depicted the highest sensitivity as compared to Escherichia coli. The zone of inhibitions for Staphylococcus aureus increased from 8.5 to 13.43 mm (for silver coated) and 9.5 to 15.5 mm (for copper coated), while for Escherichia coli it increased from 7 to 11.78mm (for silver coated) and (7.5 to 12 mm for copper coated) with increasing number of dipping cycles.

3.5 Durability in Electrical Conductivity

The durability of conductive fabrics under washing and rubbing have been a critical challenge. To investigate these properties, the electrical resistivity of samples was measured before and after washing cycles. A standard washing of samples was performed. The conductivity was again checked for the washed samples and reported in Table 6.

Table **1:** Electrical conductivity of conductive fabrics before and after washing

Fabric samples	Electrical Resistivity Ω	
	Before washing	After washing
Copper treated 5 cycles	1734	1757
Copper treated 10 cycles	1024	1039
Copper treated 15 cycles	756	762
Silver treated 5 cycles	1403	1422
Silver treated 10 cycles	972	960
Silver treated 15 cycles	650	643

It can be observed that there is no significant decrease in the resistivity fabrics before and after washing. It is evident that there is only a slight change in the conductivity of these samples even after washing. It means nanoparticles are attached firmly attached on the surface of fabrics. This was also verified by the SEM analysis before and after washing of the conductive fabrics samples.

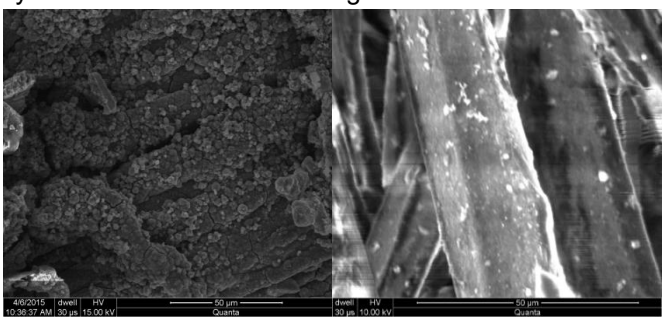

Figure 7: SEM image of silver coated fabric after washing

4. CONCLUSION

The successful application of Ag and Cu nanoparticles explained their potential applications in field of smart textiles. In addition, it was concluded that nanoparticle take up can be improved by increasing the number of dips for better covering of the fabric surface. Further, the morphology of coated fabrics and particles was studied from dynamic light scattering, SEM and XRD techniques. The utility of conductive fabrics was analyzed for electromagnetic shielding ability over frequency range of 30 MHz to 1.5 GHz by coaxial transmission line method. The sample produced from 5 dipping cycles revealed the lowest electromagnetic shielding effectiveness of about 6.10 dB for copper and 9.55 dB for silver coated fabrics in frequency range of 600 MHz–1.5 GHz. On the other hand, the sample produced from 80 dips exhibited the shielding ability of 18.54 dB for silver and 12.65 dB for copper coated fabric for respective frequency 1.5 GHz. For multifunctional behavior, the conductive fabrics were further examined for antibacterial properties against pathogenic bacteria such as Staphylococcus aureus and Escherichia coli. The zone of inhibitions for Staphylococcus aureus and Escherichia coli significantly increased with increasing number of dips. Towards the end, the durability of conductive fabrics was examined against several washing cycles. The fabrics showed good retention of the nanoparticles, proved by SEM microstructures and small loss in the conductivity of the material after washing. Therefore, the outcome of this work could provide alternative inexpensive and easier ways to obtain.

References

[1] Chung, C.,Lee, M.,Choe, MK. (2004) .Characterization of cotton fabric scouring by FT-IR ATR spectroscopy. Carbohydr Polym, 58:417–420

[2] Shateri-Khalilabad MEY,M.(2017). Fabricating multifunctional silver nanoparticles-coated cotton fabric. Arab J Chem, 10:1016

[3] Gan, X., Wu, Y., Liu, L., et al. (2008). Electroless plating of Cu-Ni-P alloy on PET fabrics and effect of plating parameters on the properties of conductive fabrics. J Alloys Compd, 455. 313

[4] Zhao ,Y., Cai, Z., Fu, X., et al. (2013). Electrochemical deposition and characterization of copper crystals on polyaniline/poly(ethylene terephthalate) conductive textiles. Synth Met, 175:1–8.

[5] Studer, A.M., Limbach, L.K., van Duc., et al. (2010) Nanoparticle cytotoxicity depends on intracellular solubility: Comparison of stabilized copper metal and degradable copper oxide nanoparticles. Toxicol Lett 197:169–174

[6] Chattopadhyay, Patel BH (2010) Effect of nanosized colloidal copper on cotton fabric. J Eng Fabr Fibers 5:1–6

MECHANICAL AND PHYSICAL PERFORMANCE OF EXTRUDED CEMENTITIOUS MATRICES REINFORCED WITH BASALT FIBROUS WASTES

Promoda Kumar Behera[1], Vijay Baheti[1], H. Savastano JR[2] and Jiří Militký[1]

[1]Department of Material Engineering, Faculty of Textile Engineering, Technical University of Liberec, Liberec 46117, Czech Republic

[2]Faculdade de Zootecnia e Engenharia de Alimentos, Universidade de São Paulo - Avenida Duque de Caxias Norte, 225, 13635-900 – Pirassununga/SP, Brazil.

Corresponding author e-mail: promodabehera@gmail.com

Abstract

The objective of this work was to analyze mechanical, physical and microstructure performance of extruded cementitious matrices reinforced basalt fibrous wastes of two different several formulations (2% BF and 2% BMF) compared with reference specimens. Basalt fiber is used as an alternative to vegetable fiber because of its high alkali resistant. The aim of this study was to evaluate the physical and mechanical properties of extruded cementitious matrices reinforced with micro and macro basalt waste fiber. Apparent porosity (AP), bulk density (BD), water absorption (WA), modulus of rupture (MOR), LOP, MOE and SE were evaluated. The 2% BF reinforced with the cement showed the highest values for BD and the lowest values for AVV and WA. No statistical differences were found between 2% BMF reinforced cement and reference sample for both WA and AVV values.

Key words

Basalt fibre, mechanical properties, extrusion process, building materials, ordinary Portland cement

1. INTRODUCTION

The use of fibers as reinforcement in cementitious matrix is quite common due to the low tensile strength and brittle nature of the cement-based products [1,2]. Nowadays many countries already prohibited the use of asbestos as reinforcement in cement based materials, due to the possible dangers associated with the inhalation of this fibrous mineral. Then, several investigations have been done regarding the use of alternative synthetic and vegetable fibers [3,5]. Basalt fibers have being increasingly used as reinforcement in cement-based materials in low cost construction in most developing countries [6,9]. Among kraft pulps, Eucalyptus kraft pulp is the most abundant and has become increasingly more available. However, the kraft process generates some industrial residues that have not appropriate destination but still presents good fiber quality, and deserves to be explored as reinforcement in non-structural materials for example. The extrusion process involves the formation of cohesive fiber-cement composites by forcing it through a die that can be adjusted to the various shape configurations [7]. This process is continuous, making it most suitable for industrial production and with great potential for low cost commercial applications. The advantage of extrusion is that it is an economical mass-production method capable of producing not only flat shapes, but also structural and hollow shapes. This process allows the use of a variety of waste materials that can be successfully incorporated into the matrix, including the use of basalt fibers as reinforcing raw materials in the production of fiber-cement composites. The aim of this work is to understand the impact of inclusion of waste basalt particles/fibers and different additions (limestone filler and metakaolin), on the physical and mechanical properties of cement-based composites.

The extrusion process involves the formation of cohesive fibre-cement composites by forcing it through a die that can be adjusted to the various shape configurations. These sections are then cut to the desired length [8]. The process is continuous, making it most suitable for industrial production. The advantage of extrusion is that it is an economical mass-production method capable of producing not only flat shapes, but also structural and hollow shapes. Extrusion technology is a potential candidate for low cost commercial applications [9]. This process allows the use of a variety of waste materials have been successfully incorporated into the matrix, including fly ash [10], silica fume [11,12] and slag [13]. This process also permits the use of vegetable fibres as raw materials in the production of fibre-cement such as ceiling elements. An interesting alternative for achieving low cost reinforcement of cementitious materials is the use of natural fibres which grow abundantly in nature. Many attempts have been made to obtain practical applications. These include studies of fibres from rice husk [14], sugar cane bagasse [15], zacate [16], jute [17], sisal [18], and bamboo [19], among others.

2. EXPERIMENTAL

2.1. Materials and mix design

Waste Basalt Fiber

For reinforcement, two types of Basalt fiber were used: short basalt fibrous waste (Macro fiber) and basalt waste milled fiber (Microfiber). The short basalt fibrous waste was obtained from the VEBA Industries, Czech Republic. The basalt fibers had density of 2.65 g/cm^3, elastic modulus of 95 GPa, tensile strength of 4000 MPa, elongation at break of 3 % and water absorption of less than 0.5 %. The length of the individual fibre is between 15 and 19 mm, with 13 μm in diameter. The chemical composition of basalt fibers as measured from elemental analysis is shown in Table 1.

Cement

The cement used in this study was the Brazilian Cauê brand ordinary Portland cement type CP V-ARI (high initial strength), in accordance with [20]. This type of cement, as described by [21] is selected for the Fiber-cement industry due to the finer particle size and higher reactivity in comparison to other blended cements available on the Brazilian market. The PC V-ARI was analyzed with a LA-950 Laser Diffraction Particle Size Distribution Analyzer which showed that 50% of the particles were finer than 11.88 μm.

Limestone

The filler used in this study was the Brazilian Itaú brand ground limestone. This filler was chosen because it is commonly used in the fabricated elements industry for partial substitution of Portland cement to reduce OPC consumption and increase stability (reducing shrinkage) [22]. The ground limestone was analyzed with a LA-950 Laser Diffraction Particle Size Distribution Analyzer which showed that 50% of the particles were finer than 12.38 μm.

Preparation of basalt micro fibrils

The short basalt fibrous waste was dipped in acetone for 24 h to remove the surface finish and impurities. They were later transferred to high energy planetary ball milling machine Fritsch pulverisette 7, Germany for mechanical activation of surface and grinding to the scale of basalt microfibrils. The dry pulverization was carried out based on previous research experience [23]. The sintered corundum container of 80 ml capacity and zirconium balls of 10 mm diameter were chosen for 30 min of dry milling. The ball to material ratio was kept at 10:1 and the speed was kept at 850 rpm.

Particle size distribution of dry milled basalt particles was obtained from Malvern zetasizer nano series based on dynamic light scattering principle of Brownian motion of particles. Deionized water was used as dispersion medium and it was ultrasonicated for 5 min with bandelin ultrasonic probe before characterization. In addition, microstructure of basalt particles was observed on scanning electron microscope (SEM) of Hitachi-model TM-3000 at accelerated voltage of 15 kV.

Composites production

The hybrid composites and the composites reinforced only with pulp were produced by the extrusion process. The formulations listed in Table 1 and Table 2. The mixture like cement CP-V ARI, Limestone, EB pulp, short basalt fibrous waste, basalt waste milled fiber and super plasticizer was homogenized in a mechanical Amadio planetary mixer (capacity of 20 L) during 5 min at 125 rpm, 5 min at medium speed (220 rpm) and finally 5 min at high speed (450 rpm). The water-cement (*w*/*c*) ratio was 0.41. The homogenized mixture was transferred to a Gelenski MVIG-05 laboratory extruder following the procedures adjusted in previous work [24]. The linear speed of the extruder was approximately 4 mm/s and cross section die width/height ratio was 3.3. The mixture was re-circulated into the extruder for 5 min before tailoring the samples. Samples of 15 mm × 50 mm × 200 mm were extruded and immediately transferred to the steel plates for hardening and initial curing.

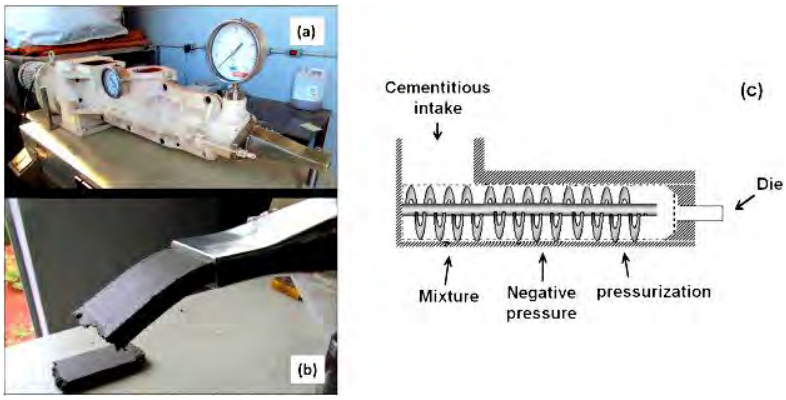

Figure 1 – (a) Details of the operating mechanism of the extrusion process (b) placing the extruded composite on a metal plate.

3. Results and discussion

3.1. Characterization of basalt microfibrils

For uniform dispersion of basalt fibers in cement matrix system, their surface was mechanically activated with further size reduction using 30 min dry pulverization in high energy ball milling. Fig. 3 shows the particle size distribution results of basalt particles obtained after 30 min of dry milling. It can be seen that short basalt fibrous waste was converted into basalt particles of micro to nano scale in multimodal distribution. This behavior was attributed to rise in temperature of ball mill and subsequent cold welding of basalt particles on milling container. For further uniform refinement of basalt particles to nano scale, it is necessary to pulverize them for prolonged duration by overcoming the rise in temperature of ball mill. Fig. 2 showed the SEM image of microstructure of basalt particles after 30 min of dry milling. The shape of basalt particles was observed predominantly in the form of microfibrils with few particles below 10 μ scale.

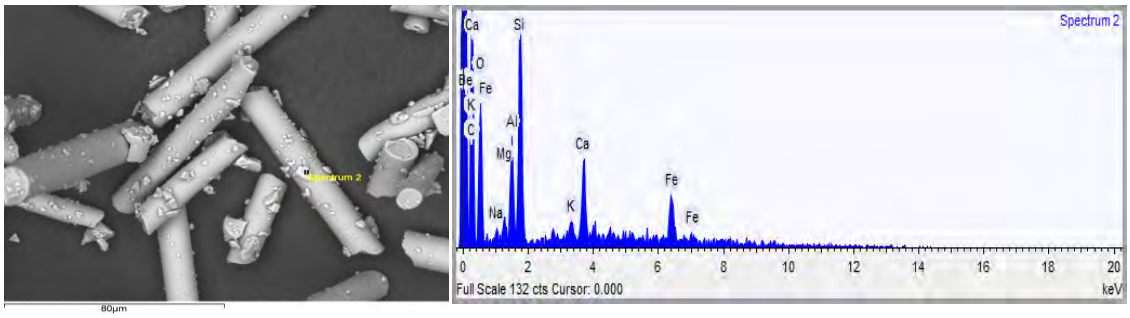

Figure 1 SEM and EDS image of basalt microfiber after 30 min dry milling

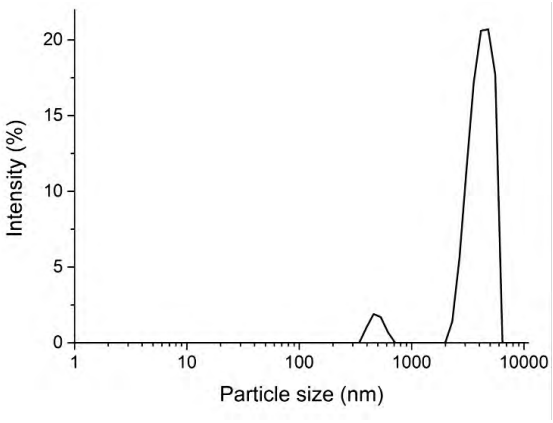

Figure 2 Particle size distribution of basalt particles after 30 min dry milling

The flexural performance of the fiber-cement composite containing waste basalt fibers at 2%BMF, 1%BF+1%BMF and 2%BF volume fractions. It is clear that the chopped waste fibers (2%BF) improved the maximum load bearing capacity of plain cement matrix. The maximum flexural stress decreased of 2% BMF with a decrease in size the same fiber volume fractions. This behavior is due to the fact that mechanical performance of fiber reinforced cementitious composites depends on the aspect ratios of fiber volume fractions we used in this experiment.

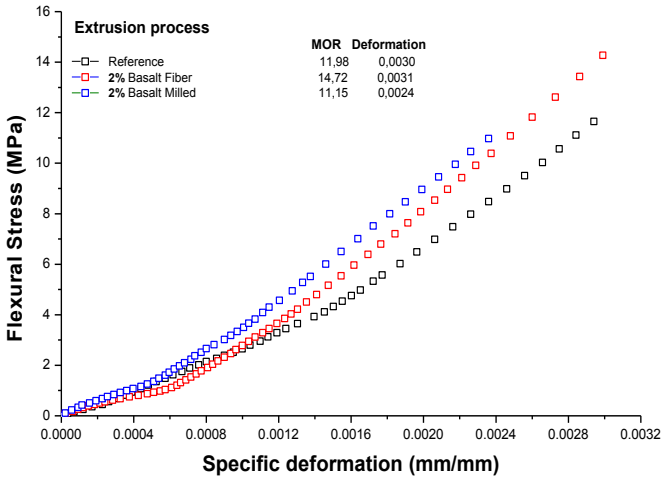

Figure 4 Typical stress × strain curves of the composites containing Reference, 2% BF and 2% BMF during flexure tests after 8 days of thermal curing.

The average values of the physical properties – the water absorption (WA), apparent void volume (AVV) and bulk density (BD) – and the mechanical properties obtained from the flexural test, such as the modulus of rupture (MOR), limit of proportionality (LOP), ratio MOR/LOP, modulus of elasticity (MOE) and specific energy, of the composites reinforced with Reference, 2% BF and 2% BMF after thermal curing for eight days. Physical and mechanical properties of composites reinforced with Reference, 2% BF, 1% BF+1% BMF and 2% BMF after thermal curing.

The post-failure aspects of the test specimens showed that, in the case of 2% BF, 2% BMF and 1% BF+1%BMF reinforced cement composites as similar like unreinforced specimens, a brittle failure occurred by separation of the elements into two parts, while 2% BMF and 1% BF+1%BMF reinforced specimens showed a less brittle behavior as compared to unreinforced specimens. The FRC as same like unreinforced specimens were at failure deformed, but in all cases brittle failure by fracture of the specimens into two parts take placed. In fact, the fibers on the fracture surface did not bridge the cracks and detached the two parts of the element. This shows up the presence of factual cracks.

4. CONCLUSIONS

- The addition of 2% basalt macro fibers resulted in an increase in flexural strengths. However the increase in strength was more prominent in case of BFRC where a gradual increase was observed with increasing fiber dosage. However, no significant change in flexural strengths was observed in between 2% BMF and 1% BF+1% BMF reinforced cement composites.

- Fiber addition had no significant effect on the modulus of elasticity of Reference and 1% BF+1% BMF reinforced cement composites. However, the modulus of elasticity of concrete slightly reduced when dosage of basalt fiber was 2% BMF.

- An increase in specific energy was observed for reinforced cement composites at the dosage of 2% Basalt macro fiber. However significant decrease was observed at 2% BMF dosage and fracture energy decreased by more than 50% at 2% BMF fiber inclusion for basalt fibers.

- BFRC shows brittle failure pattern though fiber pulled out was happened due to better interlocking in between fiber and hydrated cement composites.

ACKNOWLEDGMENT

Financial support for this research project was provided by Fundação de Amparo à Pesquisa do Estado de São Paulo (FAPESP) in Brazil.

References

[1] F.F.M. Lopes, G.T. Araujo, S. Luna, J.W.B. Nascimento, V.R. Silva, Modification of the properties of curauá fibers by acetylation. Revista Brasileira de Engenharia Agrícola e Ambiental. 15 (2011) 316–321.

[2] G.H.D. Tonoli, R.F. Mendes, G. Siqueira, J. Bras, M.N. Belgacem, Isocyanate-treated cellulose pulp and its effect on the alkali resistance and performance of fiber cement composites. Holzforschung, 67 (2013) 853-861.

[3] S. Ikai, J.R. Reichert, A.V. Rodrigues, V.A. Zampieri, Asbestos-free technology with new high toughness polypropylene (PP) fibers in air-cured Hatschek process. Construction and Building Materials. Guildford, 24 (2010) 171-180.

[4] J.H. Morton, T. Cooke, S.A. Akers, Performance of slash pine fibers in fiber cement products. Construction and Building Materials. 24 (2010) 165-170.

[5] . . e ndes .A. . oschi .E.R. aula R. . endes .B. uimar es r., F.A. Mori, Utilization potential of wood clones of Eucalyptus urophylla in the production of wood-cement panels, Cerne. 17 (2011) 69-75.

[6] G.H.D. Tonoli, S.F. Santos, J.A. Rabi, W.N. Santos, H. Savastano Jr., Thermal performance of sisal fiber-cement roofing tiles for rural constructions, Scientia Agricola. 68 (2011) 1-7.

[7] R.S. Teixeira, G.H.D. Tonoli, S.F. Santos, J. Fiorelli, H. Savastano Jr., F.A. Rocco Lahr, Extruded cement based composites reinforced with sugar cane bagasse fibres. Key Engineering Materials. 517 (2012) 450-457.

[8] Y. Shao, S.P Shah, Mechanical properties of PVA fibre reinforced cement composites mfabricated by extrusion processing, ACI materials Journal. 94 6 (1997) 555-564.

[9] C. Aldea, S. Marikunte, S. Shah, Extruded Fibre Reinforced Cement Pressure Pipe, Advanced Cement Based Material. 8 2 (1998) 47–55.

[10] A. Peled, S. Shah, Processing effects in cementitious composites: extrusion and casting, Journal of Materials in Civil Engineering. 15 2 (2003) 192-199.

[11] Y. Shao, S. Moras, N. Ulkem, G. Kubes, Wood fibre-cement composites by extrusion, Canadian Journal of Civil Engineering. 27 3 (2000) 543-552.

[12] B. Mua, Z. Li, J. Peng, Short fibre-reinforced cementitious extruded plates with high percentage of slag and different fibres, Cem. and Concr. Res. 30 8 (2000) 1277-1282.

[13] A. Alvarez-Castillo V. . Castaño . A. once R. Salgado . R. a rtínez, U. Aguilar and R. Bailón in: roc. 2nd Simposio Ibero-Americano de Polimeros/4th Simposio Latinoamericano de polímeros/6th International a cromolecular Colloquium ramado Brasil (1994) p. 101.

[14] R. ó pez V. . oblano A. i cea-Claveríe . Avalos, A. Alvarez-Castillo V. . Castaño Alkaline surface modification of sugar cane bagasse. Advanced Composite Material. 9 2 (2000) 99-108.

[15] . arcía-Zetina E. a rtínez A. Alvarez-Castillo V. . Castaño Numerical Analysis of the Experimental Mechanical Properties in Polyester Resins Reinforced with Natural Fibres, J. Reinf. Plast. Comp. 14 6 (1995) 641-649.

[16] F. Khan and S.R. Ahmad, Chemical modification and spectroscopic analysis of jute fibre, Polym. Degrad. Stabil. 52 3 (1996) 335-340.

[17] S. Varghese, B. Kuriakose and S. Thomas, Stress relaxation in short sisal-fibre-reinforced natural rubber composites, J. Appl. Polym. Sci. 53 8 (1994) 1051-1060.

[18] U.C. Jindal, Development and Testing of Bamboo-Fibres Reinforced Plastic Composites, J. Compos. Mater. 20 1 (1986) 19-29.

[19] American Society for Testing and Materials – ASTM C150/C150 M-11. Standard specification for Portland cement, 2011

[20] S.F. Santos SF, R. Schmit, A.E.F. Almeida, G.H.D Tonoli, H. Savastano JR; Supercritical carbonation treatment on extruded fibre–cement reinforced with vegetable fibres; Constr. Build. Mater., 56 (2015), pp. 84-94

[21] A. Bentur, S. Mindess; Fiber Reinforced Cementitious Composites Technology & Engineering. Taylor & Francis group, New York (1990)

[22] V. Baheti, S. Naeem . ilitký . Okrasa B. Tomková; Optimized preparation of activated carbon nanoparticles from acrylic fibrous wastes Fibers Polym., 16 (2015), pp. 2193-2201, 10.1007/s12221-015-5364-0

[23] V. Baheti, J. Militký; Reinforcement of wet milled jute nano/micro particles in polyvinyl alcohol films Fibers Polym., 14 (2013), pp. 133-137, 10.1007/s12221-013-0133-4

[24] Sérgio F. Santos, R. Schmidt, Alessandra e.f.s. Almeida, Austavo h.d. Tonoli, Holmer Savastano; Supercritical carbonation treatment on extruded fibre–cement reinforced with vegetable fibres ; Cement and Concrete Composites, Volume 56, February 2015, Pages 84-94

HEAT AND HUMIDITY TRANSFER IN SANDWICH TEXTILES FOR AUTOMOTIVE SEATS

Zuzana Drapáková[1], Vladimír Bajzík[2] and Luboš Hes[2]

[1] ŠKODA AUTO a. s., Technical development, tř. Václava Klementa 869, 29301 Mladá Boleslav, Czech Republic (Technical University of Liberec, Dept of Textile Evaluation, Studentská 2, 46117 Liberec, Czech Republic), e-mail: zuzkamail@gmail.com

[2] *Technical University of Liberec, Dept of Textile Evaluation, Studentská 2, 46117 Liberec, Czech Republic, e-mail:* vladimir.bajzik@tul.cz

Abstract

The paper is about improving heat and humidity transfer coming from passenger through the car seat cover. A new composition of sandwich cover material for car seat has been developed to improve the comfort of the passenger seat. The replacement of polyurethane foam between the top design layer and the lower smooth layer, which serves to simple cover car seat, and the way these parts are joined to the sandwich is the fundamental change. A spacer knit has replaced polyurethane part of the sandwich. By doing this, the bottom layer is no longer needed; the material is sufficiently sliding for coating the car seat. The aim of the development of sandwich cover material was to improve its attributes by using existing design materials. It was not intended to develop or change the design material for another, the new one that would be more breathable and would have higher water vapor permeability. By measuring, we have found out which of the used design materials are the most suitable for the coating, which ones have the highest air and water vapor permeability and are therefore the most suitable for the new sandwich and car seat. The materials were tested on the Permetest and Textest FX3300 measuring devices. Changing the cover sandwich, increasing passenger comfort during summer months, was also meant to lead to the change in the development of new cover sandwich.

The measurement shows, that thanks to this change the new car seat with the new cover material has a better permeability by 30% compared to the car seat with the concept of cover seat used so far. Complete seat measurement was carried out using a specially adjusted measuring head simulating the passenger position. The measured values in permeability of the car seat with standard seat cover was taken as 100% when compared to the new, for the better idea of the difference in functionality.

The innovative coating material not only has better attributes when taking into consideration the driver´s or passenger´s comfort but is also better recyclable. Compared to the original state in which there is the polyurethane foam bonded between the two polyester materials by the upper and lower layer with flame lamination, in this case polyester spacer knit bonded by glue is used.

Key words

sandwich seat cover materials, air-permeability, vapor-permeability, thermal-comfort

1. Introduction

Thermal comfort is important primarily for drivers in terms of focusing on driving. If the comfort isn't sufficient it may cause tiredness, sleepiness or irritation. Comfort is equally crucial for the rest of the passengers when it comes either to short term or long-term journeys. For this reason, emphasis should be placed on choosing the right material, on which passengers spend quite a bit of time

seated. Emphasis should be placed on the qualities of material, in this case the qualities of sandwich material and its ability to draw water vapor [1].

Presently car seats with heating are axiomatic part of the equipment of vehicles, which is ideal for winter season. Contrarily for the summer season active air-conditioned car seats are not a common matter. A more affordable option could be a passive air-conditioned seat, which would at least partially replace the missing and comfort-improving active air-conditioned car seat that is currently technologically and financially more demanding.

The functionality of the sandwich cloth assembly needs to be verified by measurement. Ideally, in a both objective and subjective way. Objectively using a permetest device that measures water vapor permeability and material breathability using the Textest 3300 device. The best way to do subjective measurement is to get as close as possible to the real situation, which in this case would be a road test on a car seat with an innovative coating.

2. Experimental

2.1. Measurement instruments

The measurement of materials was carried out on KHT TU Liberec on Permetest for measuring water vapor permeability and thermal resistance of textiles (Figure 1) [2] and TexTest FX3300 Air Permeability Tester III (Figure 2) for measuring air permeability [3].

Figure 1. Permetest

Figure2. Textest FX3300

2.2. Materials

The cover is made of sandwich material and consists of 3 parts (Figure 3):

1. The top part - design material - is made of polyester textile materials.
2. Medium part - filling, polyurethane foam in the central part with a height of 6-8 mm
3. Bottom - lining made of glove-knit polyester fabric for easy padding of the car seat.

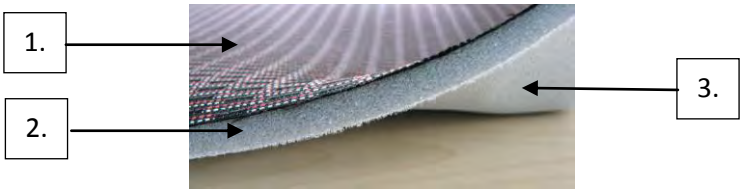

Figure 3. Sandwich material cover for car seats

Design material for the innovative car seat cover has been selected with existing coating materials. It was not desirable to create an entirely new material for both time and, above all, financial reasons. These materials must meet certain technical parameters according to the regulations. For example, abrasion resistance, tensile strength, bonding of layers, etc [4]. An important condition of materials is also a fulfilment of design requirements. For these and other reasons, design (top) materials for car seat coverings have been selected for further research.

For the middle part (layer), two materials were designed:

1. Reticulated foam (Figure 4) - foam material where the foam pores are opened by their controlled explosion in a closed box where the air is sucked out and oxygen and hydrogen supply a controlled reaction resulting in cracking of the contact bubble boundary. The pores remain open [5].
2. Distance knitting (Figure 5) - 3D knitted fabric made from 100% PES, which is made by joining two flats, independently created knitted fabrics with another dense monofilament thread set [6].

Figure 4. Reticulated foam

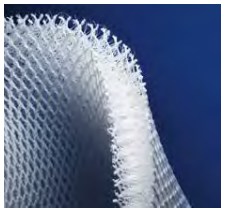

Figure 5. Distance knitted fabric

2.3. Methods

Three bonding options were selected for joining the sandwich layers:

1. sewing
2. bonding with powder glue
3. point bonding – hot melt

Based on the tests the permetest with added reference sample, 2 design materials with the best result of permeability and breathability were selected.

When it comes to the second part (middle) of the sandwich, the distance knitting has better qualities compared to the reticulated foam. Even if the reticulated foam has open pores, it is not sufficient for efficient vapor and air throughput. It no longer has the required stiffness. In addition, it is necessary to solve the lining for easy way to cover the car seat.

The third part was omitted due to the gliding qualities of the surface of the distance knitting. It is not necessary. The ease of coating was maintained without further modification or addition of the lining.

Based on these tests, the prototype of the cover for two car seats was made from the final samples:

1. design material with embossing
2. design material without any further final changes

The material of the sample number 2 had the best qualities, but the way of embossing had to be tuned so that the pattern was visible and the fibres of the distance knitting would not break, and it is also an extra operation, where you operate with heat and pressure to close other openings for the drainage of water vapours and air and thus the functionality of the whole sandwich decreases. However, not so much that the material of sample 2 is worse than sample material number 1, but it was our goal to test the subjective feeling of comfort on both materials - whether the embossing in conjunction with the distance knitting changed the perception of comfort. The material felt harder, stronger. The distance

knitting is not so soft as the polyurethane foam, so the first time using it can be negatively evaluated, and it can also be negatively rated from a long-term ride test.

Figure 6. Serial sandwich of sample 2

Figure 7. Design material of sample 2 with distance knitting

Based on this information, two prototype car seats with other design material were built for subjective testing and also for the measurement of the permeability of the car seat (see Figure 6 and 7). The breathability of the whole car seat was measured by colleagues from the Department of Machine Parts and Mechanisms under the guidance of Mr. doc. Fliegel.

Higher breathability has been confirmed on the entire car seat by 30% compared to the current state. The comfort of the car seat has been accepted and positively evaluated as part of the subjective assessment for long-term road tests, including in the car seat with embossing.

The entire car seat has not been tested for the vapor permeability yet because an extra measuring device would have to be made for this measurement, which would be a further financial and time burden.

Based on the measurement of the individual design materials for breathability and vapor permeability, the whole car seat for breathability and also based on a positive subjective assessment on long term road tests on hot summer days, it was decided that it is not necessary to measure the whole car seat for vapor permeability.

4. Results and discussion

Altogether, more than 50 samples of materials were measured. Approximately 8 lamination methods have been tested. Several samples of foam seat castings with an upgraded central part have been tested to improve comfort in the passive climate control of car seats and several prototype car seats have been built.

The table 1 shows the results of breathability and vapor permeability measurements of selected sandwich materials with PUR interlayer and PES lining, and the results of breathability and vapor permeability measurements of these selected materials, their design top part, interlayer with distance knitting, and a way of lamination for the building of prototype car seats of the sample 1 and sample 2.

Sample of textile	Sandwich with PUR interlayer and lining				Sandwich with distance knitting			
	Air-permeability	Vapor permeability			Air-permeability	Vapor permeability		
	$\bar{x}$ - Flow [l/m²/s]	p[%] $R_{et}\left[Pa.m^2.W^{-1}\right]$	$\bar{x}$	v [%]	$\bar{x}$ - Flow [l/m²/s]	p[%] $R_{et}\left[Pa.m^2.W^{-1}\right]$	$\bar{x}$	v [%]
Sample 1 	128	10,3		9,2	229,3	18,8		5,2
		33,2		10,1		19,7		7,3
Sample 2 	280	7,7		19,0	510	13,5		17,2
		45,7		21,7		32,4		23,5

Table 1. Serial samples of sandwich material with PUR foam

According to the results, the improvement of sandwich material in permeability and vapor permeability is evident [7].

Figure 8 shows the measurement of the overall breathability of the seat on three foam casting samples with an innovative sandwich coating and a comparison with the existing design of the car seat with standard foam casting and sandwich coating where the topcoat, PUR interlayer and lining are joined by flame lamination. Verification of breathability on the complete car seat showed an improvement of almost 30% compared to the standard car seat.

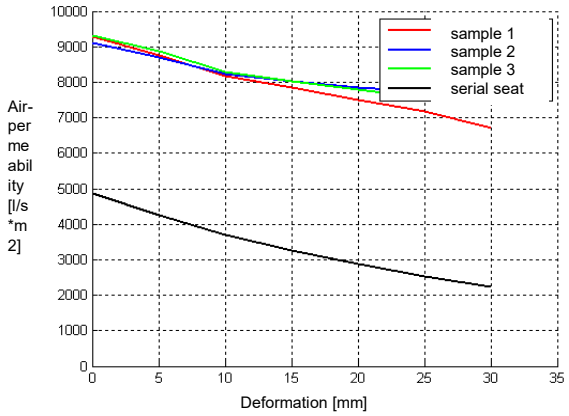

Figure 8. Measurement of the overall breathability of the seat on three foam samples with an innovative sandwich coating. Comparison with the existing car seat design

5. CONCLUSIONS

An objective evaluation of the innovated sandwich according to the measurement result shows a visible improvement in permeability and water vapor permeability. For material processing, the visual quality of the coating is also suitable for spot bonding lamination. Seating comfort is not negatively affected by this composition while maintaining at least 5 mm of the thickness of the distance knitting. Also, this cover concept does not affect other related seat components such as heating and SBR sensors.

In the subjective assessment of the car seat with an innovative sandwich cloth, the seat was positively evaluated in the sense of maintaining the existing comfort criteria and a visible improvement in thermal comfort. The passenger sweats less and the seat even contributes to comfort in the hot weather when driving longer.

ACKNOWLEDGEMENTS

Acknowledgements for support belong to KHT TU Liberec, ŠKODA AUTO A.S., Proseat and Fezko.

References

[1] Hes, L., Sluka, P.: Úvod do komfortu textilií. Liberec: Technická univerzita v Liberci, 2005. ISBN 80-7083-956-0.

*[2] Hes, L.: Permetest. Liberec: S*ensora instruments & consulting, 2008. 1.

[3] Textest AG; [online]. Poslední revize 07. 08. 2008, [cit. 2008-08-07]. Dostupné z: <http://www.textest.ch/en/FX3300-Lab-Air.html>.

[4] Nolis, VW Koncernorm. Koncernorm VW50105. NOLIS nolis.wob.vw.vwg. [Online] VW, 7. 8 2010.[Citace:15.9.2012.] http://nolis.wob.vw.vwg:15233/showprop/?id=651648&key=cbdmP26x1yHctM2Y4C0.

[5] Janda P. Vlastnosti polyuretanový a retikulovaných pěn. [Dokument] Mladá Boleslav : PROSEAT, 2014. 1.

[6] Tylex Letovice: Distanční 3D úplety. http://www.sindat.cz/. [Online] SINDAT, 15. 5. 2012. [Citace 29. 10 2012]. http://www.sindat.cz/technicke-pletene-textilie/en/dwn/distancni-3d-uplety.pdf.

[7] Nolis, VW Koncernorm. Textilien - Bestimmung der Luftdurchlässigkeit von textilen Flächengebilden (ISO 9237:1995). Burscheid : Konzernorm Volkswagen, 1995. 1.

INTUMASCENT FLAME RETARDANT BILAYER COATINGS ON COTTON FABRIC OF CASEIN AND AMMOIUM POLYPHOSPHATE VIA BILAYER ASSEMBLY

Sajid Faheem, Vijay Baheti, Maroš Tunák, Jakub Wiener, Jiří Militký

Department of Materials Engineering, Faculty of Textile Engineering, Technical University of Liberec, Studentská 1402/2, 46117 Liberec 1, Liberec, Czech Republic. Tel: +42048531111

Author: Sajid Faheem; msajidfaheem@gmail.com
Corresponding Author: Vijay Baheti; vijaykumar.baheti@gmail.com

Abstract

The objective of present study was to investigate the effect of bilayer coating of different concentrations of APP and casein on thermo-oxidative properties, flame retardant behavior as well as thermal conductivity of cotton fabrics. The flame retardant behavior was found to increase predominantly with increase of APP concentration than the casein concentration due to greater release of phosphoric acid and ammonia from APP. Whereas, the higher concentration of casein was found more advantageous to form the distinct layer of intumescent char formation, where cotton fabric samples coated with 15% casein and 7.5% APP contents produced maximum char of 44%.

Key words

Green flame retardants; Casein; Ammonium Polyphosphate; Cotton; Thermo-oxidative stability.

1. INTRODUCTION

Cotton fiber is ideally used in apparels, draperies, tents, pillowcases, towels, bed sheets, etc because of its soft, comfortable, and breathable features [1]. However, cotton fiber also poses many challenges due to its flammable and hydrophilic nature where heat and humidity combine to form fire conducive environments [2]. Once cotton fabric is ignited, the flame spreads fast and is difficult to extinguish. The limiting oxygen index of cotton is only about 19 % and the combustion temperature is 360–425 °C [3].

In recent years, the intumescent systems (i.e. combination of acid source, carbon source and blowing agent) are considered as the most performing solution available to withstand the fire threat [4, 5]. Intumescent fire resistant coatings can foam and bubble when they encounter flame or high temperatures [6]. The subsequent formation of swollen multicellular thermally stable char thus can prevent the heat, fuel and oxygen transfer between the flame and material [7, 8].

The present paper described a simple strategy to build intumescent coatings on cotton fabric surfaces using environment friendly resources. The bilayer assemblies of positively charged casein were coupled with negatively charged APP, and deposited on cotton fabrics by traditional coating methods. The casein–APP pair can represent an intumescent-like system, in which casein can act as both carbon source and foaming agent, whereas APP is able to generate phosphoric acid at high temperatures.

2. EXPERIMENTAL METHODS

2.1. Materials

The plain woven 100 % cotton bleached fabric having 145 g/m^2 aerial density (Licolor, a.s. Czech Republic), bovine milk casein (Sigma-Aldrich, Czech Republic), Ammonium polyphosphate, APP (Aako Netherland), Sodium hydroxide and hydrochloric acid (Lach-Ner, Czech Republic) were used in this study.

2.2. *Prepartion and application of casein and APP solutions on cotton fabric*

The 5, 10, 15 wt. % of casein powder was added in deionized water. It was heated at 80 °C by adjusting the pH to 2-3 using 1M HCl in thermostatic bath with continuous stirring. The process was later stopped when the casein was completely dissolved. Whereas, the APP solutions were prepared at room temperature by addition of 2.5, 5.0 and 7.5 wt % APP powder in deionized water and by adjusting the pH to 9-11 using 1M NaOH.The bilayer assemblies of different concentrations of APP and casein were applied on cotton fabric in a climatic chamber at 30 °C and 30 % R.H through conventional coating method. In this way, the total of nine samples was prepared (see Table 1). The uptake (add on percentage) was also calculated.

Table 1. Details of coated samples

Sample Name	Casein Conc. (%)	APP Conc. (%)
CAS5+APP2.5	5	2.5
CAS5+APP5	5	5
CAS5+APP7.5	5	7.5
CAS10+APP2.5	10	2.5
CAS10+APP5	10	5
CAS10+APP7.5	10	7.5
CAS15+APP2.5	15	2.5
CAS15+APP5	15	5
CAS15+APP7.5	15	7.5

2.3. *Characterization and testing*

Bilayer coated cotton fabrics were characterized for FTIR, SEM, phosphorous element contents analysis, TGA and flame retardancy as well as the thermal conductivity of char residues, according to standard test methods.

3. RESULTS AND DISCUSSION

Data collected from characterization and testing of developed samples were analyzed and discussed to study and investigate reasons for the behavior of intumescent and flame retardant properties.

3.1. *Thermo-oxidative stability of casein-APP coated cotton fabrics*

As any polymeric material undergoes thermo-oxidation before ignition, therefore the most important issues in the design of a new flame retardant for fabrics is their thermal stability in air [9, 10]. Here, thermo gravimetric analysis was employed to study the effect of bilayer coating of different concentrations of casein and APP solutions on thermo-oxidative stability of cotton fabrics. Figure1 represent the weight loss with increase in temperature and also the different decomposition temperatures for uncoated and coated samples.

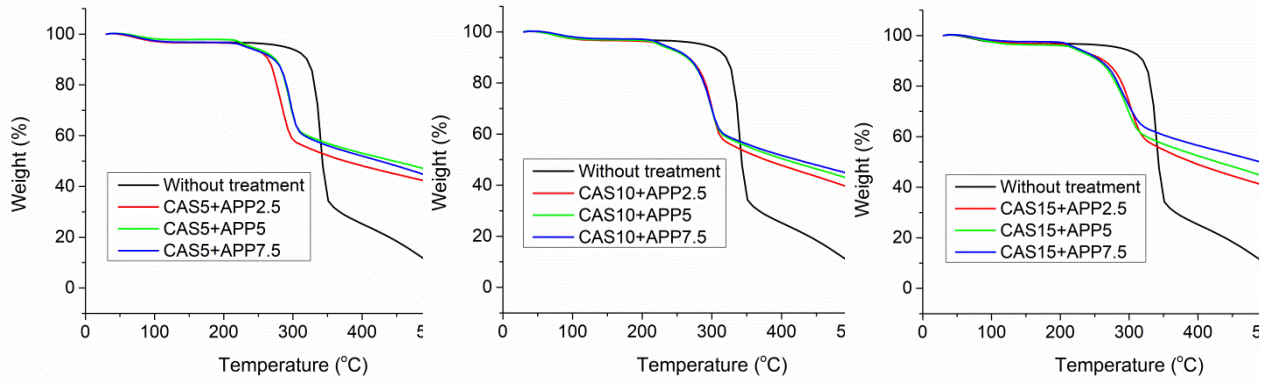

(a) 5% casein/APP (b) 10% casein/APP (c) 15% casein/APP

Figure 1. TGA curves for different bilayer assemblies coated on fabrics

The residue (%) after the first degradation step at T_{max1} was attributed to the formation of a thermally stable form of aliphatic char due to depolymerization and dehydration of cellulose. Nevertheless, on further increase of temperature, the second peak of maximum weight loss rate appeared (T_{max2}), which correspond to the carbonization and oxidation of the aliphatic char into carbon mono and dioxide. The $T_{onset10\%}$ values of cotton fabrics were found to shift towards the lower temperatures when coated with bilayer of casein and APP solutions.

3.2. Flammability properties of casein-APP coated fabrics

The combustion behavior of the uncoated and the coated cotton fabrics was assessed by horizontal flame test to describe the real fire scene. The total burning time (s), burning rate (mm/s) and residue (%) were used to estimate the resistance for flame propagation (see Table 2). When a methane flame was applied for 3 sec, the untreated cotton fabric burnt vigorously without leaving any residue. The flame lasted for 36 sec followed by prolonged afterglow. On the other hand, the bilayer coating of casein and APP solutions promoted increase in total burning time. The flame stopped after some seconds without any afterglow phenomenon depending upon the concentrations of casein and APP solutions.

Table 2. Burn characteristics of different bilayer assemblies coated on fabric

Sample	Total Burning Time (sec)	Flame Stoppage Time (sec)	Afterglow (sec)	Char residue (%)
No treatment	36	-	15	3.1
CAS5+APP2.5	-	8	-	26.8
CAS5+APP5	-	7	-	32.5
CAS5+APP7.5	-	5	-	34.3
CAS10+APP2.5	-	6	-	28.9
CAS10+APP5	-	5	-	35.4
CAS10+APP7.5	-	3	-	37.2
CAS15+APP2.5	-	5	-	32.8
CAS15+APP5	-	4	-	40.1
CAS15+APP7.5	-	2	-	43.9

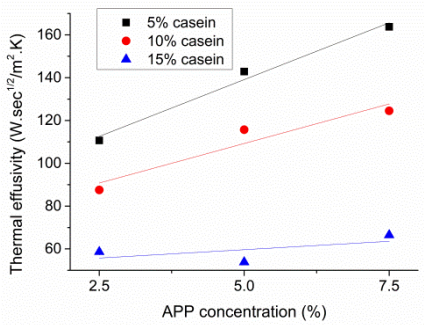

Figure 2. Thermal effusivity of char resides

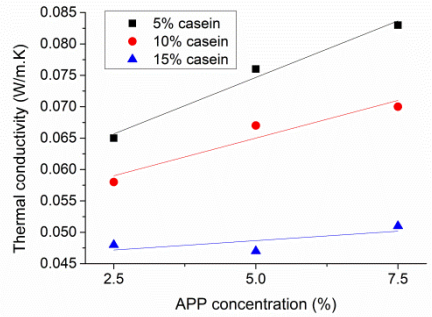

Figure 3. Thermal conductivity of char residues

In order to validate the formation of voluminous/intumescent char on surface of coated fabrics, the thermal conductivity of the residual chars were measured. From Figure 2 and Figure 3, it can be seen that thermal conductivity and thermal effusivity values of residual chars reduced with increase in APP or casein concentrations in bilayer assembly. At low APP or casein contents, the greater values of thermal conductivities can be attributed to formation of less, coherent char without any intumescences. On the contrary, lower values of thermal conductivities at high APP/casein contents indicated formation of dense, non-coherent char with more intumescences. Therefore, due to more air gaps between the layers of chars, they absorb low heat from surroundings resulting in slow and less propagation of flame. Later, the flame retardant mechanism of bilayer assemblies of casein/APP contents was investigated by observation of the surface structure of burnt samples on scanning electron microscopy (see Figure 4). At low casein concentrations, a thin protective char layer formed on the surface of fibers and few fibers fractured during the burning (Figure 4a, Figure 4b and Figure 4c). However, with increase in casein concentrations, char layer became denser and weave structures of coated fabrics greatly retained. These results indicated formation of additional char residue by catalytic dehydration of casein in the presence of APP, and thus potential use of casein as carbon source in intumescent systems. The

bilayer assemblies of lower APP contents produced globular micrometric structures at localized spaces (Figure 4a, Figure 4d, and Figure 4g), whereas more expanded globular micrometric structures (i.e. global intumescence) at enlarged spaces were observed for higher APP contents (Figure 4c, Figure 4f and Figure 4i). The globular micrometric structures are phosphorus-rich bubbles that blow up during the combustion [24].The presence of more bubbles in case of higher APP contents indicated release of more volatile ammonia gas for larger expansion of char.

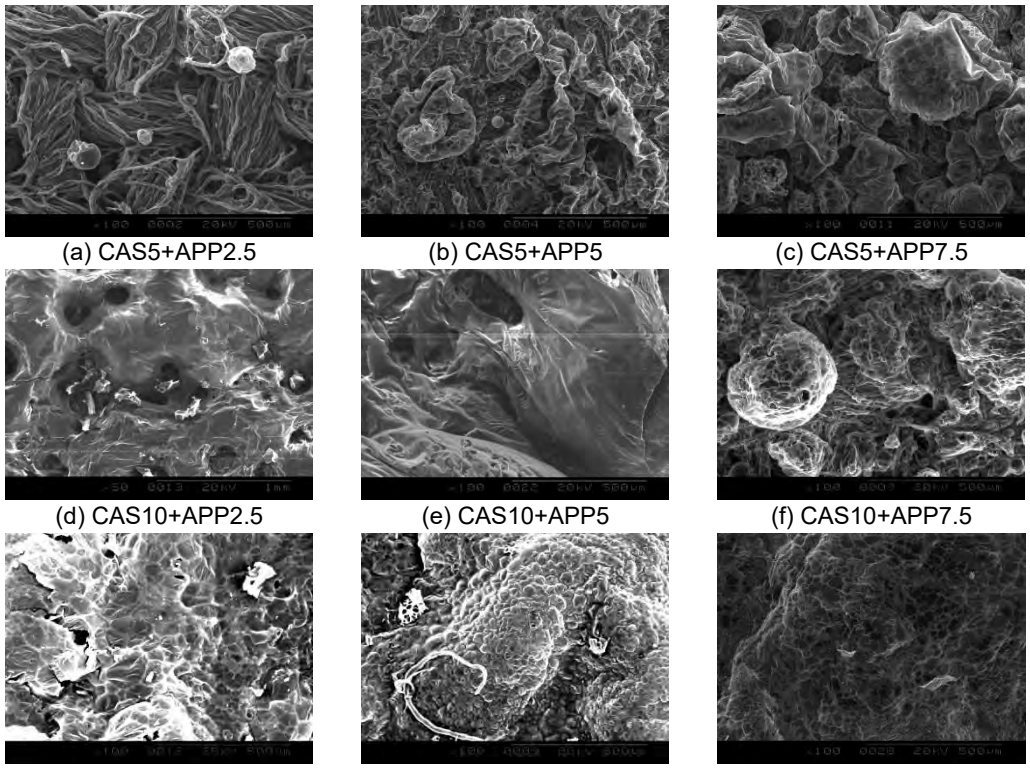

(a) CAS5+APP2.5 (b) CAS5+APP5 (c) CAS5+APP7.5

(d) CAS10+APP2.5 (e) CAS10+APP5 (f) CAS10+APP7.5

(g) CAS15+APP2.5 (h) CAS15+APP5 (i) CAS15+APP7.5

Figure 24. SEM images of char residues of different bilayer assemblies

4. CONCLUSIONS

In present work, the environment friendly intumescent system of casein and APP was applied as bilayers on cotton fabrics by simple and industrially scalable technique. The effects of different concentrations of casein and APP in bilayer assembly were studied for thermo-oxidative stability and flame resistance behavior of cotton fabrics. From TGA analysis, higher concentration of APP depicted stronger sensitization of the cellulose decomposition as compared to casein. However, the higher concentration of casein was found to produce higher char residue irrespective of the APP concentration. From horizontal flame tests, cotton fabrics coated with 15% casein and 7.5% APP contents showed maximum char formation of 44% as compared to 3% char for uncoated cotton fabrics. The images of burnt samples confirmed the formation of distinct intumescence layer of char residue at higher concentrations of casein and APP, and it was also validated from the measurements of thermal conductivity of char residues. The SEM images of residues of burnt samples showed the formation of thin protective char layer on the surface of fibers at lower casein content. Interestingly, globular micrometric structures at localized spaces were observed for the lower APP contents, and more expanded globular micrometric structure at enlarged spaces were observed for higher APP contents. In this way, the present work realized that the casein could perform number of functions such as catalyzed dehydration, accelerated charring and intumescent char formation in APP based intumescent systems.

ACKNOWLEDGEMENTS

The financial support for conducting the present research work was provided from the Student Grant Competition Technical University of Liberec no. 21241 granted by Ministry of Education, Youth and Sports of Czech Republic.

References

[1] D. Zhang, B.L. Williams, S.B. Shrestha, Z. Nasir, E.M. Becher, B.J. Lofink, et al., Flame retardant and hydrophobic coatings on cotton fabrics via sol-gel and self-assembly techniques, J. Colloid Interface Sci. 505 (2017) 892–899.

[2] Y. Liu, Y.T. Pan, X. Wang, P. Acuña, P. Zhu, U. Wagenknecht, et al., Effect of phosphorus-containing inorganic-organic hybrid coating on the flammability of cotton fabrics: Synthesis, characterization and flammability, Chem. Eng. J. 294 (2016) 167–175.

[3] Y. Feng, Y. Zhou, D. Li, S. He, F. Zhang, G. Zhang, A plant-based reactive ammonium phytate for use as a flame-retardant for cotton fabric, Carbohydr. Polym. 175 (2017) 636–644.

[4] W. Jiang, F.-L. Jin, S.-J. Park, Synthesis of a novel phosphorus-nitrogen-containing intumescent flame retardant and its application to fabrics, J. Ind. Eng. Chem. 27 (2015) 40–43.

[5] F. Fang, X. Zhang, Y. Meng, Z. Gu, C. Bao, X. Ding, et al., Construction of intumescent flame retardant and antimicrobial coating on cotton fabric via layer-by-layer assembly technology, Surf. Coatings Technol. 276 (2015) 726–734.

[6] M. Jimenez, S. Duquesne, S. Bourbigot, Intumescent fire protective coating: Toward a better understanding of their mechanism of action, Thermochim. Acta. 449 (2006) 16–26.

[7] K. Apaydin, A. Laachachi, V. Ball, M. Jimenez, S. Bourbigot, V. Toniazzo, et al., Intumescent coating of (polyallylamine-polyphosphates) deposited on polyamide fabrics via layer-by-layer technique, Polym. Degrad. Stab. 106 (2014) 158–164.

[8] J. Alongi, M. Ciobanu, G. Malucelli, Novel flame retardant finishing systems for cotton fabrics based on phosphorus-containing compounds and silica derived from sol-gel processes, Carbohydr. Polym. 85 (2011) 599–608. [9] I. Simkovic, "TG/DTG/DTA evaluation of flame retarded cotton fabrics and comparison to cone calorimeter data," Carbohydr. Polym., vol. 90, no. 2, pp. 976–981, 2012.

[10] D. Price, a. R. Horrocks, M. Akalin, and a. a. Faroq, "Influence of flame retardants on the mechanism of pyrolysis of cotton (cellulose) fabrics in air," J. Anal. Appl. Pyrolysis, vol. 40–41, pp. 511–524, 1997.

[11] J. Alongi et al., "Caseins and hydrophobins as novel green flame retardants for cotton fabrics," Polym. Degrad. Stab., vol. 99, no. 1, pp. 111–117, 2014.

INVESTIGATION OF MATERIAL BEHAVIOUR ON LIQUID MOISTURE TRANSPORT PROPERTIES OF FUNCTIONALUNDERWEARS

Sajid Hussain, Viera Glombikova, Antonin Havelka

Technical University of Liberec, Faculty of Textile Engineering, Department of Clothing Technology, Liberec, Czech Republic, Studentska 1402/2, 461 17, Liberec.
Corresponding author e-mail: sajid.hussain@tul.cz

Abstract

Liquid moisture transport of textile structures has been studied in order to manage human perspiration well. This article deals with investigation of moisture transport of single jersey knitted fabrics by sophisticated methods, such as moisture management tester (MMT) and thermography systems. Four knitted fabrics were analyzed by the above-mentioned methods. Specifically, the distribution of liquid drops on samples was compared with the results of vertical wicking phenomena. There is a strong co relation between OMMC and accumulative one way transport index % with vertical wicking of knitted samples.

Key words

Moisture Transportation, breathability, Moisture Management Tester, Wicking.

1. INTRODUCTION

Moisture transport properties are significant to safe total physiological comfort of a wearer. Larger amount of sweat and higher body temperature are the outcome of intense activities such as sports and exercises or higher ambient air temperature. If the heat and moisture are not released effectively from the body, heat stress may occur and the wearer's performance will be negatively affected [1].

The underwear should transport this liquid moisture away from the skin or inner fabric surface to the outer surface as soon as possible to ensure a safe level of comfort for users [2].

The moisture management tester (MMT) is sophisticated test equipment that evaluates absorption properties of fabric and suitably complements standardized vertical or horizontal wicking testers. MMT investigates horizontally dynamic spreading of liquid drops on the surface of samples and in addition evaluates liquid transfer from the fabric's inner surface to its outer surface [3].

Wicking methods are used for the capillary phenomenon to analyse liquid transport properties of fabrics. Wicking phenomena takes place when sweat travels along the surface of the fibre but is not absorbed inside the fibre [4]. Nemcokova R. et al. [5] applied technique based on the combination of thermography system and image analysis system for the evaluation of both vertical wicking of fabrics and horizontal wetting of fabrics. Thermography system took the advantage of a physical rule: during water evaporation heat arises.

Functional under wears maintains the temperature of human body under different climates. During alpine skiing and snowboarding[6], athletes experience alternating phases of physical activity and in these state functional underwears create an environment that maintains stable body climate in order to prevent the body from overheating or cooling down too much [7]. Fabrics having good moisture transport properties and fabric drying properties are necessary for sportswear, underwear or other type of clothing which have direct contact with human skin [8]. Cotton fabric has good water absorbing property. Cotton fabric keeps absorbed water inside its structure and its moisture transfer property is not very good especially during exercise in a humid and warm environment [9]. Polypropylene is a

good performer in moisture management due to its hydrophobic nature and due to its good thermal characteristics; it keeps the wearer warm in cold weather and cold in warm weather [10].

2. EXPERIMENTAL

2.1. Materials

Four knitted fabrics (see Table 1) were developed on circular knitted machine having same machine settings. Single Jersey Knitted fabrics are made of five raw materials having same pattern of construction.

Table 1. Characteristics of tested knitted fabrics

1st component	2nd Component	3rd Component	Fabric Thickness (mm)	Fabric Weight (GSM)	Sample Codes
50% Cotton Linear Density : 36/1 Ne	25% Coolmax Linear Density : 36/1 Ne	25 % Micro denier Multi filament Polypropylene Linear Density : 100 Denier	0.74	288	A
50% Modal Linear Density : 36/1 Ne	25% Coolmax Linear Density : 36/1 Ne	25 % Micro denier Multi filament Polypropylene Linear Density : 100 Denier	0.74	285	B
50% Viscose Linear Density : 36/1 Ne	25% Coolmax Linear Density : 36/1 Ne	25 % Micro denier Multi filament Polypropylene Linear Density : 100 Denier	0.74	292	C
50% Cotton Linear Density : 60/1 Ne	25% Coolmax Linear Density : 36/1 Ne	25 % Micro denier Multi filament Polypropylene Linear Density : 100 Denier	0.73	250	D

2.2. Methods

Moisture management properties of fabric samples were tested using Moisture Management Tester (MMT, by SDL Atlas) according to AATCC Test Method 195-2009. Vertical Wicking of knitted samples was tested by Thermography system .Thermography system takes the advantage of a physical rule: during water evaporation heat arises. This process is possible to be captured on a thermograph by a thermography system. Obtained thermographs are evaluated by an image analysis system to find moisture management parameters of weft knitted structures.

3. RESULTS AND DISCUSSION

All moisture management parameters like wetting time, absorption rate %, spreading speed, accumulative one way transport index and OMMC were measured results are shown in Table No. 2.

Table 2. MMT results of knitted samples.

Samples	Top Wetting Time (Sec)	Bottom Wetting Time (Sec)	Top Absorption Rate (%/Sec)	Bottom Absorption Rate (%/Sec)	Top Spreading Speed (mm/Sec)	Bottom Spreading Speed (mm/Sec)	Accumulative one way transport index %	OMMC
A	2.34	2.47	59.79	68.02	9.52	8.80	125.10	0.60
B	2.26	2.36	58.60	65.96	9.63	9.37	112.29	0.59
C	2.32	2.39	60.01	68.48	11.75	11.37	136.20	0.62
D	1.97	2.06	38.50	58.30	11.33	9.71	387.00	0.84

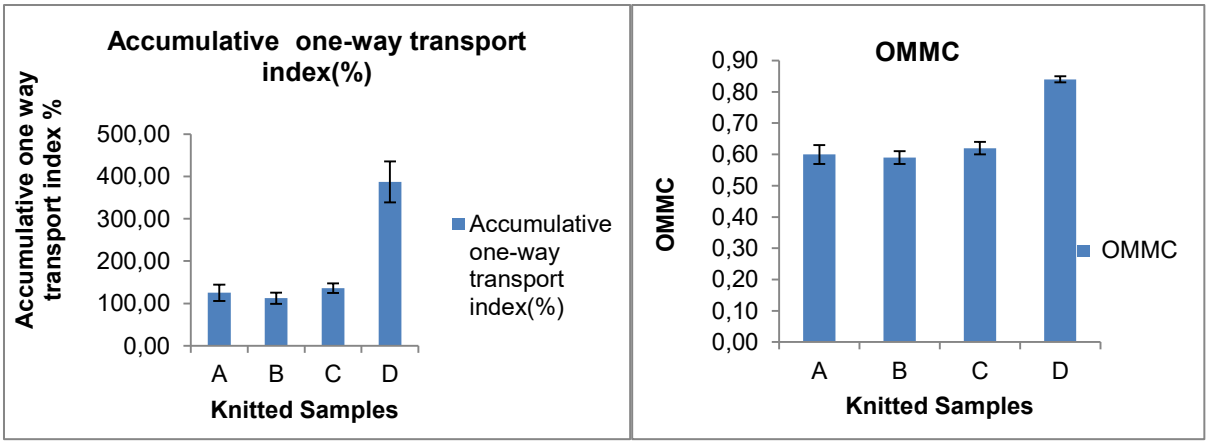

Figure 1. Accumulative one way transport Index % and OMMC results of Knitted samples

Vertical wicking results of all samples are given in Table 3.

Table 3. Vertical Wicking of Samples (Course Wise and Wales Wise)

Sample	Course wise Wicking (mm)				Wales wise Wicking (mm)			
	20 Sec	40 Sec	60 Sec	600 Sec	20 Sec	40 Sec	60 Sec	600 Sec
A	31.9	45	51.4	104.2	14.1	15.8	17.2	75.8
B	34.2	46.3	52.4	109.5	15.7	19.4	21.9	92.9
C	34.4	47.5	53.3	111.5	14.4	15.8	17.2	86.2
D	41.6	52.7	61.3	122.2	16.2	21.9	24.5	97.6

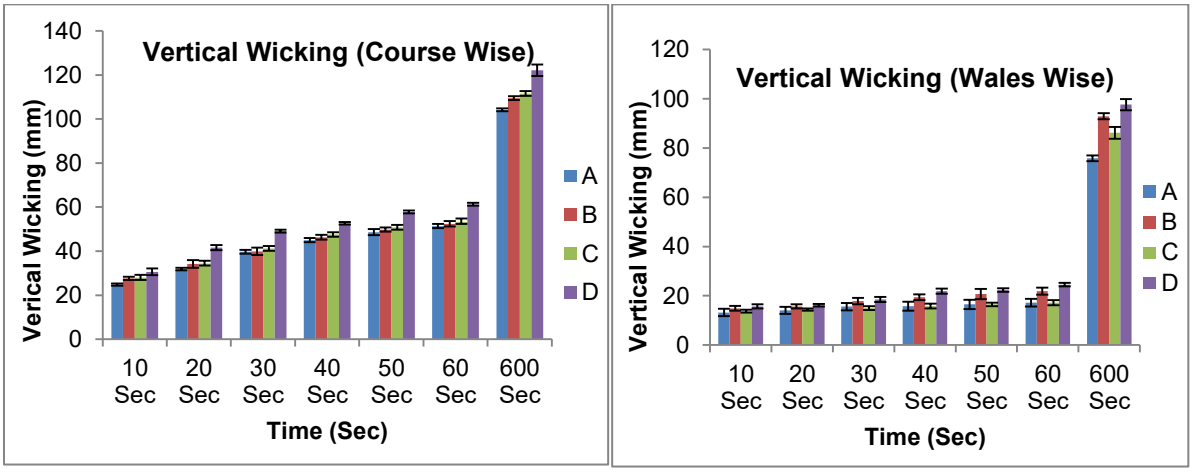

Figure 2. Vertical Wicking (Course wise and Wales Wise)

Co- Relation of OMMC with Vertical Wicking.

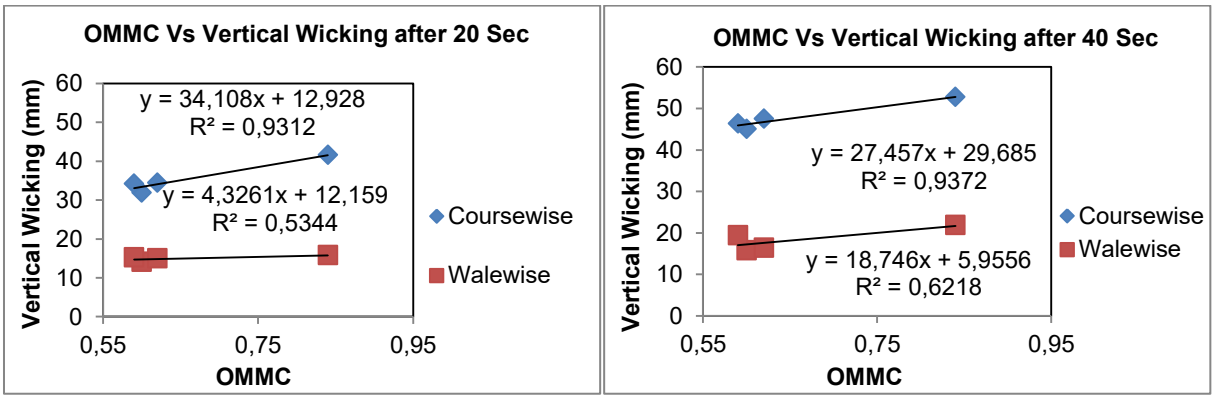

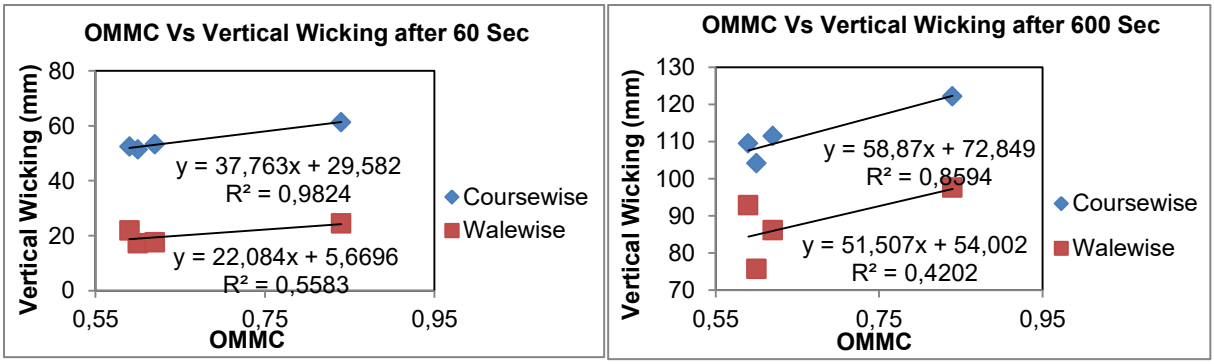

Figure 3. Co-Relation of Vertical Wicking with OMMC

4. CONCLUSIONS

Four knitted fabric samples having 50% courser cotton, 50% modal, 50% viscose, 50% fine cotton respectively were developed with 25% coolmax and 25% multifilament polypropylene.

According to the results it was concluded that sample D showed fast wetting , less absorption , very fast spread ability of liquid moisture , higher values of accumulative one way transportation and OMMC values as compared to samples A, B and C. Similarly in case of vertical wicking results, it was concluded that sample D showed maximum uptake of liquid moisture at every segment of time from start to 10 minutes of time. Sample D comprises 50 % finer cotton while other three samples are comprised of course counts of cotton, modal and viscose. So from this study it can also be concluded that if finer counts are used for these materials, best results can be achieved. There is a strong positive co-relation of accumulative one way transport index % and OMMC with vertical wicking specially in course wise direction.

References

[1] Ho, C.P, et al., (2011). Improving Comfort in Apparel, Woodhead Publishing Limited, Cambridge, UK, Improving thermal comfort in apparel, ISBN 978-1-84569-539-2.

[2] Bao-guo, Y., et al., (2006). An Improved Test Method for characterizing the dynamic liquid moisture transfer in porous polymeric materials. Polymer Testing, 25 (5), 677- 689.

[3] Oner, E., et al., (2013). Evaluation of Moisture Management Properties on knitted fabrics, Journal of the Textile Institute, 104 (7), 699-707.

[4] et al. Machova, K., "Air Streaming in Spacer Fabrics to Support the Wear Comfort of Sport and Outdoor Clothing," Melliand, vol. 6, pp. 23–28, 2006.

[5] R. Nemcokova, V. Glombikova, and P. Komarkova, "Study on liquid moisture transport of knitted fabrics by means of MMT, thermography and micro tomography systems" vol. 15, no. 4, 2015.

[6] B. Schindelka, S. Litzenberger, and A. Sabo, "Body climate differences for men and women wearing functional underwear during sport at temperatures below zero degrees Celsius," Procedia Eng., vol. 60, pp. 46–50, 2013.

[7] R. Fangueiro, P. Gonçalves, F. Soutinho, and C. Freitas, "Moisture Management Performance of Multifunctional Yarns Based on Wool Fibers," Indian J. Fibre Text. Res., vol. 34, pp. 315–320, 2009.

[8] M. Weder, R. M. Rossi, C. Chaigneau, and B. Tillmann, "Evaporative cooling and heat transfer in functional underwear," Int. J. Cloth. Sci. Technol., vol. 20, no. 2, pp. 68–78, 2008.

[9] M. Brazaitis, S. Kamandulis, A. Skurvydas, and L. Daniusevičiute, "The effect of two kinds of T-shirts on physiological and psychological thermal responses during exercise and recovery," Appl. Ergon., vol. 42, no. 1, pp. 46–51, 2010.

[10] N. Ozdil and S. Anand, "Recent Developments in Textile Materials and Products Used for Activewear and Sportwear," Electron. J. Text. Technol., vol. 8, no. 3, pp. 68–83, 2014.

SUPERHYDROPHOBIZATION OF COTTON FABRIC WITH FLY ASH FOR DURABLE UV PROTECTION AND OIL/WATER SEPARATION PROPERTIES

Muhammad Zaman Khan, Vijay Baheti and Jiri Militky

Technical University of Liberec, Faculty of Textile Engineering, Department of Material Engineering, Czech Republic
Corresponding author: zamankhan017@yahoo.com

Abstract

In the present research work, multifunctional cotton fabric with good super-hydrophobic, UV-protection and good oil/water separation properties was developed by coating fly ash nanoparticles and subsequent hydrophobization. After treatment of Trimethoxy(octadecyl)silane (OTMS) on fly ash coated fabrics, the water contact angle was increased to 143°, 147° and 153° for fly ash concentration of 1, 2 and 3 wt% respectively. Furthermore, the coated fabrics showed great potentials for removal of floating oil layer, underwater oil droplet and oil/water separation function. The surface morphology and elemental composition of coated fabric has been characterized with SEM and EDX respectively.

Key words

Cotton fabric, Contact angle, Fly ash, Oil water separation

1. INTRODUCTION

The superhydrophobicity of solid surfaces has been investigated with considerable attention over the past few years and remarkable progress has been achieved. The lotus flower is considered as a symbol superhydrophobicity. Surface roughness plays vital role in producing extreme repellence against liquid droplets [1, 2]. Superhydrophobic surfaces with physical self cleaning properties are due to water-repellent double structures of the surfaces. These hierarchical double structures can be achieved by surface roughness due to the micro/nano structures and hydrophobicity due to low-surface energy materials on top of the rough structures. To develop superhydrophobic surfaces, modification of surface chemistry in conjunction with the surface roughness is important [3–5]. The superhydrophobic surfaces are generally made by controlling the surface roughness and surface chemistry of various substrates using expensive materials, which are then applied by means of complex and time-consuming processes. Therefore, it is a technical challenge to achieve surface roughness and low-surface energy characteristic by simple and cheap method. In recent years, lot of work has been done on development of functional superhydrophobic textile by using nanoparticles of ZnO, Ag, SiO_2, MgO and TiO_2 etc [6–9].

In present study, superhydrophobic cotton fabric was developed by using mechanically activated fly ash and non-fluorinated silanes. Milled fly ash was used to achieve micro-nano roughness on the surface of the fiber and selected non-fluorinated silanes to impart low-surface energy characteristic. UV protection and oil/water separation properties of the developed fabrics were also investigated. It was also found first time that fly ash can be used as a potential UV protective material. The durability was assessed via comparing the results of the fabric before and after washing.

2. EXPERIMENTAL

2.1. Materials

Fly ash was obtained from the city of Plzeň located in the Czech Republic with the help of SILO Transport organization. The Trimethoxy(octadecyl)silane (analytical grade) was purchased from Merck. To investigate oil in water separation performance, four model oils of varying density (i.e. toluene, n-hexane, chloroform, petro ether) were used from laboratory. Plain woven bleached cotton fabric was used as substrate to create superhydrophobic surface.

2.2. Methods

Preparation of mechanically activated fly ash

Mechanical activation of fly ash was carried out using high-energy planetary ball mill of Fritsch Pulverisette 7 in a sintered corundum container of 80 ml capacity using zirconia balls of 10 mm diameter for the duration of 30 min. The ball mill was loaded with ball to fly ash weight ratio of 5:1. The rotation speed of the planet carrier was kept at 850 rpm. Moreover, milled fly ash particles were taken out to test particle size distribution on Malvern Zetasizer Nano based on dynamic light scattering principle.

Preparation of superhydrophobic cotton fabrics

To make fly ash dispersion different concentrations (1%, 2%, 3%) of FA were added into distilled water and sonicated for 10 min using ultrasonic system (Bandelin Sonopuls HD 3200, 20 kHz, 200 W, 50% efficiency). FA dispersion was applied to cotton fabrics through a dip-pad-dry-cure process. The fabric was immersed in the solution for 2 min and then it was passed through a padder. The fabric was dried at 90°C in a drying oven and cured at 120°C for 3 min. The fabric coated by fly ash was added into hydrolyzed OTMS solution (8%, w/w) to modify for 2 hr at room temperature. The treated samples were then dried in air and cured at 120°C in a drying oven for 1 hr. Figure. 1 shows the schematic of fabrication of superhydrophobic surfaces.

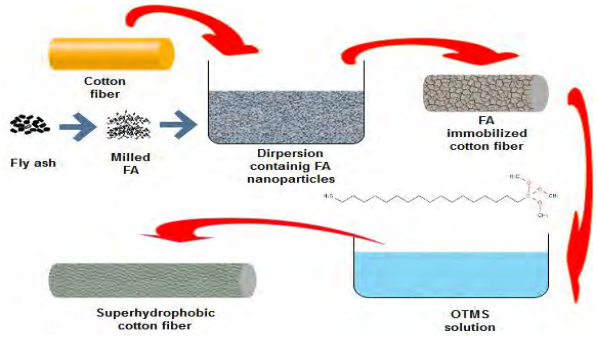

Figure 1. Schematic representation of superhydrophobic cotton fabric via immobilization of fly ash on the fabric with OTMS modification

Surface morphology and elemental analysis

The surface morphology of control and coated fabrics was observed by using a Scanning Electron Microscope TS5130 VegaTescan at 30 kV acceleration voltage. The elemental analysis of samples was carried out using Energy-dispersive X-ray spectroscopy.

Water contact angle and sliding angle measurement

Contact angle was measured by surface energy evaluation system of Advex Instruments. It is based on the goniometric method to calculate the contact angle between liquid and solid with 5 µl of water droplet. Six measurements were made on each sample for the determination of the average CA values. Water sliding angle was measured by using a custom-made device, which can measure sliding angle with an accuracy of 1°. On each sample, six measurements were made and mean value was taken.

UV protection properties

The ultraviolet radiation blocked or transmitted by textile fabric was determined by using the standard test method of AATCC 183-2000. Mean UPF, UVA and UVB blocking percentage of samples were calculated using UV-vis-NIR Spectrophotometer (UV-3101PC). For each sample, four measurements were performed and the average of all four scans was taken as a final UPF value.

Oil/water separation test

The as-developed cotton fabric was tested for separating oil/water mixture. Mixtures of oils (n-hexane, toluene, chloroform, petro ether) and water (50% v/v) were used for oil/water separation test. The oil/water separation efficiency was calculated using formula $K_s = m_1/m \times 100\%$. Where "m'' is amount of oil mixed with water to form oil/water mixture and "m_1" is the volume of oil after separation.

3. RESULTS AND DISCUSSION

3.1. Superhydrophobicity of cotton fabric

As expected, the water dyed with orange II was absorbed rapidly to the pristine cotton fabric (Figure 2(a)), while the orange colored water droplet exhibits a spherical shape on the surface of as-prepared cotton fabric with fly ash concentration of 3 wt.% (Figure 2(b)). The optical image of superhydrophobic fabric submerged in water, while a layer of minute bubble can be seen on the interface between the superhydrophobic fabric and water (Figure 2(c)). The mirror-like phenomenon is due to total reflectance of light at the air layer trapped in the superhydrophobic cotton surface.

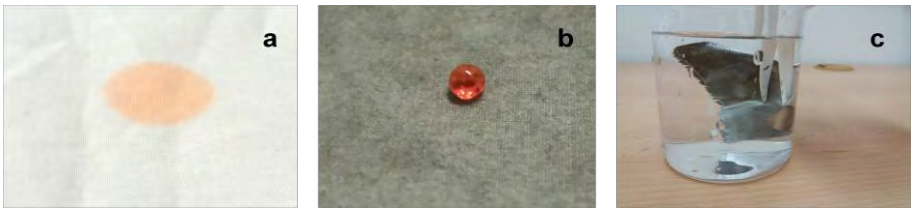

Figure 2. (a) Photographs of water droplet on pristine cotton , (b) cotton with FA-OTMS and (c) Superhydrophobic fabric immersed in the water via external force.

The surface morphology is important to obtain the superhydrophobic property. Figure. 3 show the SEM images of fly ash coated fabric surfaces. The surface of cotton fiber was uniformly covered by fly ash particles. Moreover, dense coatings with obvious hierarchical structures were formed when increasing the fly ash concentration. A micro/nanoscale surface mimicking the surface of lotus leaf was formed with each fiber of approximately 10 μm diameter, and the fly ash particles of below 1000 nm size. A good adhesion between the fly ash particles and cotton fibers can be attributed to the presence of hydroxyl groups and formation of hydrogen bonds between them.

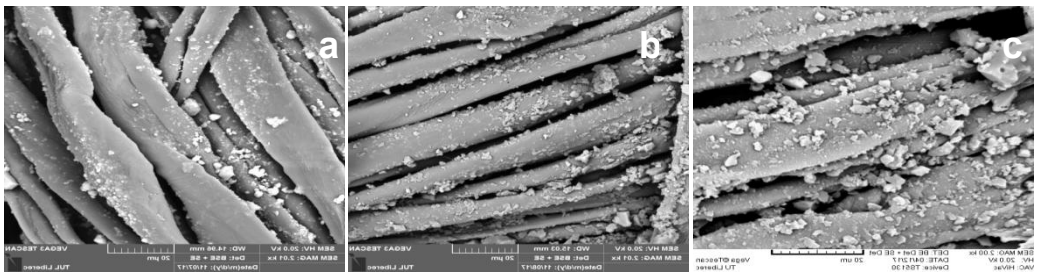

Figure 3. SEM images of cotton fabric coated with 1 wt% fly ash (a), 2 wt% fly ash (b) and 3 wt% fly ash (c).

The effect of fly ash particles on the superhydrophobicity of the fly ash-OTMS coated fabrics was investigated from measurements of water contact angle and water sliding angle (see Figure. 4). The surface of uncoated cotton fabric was completely wetted by the water droplet without any contact angle, whereas the water droplet exhibited a spherical shape on the surface of fly ash-OTMS coated. Cotton fabrics coated with only OTMS, the water contact angle and sliding angle were measured around 130° and 22° respectively. When fly ash particles were applied on cotton fabric with subsequent treatment of OTMS, the contact angle was enhanced and sliding angle was further decreased. The water contact angle of 143°, 147° and 153° and roll off angle of 13°, 8° and 5° was measured for fly ash concentration of 1, 2 and 3 wt% respectively.

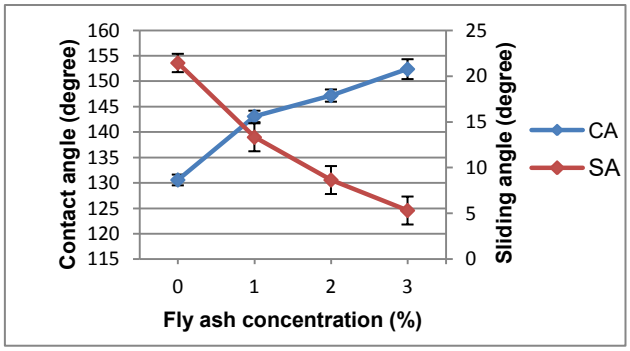

Figure 4. Effect of fly ash concentration on contact angle and sliding angle

3.2. UV protection performance of fly ash coated cotton fabrics

From Table 1, the UV transmittance was found to reduce with increase in concentration of fly ash particles on fabric surface. The maximum UV blocking was observed in case of cotton fabric coated with 3 wt% fly ash. The untreated cotton fabric showed a low UPF of 9.49, however all the cotton fabrics decorated with fly ash particles exhibited large increase in UPF values. The maximum increase in UPF was observed for 3 wt% fly ash concentration, where the UPF value was increased to 1777.43.

Table 1. UV transmission of fly ash coated cotton fabrics

Samples	UVA Blocking %	UVB Blocking %	Mean UPF
Control	84.30	90.72	9.49
1% FA	99.46	99.7	299.4
2% FA	99.82	99.89	801.44
3% FA	99.92	99.95	1777.43

3.3. Oil/water separation performance of superhydrophobic cotton fabrics

Toluene was used to observe the oil removal from the surface of water, whereas chloroform was used to observe the underwater oil removal from water. The toluene and chloroform oil was dyed by red orange before adding into the water. Due to low density of toluene, it was floated on water surface as shown in Figure. 5(a) . Whereas, due to high density of chloroform, it reached to the bottom of water surface as can be seen in Figure. 5(b). A piece of superhydrophobic cotton fabric was immersed into the water, both the oils were completely absorbed into the coated fabric structure within few seconds leaving any color in water. Moreover, the oil separation efficiency of superhydrophobic cotton fabrics was tested in separate experiments. The separation efficiency of 98%, 96%, 97% and 95% was obtained for toluene/water, n-hexane/water, chloroform/water and petro ether/water, respectively.

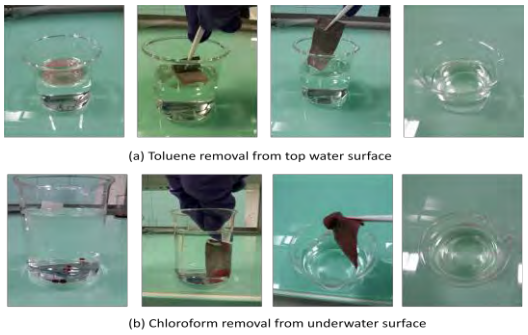

Figure 5. Oil in water removal performance of fly ash-OTMS coated cotton fabrics

3.4. Durability of superhydrophobic cotton fabrics

Figure 6. shows the results of contact angle measurements for characterization of durability of fly ash-OTMS coated cotton fabrics against laundering, Similarly, the contact angle was reduced for all the concentration of fly ash after five laundering cycles. However, it was still higher than 150° for 3 wt% fly ash sample. This demonstrated that fly ash particles were robust and stable on cotton surfaces, and only few fly ash particles were removed due to shearing and friction forces of laundering process.

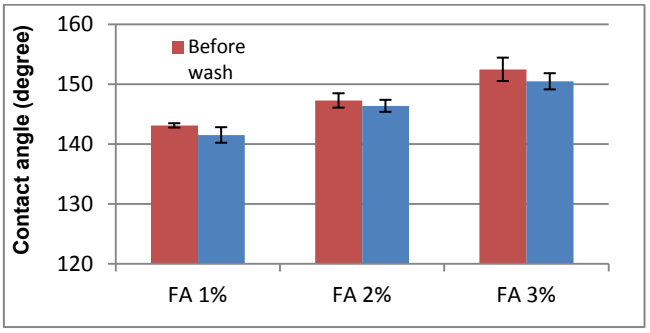

Figure 6. Durability of fly ash-OTMS coated cotton fabrics after washing.

4. CONCLUSIONS

In this study, fly ash particles were used to create superhydrphobic and UV protective cotton fabrics. Superhydrophobic properties were achieved by coating non-fluorinated silane on previously fly ash coated fabrics. The water contact angle was measured around 130° for coated fabrics of OTMS alone. However, when fly ash concentration of 1, 2 and 3 wt % was applied; the contact angle was improved to 143°, 147° and 153°, respectively. The coated fabrics exhibited large increase in UPF values due to their high refractive index and presence of metal oxide constituents. The fly ash-OTMS coated fabrics showed good oil in water separation performance for toluene/water, n-hexane/water, chloroform/water and petroether/water, respectively.

ACKNOWLEDGEMENTS

This work was supported by the student grant competition 21247 at Technical University of Liberec.

References

[1] *Yan Y.Y., Gao N, Barthlott W. (2011). Mimicking natural superhydrophobic surfaces and grasping the wetting process: A review on recent progress in preparing superhydrophobic surfaces. Adv Colloid Interface Sci; 169: 80–105.*

[2] *Feng L, Li S, Li Y, et al. (2002). Super-hydrophobic surfaces: From natural to artificial. Adv Mater; 14: 1857–1860.*

[3] *Gustafsson E, Larsson P.A, Wågberg L. Treatment of cellulose fibres with polyelectrolytes and wax colloids to create tailored highly hydrophobic fibrous networks. Colloids Surfaces A Physicochem Eng Asp 2012; 414: 415–421.*

[4] *Shirgholami MA, Shateri Khalil-Abad M, Khajavi R, et al. (2011).Fabrication of superhydrophobic polymethylsilsesquioxane nanostructures on cotton textiles by a solution-immersion process. J Colloid Interface Sci; 359: 530–535.*

[5] *Bae GY, Min BG, Jeong YG, et al. Superhydrophobicity of cotton fabrics treated with silica nanoparticles and water-repellent agent. J Colloid Interface Sci 2009; 337: 170–175.*

[6] *Ashraf M, Champagne P, Campagne C, et al. (2014). Study the multi self-cleaning characteristics of ZnO nanorods functionalized polyester fabric. J Ind Text; 1–17.*

[7] *Huang J.Y, Li S.H, Ge M.Z, et al. (2015). Robust superhydrophobic TiO_2 @fabrics for UV shielding, self-cleaning and oil–water separation. J Mater Chem A; 3: 2825–2832.*

[8] *Roach P, Shirtcliffe N.J, Newton M.I. (2008).Progess in superhydrophobic surface development. Soft Matter; 4: 224.*

[9] *Nosonovsky M, Bhushan B. (2007). Hierarchical roughness optimization for biomimetic superhydrophobic surfaces. Ultramicroscopy; 107: 969–979.*

CONDUCTIVE TRACKS USED IN SMART CLOTHING

Ing. Michal Martinka, Ing. Eva Hercíková, doc. Ing. Antonin Havelka CSc.

Technical University of Liberec, Faculty of Textile Engineering, Department of Clothing technology, Studentská 2, 461 17 Liberec, Czech Republic , michal.martinka@tul.cz

Abstract

One of the most important components for wearable electronics there are fabric interconnectors. The human body is not straight, hard and firm, but consists of many curves, it is soft and flexible. Even in seeming idle mode it is still moving and it is necessary for the clothing to respect these changes on the market we can find money of variants and types of interconnectors. Their choice is very important for the optimal operation of all electronic components in the system. Their suitability or inappropriateness must be judged on the basis of many factors they have to carry out.

Key words

Smart textiles, electric resistance, interconnectors, conductive tracks

1. INTRODUCTION

In the 21st century, the user no longer wants to wear plain clothes, but requires certain features, whether it be monitoring the health of the wearer or his surroundings, or facilitating communication with other mobile devices (watches, smartphones ...). Such clothes are called SMART fabrics, or smart clothes. The aim of this experiment was to analyse available types of conductive pathways for future use [6][7].Main text / Arial, 10 point, 2Justified

2. SMART TEXTILES

Smart or intelligent fabrics add some added value. They either react actively or passively to objects from their surroundings, using MEMS (microelectromechanical systems) implemented into the structure of the garment itself. The basis is that MEMS systems do not aggravate the physiological properties of the garment and prevent the wearer from moving and, on the contrary, with their functions, increase the useful properties of smart garments. After removing the power supply, MEMS-fitted clothing can be maintained in a standard way, such as washing and ironing, but with respect to the electronics used. In the future, SMART fibers and sensors are directly incorporated into the fabric. Thanks to this, we can neglect any maintenance restrictions created by using MEMS [1]

Smart clothing is the kind of apparel that has implemented electronic parts, in particular, microcomputers and sensors. It’s worn as ordinary clothing, providing additional value to the user by virtue of innovative technologies. [6][7].

2.1. Classification of smart textiles

Main text Arial bold italic, 10 point, Justified

Smart fabrics are divided into three groups depending on their "intelligence"[8][9][10]:

- Passive smart fabrics - belongs to the first generation of intelligent textiles. These fabrics include a detection unit (s) that is connected to an external control system that evaluates the data and sends it to the monitoring unit. An example of a passive wearable electronics can be a cycling jacket with a light signaling to change the direction of travel. [3] [8][9][10]

- Active Smart Fabric - belongs to the second generation of intelligent textiles. The fabric is equipped with sensors, but also a control unit and a battery. They react directly to the impulse. They are able to change color, retain heat or regulate breathability. If we place the garment on the UV radiation sensors, clothing can alert us if the radiation intensity is too high either by changing the color of the garment or by lighting or acoustic signaling. The same principle can be applied to measuring radiation. [2] [8][9][10]

- Super Smart Textiles - Developed Third Generation. These textiles are capable of learning, responding to stimuli from the environment and adapting to their function. Textiles are gradually learning to respond to new subjects, memorizing reactions to these stimuli, which will allow for a quicker response when repeating them. [3][8][9][10]

3. CONNECTION

The application of electronics to SMART clothing is governed by a simple scheme which regardless to

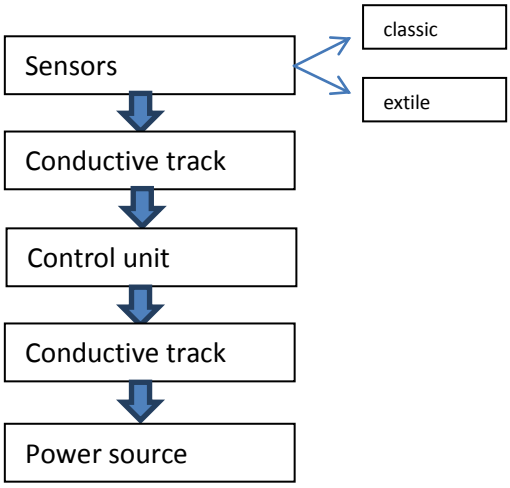

the use has to include:

Sensors transforms a signal into another signal that can be read and understood by a predefined reader, which can be a real device (electric signals) or a person [11].

4. CONDUCTIVE PATH

4.1. Types of conductive tracks

Conducting tracks exist in many forms [4][2][3]:

- Conductive sewing threads – ultra fine metal or chemical fiber in combination with synthetic filament, for example polyester or polyamide. The advantage of conductive sewing threads is to be used in a standard sewing machine. Their use does not affect the physical properties of SMART clothing itself. [4][2][3]
- Electrically conductive wires (copper wires) - Standard copper wires of different diameters depending on the required resistance or use. For transmission of energy to the system, a different diameter is used than the heating system.
- Conductive ribbons - Insulated or non-insulated conductive wires embedded in a textile ribbon. They may be two, three, four or even six veins depending on the use.
- printed conductive tracks (silver, graphite)
- 3D printing - special conductive strings to a 3D printer based on PES or ABS, depending on the type of use. Scattered carbon particles perfectly transfer the electrical energy into the printed structure.

4.2. Types of conductive tracks

Although a number of conductive tracks are on the market, not all of them is possible to use for textile industry and to SMART apparel. The most important parameter in conducting paths is the electrical resistance R [Ω]. Electrical resistance is the ability of the material to conduct electrical current. Mathematically, it can be expressed using Ohm's law

$$R = \frac{U}{I} [\Omega]$$

Where U is the voltage at the ends of the conductor and I is the current passing through the conductor [5]

5. TESTING CONDUCTIVE TRACKS

To test was chosen twenty types of conductive tracks ranging from standard sewing thread to the conductive ABS created using 3D printing.[3][4]

Tested conductive path:

- 4-conductor ribbon fiber spun into a textile ribbon (sample b))
- The conductive sewing thread consists of 31% PESh and 68% (8x) brass wire (sample a1-a8)
- Painted conductive strip on the underlying material (silver conductive strip) (sample e1-e6)
- Conductive rubber (sample c)
- Conductive Velcro (arrested metallic flute) (sample d)

The samples were sutured onto the 15 cm non-conductive substrate shown in **Chyba! Nenalezen zdroj odkazů.**.

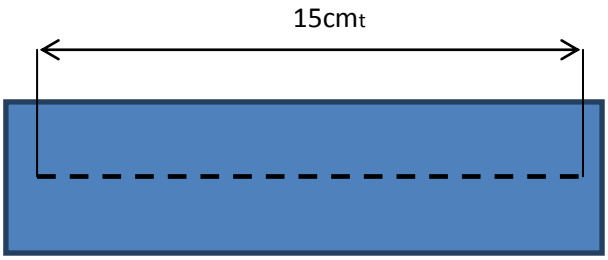

Figure 1 Design of the test sample

The electrical resistance R was measured on the UT71B multimeter.

Measured values are displayed in Table 1.

Table 1. Measured values

Electric resistivity [Ω]		
Sample	**Average**	**Standard deviation**
a1	57,2	5,134199061
a2	50,6	1,113552873
a3	52,4	1,907878403
a4	2746,0	73,78346698
a5	3,9	0,110566722
a6	3,2	0,579461819
a7	29,2	2,821347196
a8	17,7	2,002498439
b	15,5	2,197529477
c	4,7	0,920649261
d	0,2	0,040399242
e1	154,4	16,94130644
e2	411,0	48,67237409
e3	415,0	18,57417562
e4	470,0	135,4990775
e5	690,5	209,8147993
e6	837,0	26,0959767

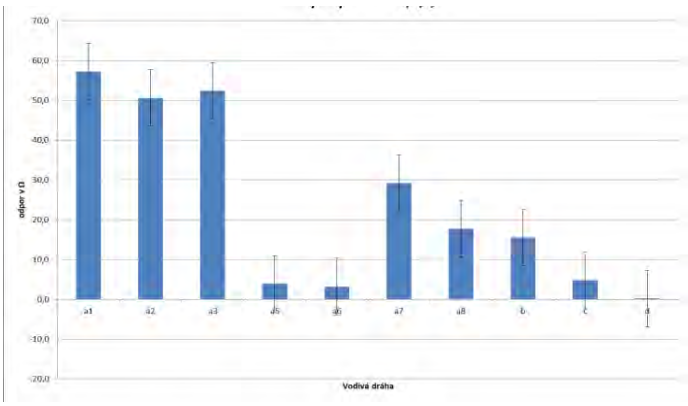

Figure 2 Average resistance a1-a8,b,c,d

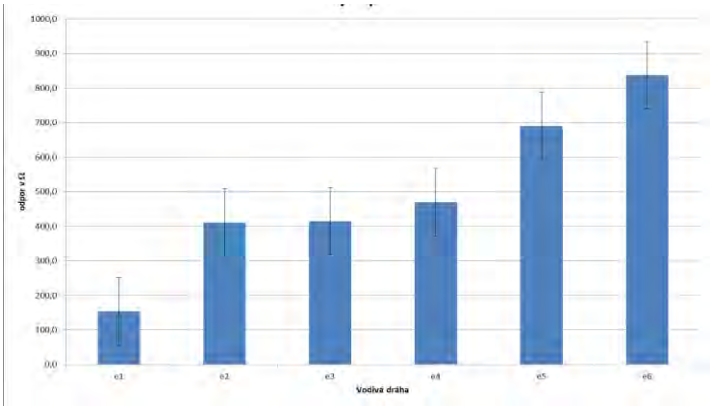

Figure 3 Average resistance e1-e8

5.1. Selected type of conductor

For further use, the most suitable sample b was chosen which had the best results in terms of measured values. These ribbons achieved the best conductive properties. Their other great advantage as opposed to printed paths (samples e1-e6) there is ease of application. Printed conductive tracks there are preparation-intensive, their application is limited as well as requires special maintenance.

6. CONCLUSION

Proper choice of conductive path affects the overall functionality of SMART garment. If we choose the conductive path incorrectly, the electronics contained in SMART clothing may not work properly. Poorly chosen diameter and electrical resistance can cause heating and mechanical damage as well as injury to the wearer. It is important to know what the electronics in the garment should serve, to use heating conductors with parameters other than pure sensor-battery connections.

References

[1] Hubálek J., Mikrosenzory a mikroelektromechanické systémy, nakladatelství VUT, Brno, 2009, 80-7284-305-X

[2] Tao, Xiaoming. Smart fibres, fabrics and clothing. Boca Raton: CRC Press, 2001. ISBN 978-1-85573-546-0.

[3] Tao, Xiaoming, ed. Handbook of smart textiles: with 565 figures and 66 tables. Singapore: SpringerReference, [2015]. ISBN 978-981-4451-44-4.

[4] Elektrotechnická měření. Praha: BEN - technická literatura, 2002. ISBN 80-7300-022-9.

[5] Clevertex: Special, protective and functional textiles [online] © 2018 – CS Technologies s.r.o. (cit. 20.7.2018) dostupné z: http://www.clevertex.cz/en/threads/electrically-conductive-hybrid-threads-detail-761

[6] Kumar, L. Ashok a C. VIGNESWARAN. Electronics in textiles and clothing: design, products and applications. Boca Raton: CRC Press, [2016]. ISBN 9781498715515.

[7] Van Langenhove, Lieva, and Carla Hertleer. 2004. "Smart Clothing: a New Life." International Journal of Clothing Science and Technology 16 (1/2): 63–72.

[8] Zhang, X., Tao, X., 2001a, Smart Textiles: Passive Smart. Textiles Asia, June 2001, pp. 45-49

[9] Zhang, X., Tao, X., 2001b, Smart Textiles: Active Smart. Textiles Asia, June 2001, pp. 49-52

[10] Zhang, X., Tao, X., 2001c, Smart Textiles: Very Smart. Textiles Asia, June 2001, pp. 35-37

[11] Tao, Xiaoming. Wearable electronics and photonics. Boca Raton: CRC Press, 2005. ISBN 978-1-85573-605-4.

DIELECTRIC PROPERTIES OF EPOXY COMPOSITES FILLED WITH RECYCLED CARBON FIBERS

Jana Novotná

Technical University of Liberec, Dep. of Material Engineering, Liberec, Czech. Rep.,

e-mail: jana.novotna3@tul.cz

Abstract

It was prepared a thin samples of epoxy composites filled with 0-14% concentrations of recycled carbon fibers. Then was measurement capacitance and dielectric loss and calculated permittivity of this two phases composites with conductive and not conductive part. Furthermore is discusses the issues to the practical application of Maxwell Garnett approach to the modeling of the electric permittivity.

Key words

Recycled carbon fibers, permittivity, Maxwell Garnett theory.

1. INTRODUCTION

Polymers belong to dielectrics. The dielectric properties of fiber-filled composites are a suitable tool for their characterization [1]. The polarizability of the polymer expresses the dielectric properties of the relative permittivity *ε* and the loss factor (or dielectric loss) *tan δ*. Dielectrics are non-conducting, electrons and protons do not move freely there, only a small shift occurs. By the action of an external electric field, electrical charges are formed in the dielectric. Positive and negative charges move in the opposite direction, the dielectric obtains dipole moment which is macroscopically expressed by the polarization vector.

Table 1. Relative Permittivity of materials at 20ºC by the frequency 100Hz [2]

	ε[-]
vakuum	1,0
PAD	2,6
epoxy	5,0
bakelit	5,1
diamant	10,5
grafit	13,5

The real part of permitivity was calculated using a relationship [3]:

$$\varepsilon' = \frac{Cd}{\varepsilon_0 S} \quad (1)$$

where *C* is capacitance, $\varepsilon_o = 8.85 \times 10^{-12}$ *F/m* is called *permittivity of free space*. It is universal constant. Further *d* is the sample thickness and *S* is the area of the sample.

The imaginary part of permitivity *ε″* was given by the relationship:

$$\varepsilon'' = \varepsilon' tg\delta \quad (2)$$

Then complex permittivity was expressed as:

$$\varepsilon = \varepsilon' - i\varepsilon'' \quad (3)$$

2. EXPERIMENTAL

2.1. Fillers = Fibers

The initial short cut recycled carbon fiber was Carbiso Milled Carbon Fiber with a diameter of 7 μm and an average length of 100 μm. The precursor of these fibers is PAN. Fiber density is 1800 kg/m^3 [4].

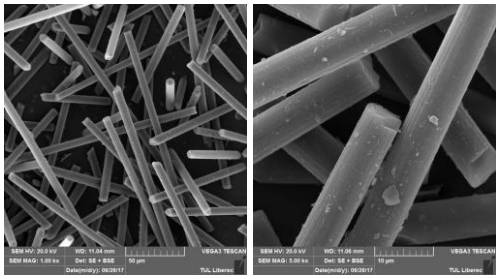

Figure 1. SEM image fibers from VEGA TS 5130

2.2. Materials = matrix

A series of samples of epoxy resin MGS L 285 / H 508 was produced, a mixing ratio of 100: 40 by weight. Laminating system L 285 was an epoxy resin from Bisphenol A and Epichlorohydrin, commonly used by most aircraft and glider manufacturers. The density of the resin was 1200 kg/m^3 and the density of hardner was 1030 kg/m^3[5].

The mixture epoxy, hardner and fibers was stirred at room temperature for 5 min. using a Hanna HI190 magnetic stirrer, then poured into pre-separated circular glass molds and then left to stand for 24 hours at room temperature. Followed curring was in an oven for 15 hours at 60 °C. The circular samples have a thickness about 0,002-0,003 m (depending on each sample) and a diameter of 0,035 m. The area of the applied electrode was 0,00067±0,00002m^2. Further details of sample preparation are specified in the work[6].

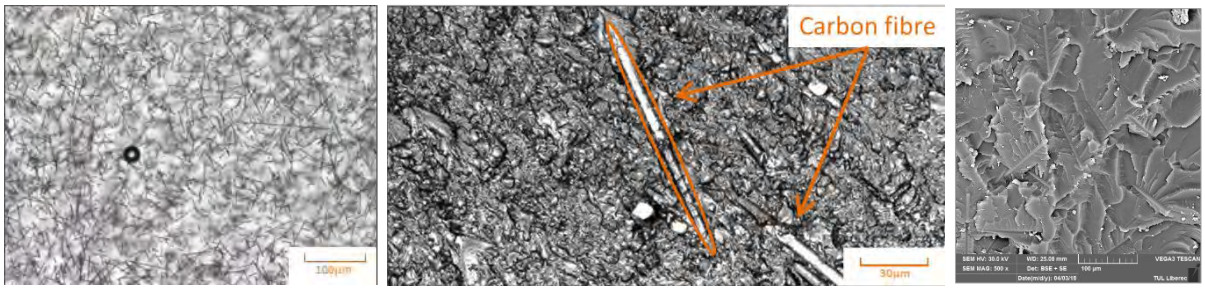

(A) (B) (C)

Figure 2. (A) Image analysis composites of the concentration of 0.1% of filler, (B) cut off sections of composites of the concentration of 2.5% of filler confocal laser scanning microscope OLYMPUS LEXT OLS 3000, (C) SEM image composites of the concentration of 1% of filler from VEGA TS 5130

2.3. Measurement

All measurements were made under climatic conditions (20 ± 2) °C of relative humidity (40 ± 2)%. It was 100 pieces of samples produced and measured. The samples for better surface adhesion were coated with the silver conductive paste ELEKTRODAG 1415 (Agar scientific) on both sides. Each sample was measured three times.

At first the permittivity *ε* was calculated using the relationship (1) and (2) where capacitance *C* and loss factor *tan δ* were measured with the RCL meter INSTEK LCR821 [7]. At second the capacitance and the tan δ were measured using an AGILENT 4294 analyzer [8].
The measured frequency was 1 kHz, measurement uses 4-wire sample holder in a shielded metal box, see Fig. 3.

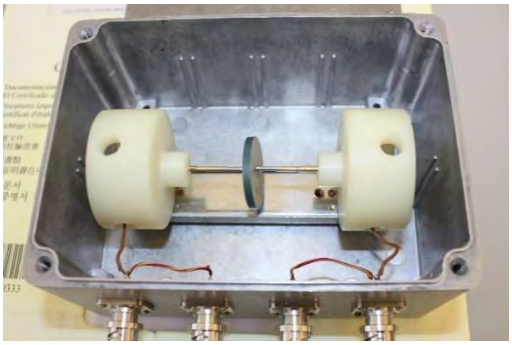

Figure 3. A 4-wire sample holder in a shielded metal box

3. RESULTS

Based on extensive experiments, it has been found that permitivity measurements are comparable and reliable,see Tab. 2 and 3. The neat resin permittivity measured values are comparable to the value 5 shown in Tab. 1.

Table 2. Permittivity results using RCL meter INSTEK

Volume fraction [%]	Permittivity ε [-]	Variation coefficient [%]	Confidence interval lower	Confidence interval upper
0,0	4,68	2,57	4,49	4,88
0,5	5,62	4,39	5,22	6,01
1,0	6,56	10,18	5,50	7,63
2,0	8,81	3,33	8,35	9,28
3,0	9,90	2,79	9,46	10,34
5,0	13,32	4,35	12,40	14,24
7,0	10,10	5,49	9,22	10,99
9,0	15,49	2,32	14,92	16,06
10,0	16,92	8,99	14,50	19,34
12,0	17,96	1,60	17,50	18,42
14,0	24,11	1,35	23,59	24,63

Table 3. Permittivity results using AGILENT 4294

Volume fraction [%]	Permittivity ε [-]	Variation coefficient [%]	Confidence interval lower	Confidence interval upper
0,0	4,32	3,08	3,99	4,65
0,5	5,23	1,21	5,07	5,38
1,0	6,04	1,02	5,89	6,19
2,0	8,21	2,16	7,77	8,65
3,0	9,18	2,63	8,58	9,78
5,0	11,95	4,25	10,69	13,21
7,0	9,19	6,57	7,69	10,69
9,0	14,45	2,75	13,47	15,44
10,0	14,90	4,03	13,40	16,39
12,0	17,21	4,81	15,15	19,26
14,0	22,09	0,70	21,71	22,48

4. MODELING AND PREDICTION OF ELECTRICAL PROPERTIES

Numerous studies have demonstrated that the MG (Maxwell Garnett) formula is particularly suitable to predict the complex permittivity of multiphase mixtures with *n* sorts of inclusions, conductive and not conductive [9]. In this work was used *n=2* (epoxy and fibers). If we have a composite formed of epoxy resin reinforced by randomly distributed carbon fibers. Fiber length *l = 0.1mm* and fiber diameter *d = 7 μm*, so *l> d*. We assume the distribution of fibers in three spatial dimensions with the same degree of randomness. The filaments are embedded in the dielectric permeability matrix ε_m, the following relation applies MG model[10].

$$\varepsilon = \varepsilon_m + \frac{\frac{P}{3}(\varepsilon_f - \varepsilon_m)\left[\frac{\varepsilon_m}{\varepsilon_m + \varepsilon_f} + \frac{\varepsilon_b}{\varepsilon_m + N(\varepsilon_f - \varepsilon_m)}\right]}{1 - \frac{P}{3}(\varepsilon_f - \varepsilon_m)\left[\frac{1}{\varepsilon_m + \varepsilon_f} + \frac{N}{\varepsilon_m + N(\varepsilon_f - \varepsilon_m)}\right]} \quad (4)$$

Where ε_f is fiber permittivity and *P* is volume fraction of fibers. This model is valid only for fiber concentrations below the percolation threshold. If the composite is composed of carbon fibers whose shape can be approximated by thin cylinders, we assume two depolarization factors associated with a diameter passing through the fiber axis equal to *1/2*, while a third that is connected in a direction parallel to the fiber axis can be expressed as *N*. In the case of this simplification, the expression can be expressed as:

$$N \approx \left(\frac{d}{l}\right)^2 \ln\left(\frac{l}{d}\right) \quad (5)$$

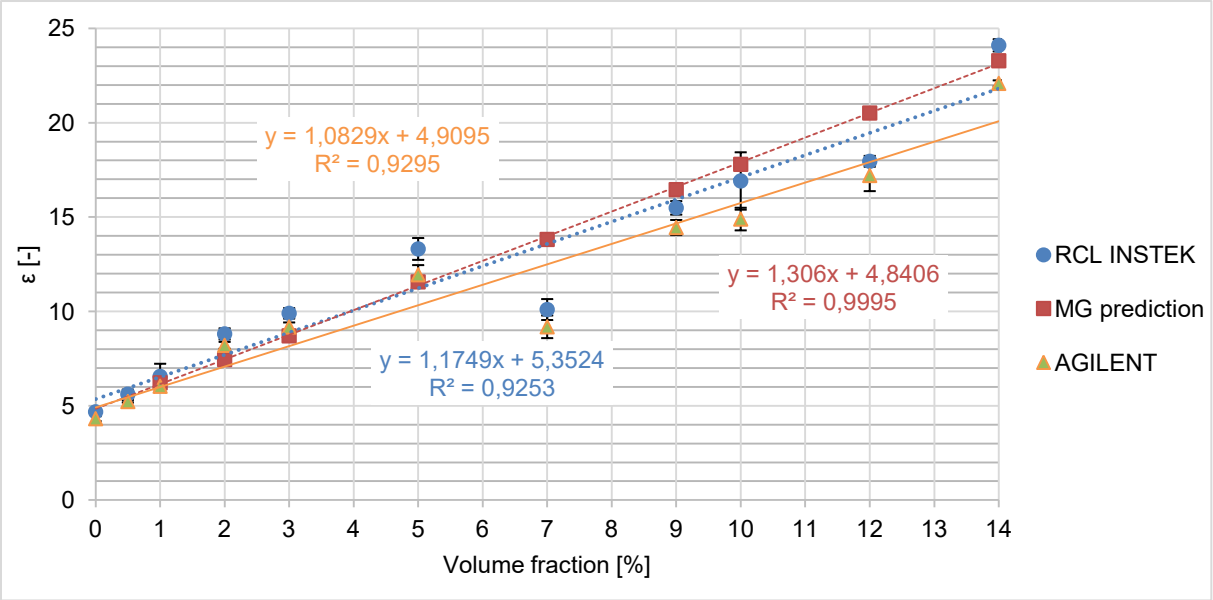

Figure 4. Comparsion experimentally obtained and MG formula predicted permittivity

In all cases, the independent variable is linearly dependent, as proved it by high correlation coefficient values, so the used MG prediction model can be recommended for predicting the permittivity epoxy composites filled with short carbon fibers, see Fig.4..

5. CONCLUSIONS

With the technology pouring recommended in [9], a wide range of thin epoxy composites filled with recycled carbon fiber Carbiso was prepared. For these samples, the dielectric properties represented the capacitance and dielectric loss was measurement and permittivity calculated.

In a static environment, many studies have demonstrated the suitability of the MG model for predicting the permittivity of composites containing conductive and non-conductive components [1], [10].This approximated model has been verified by the experimental data and can be successfully used for prediction of static permittivity, as confirmed by this work for all samples.

ACKNOWLEDGEMENTS

Author is grateful for the financial support from the Student research project 2018 No.21248 supported by Czech Ministry of Education, and by Faculty of Textile, Technical University of Liberec. Author is grateful for the useful help to prof. Mgr. J.Erhart PhD.

References

[1] A. N. Lagarkov, S. M. Matytsin, K. N. Rozanov, and A. K. Sarychev, "Dielectric properties of fiber-filled composites," J. Appl. Phys., 1998.

[2] T. Martin, "Dielektrika," 2009. [Online]. Available: http://dielektrika.kvalitne.cz/tabulky.html.

[3] D. D. L. Chung, "Composite Materials: Science and Applications," Compos. Mater. Struct. Process., pp. 1–34, 2010.

[4] "Technical Information for Carbiso Mil 10 µ Milled Carbon Fibre," 2018. [Online]. Available: http://www.easycomposites.co.uk.

[5] "Technical Information for EPIKOTE Resin MGS LR285." [Online]. Available: 2010 www.swiss-composite.ch/pdf/t-Epoxyd-Harz-L-285-LF-e.pdf.

[6] J. Novotná, J. Salačová, and M. Pechočiaková, "C/P carbon composites - Reinforcement volume effect on the electrical properties," in IOP Conference Series: Materials Science and Engineering, 2017, vol. 254, no. 4.

[7] "INSTEK LCR 821," Technical Informacion, 2018. [Online]. Available: http://www.testequipmentdepot.com/instek/meters/lcr821.htm.

[8] "Technical Information Agilent 4294A," 2013. [Online]. Available: https://www.keysight.com.

[9] A. Balzano, I. M. De Rosa, F. Sarasini, and M. S. Sarto, "Effective properties of carbon fiber composites: EM modeling versus experimental testing," in IEEE International Symposium on Electromagnetic Compatibility, 2007.

[10] V. Markel, "Introduction to the Maxwell Garnett approximation," J. Oprtical Soc. Am., pp. 1244–1256, 2016.

DEVELOPMENT OF THE FORCE SENSITIVE RESISTORS USING POLYPYRROLE COATED COTTON WOVEN FABRIC FOR PRESSURE SENSING APPLICATION

Sundaramoorthy Palanisamy[1*], Veronika Tunakova[2], Benny Malengier[3], Daniel Karthik[4], Lieva Van Langenhova[5], Jiri Militky[6]

[1,2,4&6] Department of Material Engineering, Faculty of Textile Engineering, Studentska 2, 461 17 Liberec, Czechia.

[1,3&5] Department of Materials, Textiles & Chemical Engineering, Centre for Textile Science and Engineering, Technologie Park 907, 9052 Gent, Belgium.

*Email id: sundar2026@gmail.com

Abstract

The cotton twill woven fabric is taken for coating with polypyrrole (PPy) conductive polymer by chemical oxidation method. Monomer, oxidant and dopant used are pyrrole, ferric chloride and Tetra-ethyl ammonium p-toluene-sulfonate at ratio of 4:2:1. Optimized monomer concentration of 0.4M is taken for polymerization process and processing time of 4 hours at 15 ºC. After the polymerization, the samples were washed with 2% ethanol and distilled water simultaneously until excess particle removing. The pressure sensing ability of the PPy cotton fabric is measured with change in resistivity by varying weight. The warp direction of the fabric is showing good sensitivity than weft direction. PPy cotton fabric has better sensing ability of pressure compare with standard nonwoven sample.

Key words

Cotton, Polypyrrole, Chemical oxidation, Resistivity, Woven, Nonwoven.

1. INTRODUCTION

Conductive polymers have attracted the attention of a great number of researchers in the textile field due to their potential applications in composites with natural, artificial or synthetic fibers. The affinity to several kinds of fibers, yarns and fabrics with doped conjugated polymer, permits the production of composite textiles with improved electrical properties. Polypyrrole (PPy) is one of the most suitable conductive polymers for deposition on textile materials due to its excellent conductivity and relevant environmental stability [1]. PPy is commonly produced by electrochemical synthesis or chemical oxidative polymerization in aqueous solution and shows good affinity with natural and artificial fibers. Textile substrates can be easily covered with a PPy layer by immersion of the fabric in the polymerization solution containing pyrrole, an oxidant and a doping agent [2].

The force sensing resistors (FRS) are developed for precise pressure sensor applications. The FSR is working with measuring the change in resistance by increase in force. It detects physical pressure, squeezing and weight by change in resistive value. The applications of FRS are in medical field [3], shoe insoles to detect pressure of our foot [4], video games, electrical automobiles, sporting equipments, etc, [5]. The textile spacer fabrics coated by silver on both side act as a capacitor, whose capacitance helps to measure snowboarding sock pressure during skiing [6]. Highly elastic fabric was coated with polypyrrole (PPy) polymer to measure strain in urinary bladder of urinary dysfunction. The resistance is influenced by stretching the fabric and measure strain variation [7]. Conductive PPy coated electrospun poly (vinylidene fluoride) (PVDF) fiber mat is developed for pressure sensor application; the compression stress is significantly changing the relative conductivity of PVDF/PPy mat [8].

2. EXPERIMENTAL

2.1. Materials

The pyrrole monomer is purchased from Sigma Aldrich. Ferric chloride from Sigma Aldrich is used as an oxidising agent, Tetra-ethyl ammonium p-toluene-sulfonate as a doping agent from sigma Aldrich and distilled water was used through the process as a solvent. The cotton woven twill white fabric with specification of 277 grams per square meter (GSM) and 0.71 mm thickness was taken for the process.

2.2. Methods

The pyrrole monomer was polymerised by chemical oxidation method with ferric chloride as oxidizing agent and tetra-ethyl ammonium p-toluene-sulfonate as doping agent. The optimized molarity of monomer was taken for the experiment is 0.4 M [9]. Temperature maintained through-out the process is 15 ºC and processing time is 4 hours.

In figure 1(a) shows the experimental setup and figure 1(b) shows the image of the cotton sample coated with polypyrrole polymer. Cotton woven fabric was taken and weigh in digital balance was measured to note weight of material. Then 1:40 material to solvent ratio was taken, distilled water is used as a solvent. After that, the monomer, oxidant and dopant were taken in the ratio of 4:2:1 and mixed in solvent under fume hood. Magnetic stirrer was used to dissolve the chemicals at 700 rpm for 10 minutes. Once the chemicals were dissolved then the fabric sample was dipped in the bath and continuously stirrer for 4 hours at 700 rpm in 15 ºC throughout the process. After 4 hours the samples were removed from the bath and washed in 2% ethanol solution for several times and again washed with distilled water until the excess particles were removed from the surface of the sample. Finally, the sample was dried in the hot air oven for 1 hour at 80 ºC temperature. For further analysis, the dried samples were conditioned for 24 hours at laboratory atmosphere.

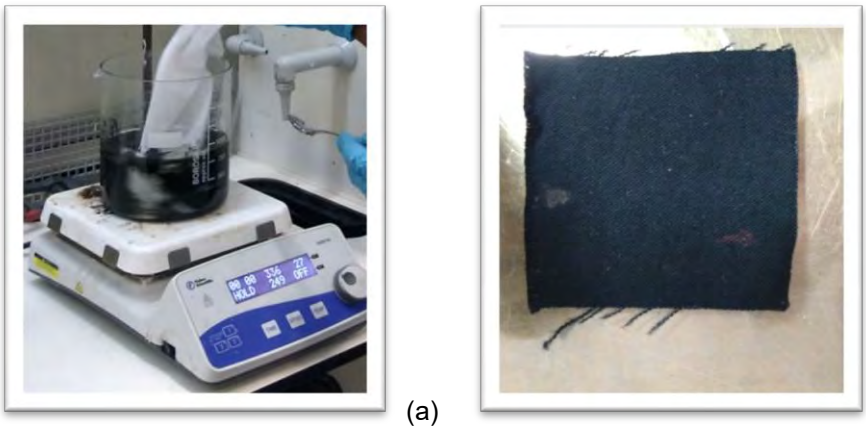

(a) (b)

Figure 1. (a) Experimental setup and (b) image of cotton fabric coated with polypyrrole polymer.

3. RESULTS AND DISCUSSION

Figure 2 shows the photographic image of the force sensitive resistor test setup with sample. In this setup, the sample was holds by connecting rods on both ends at 4 cm distance; insulation material is placed on the sample for separating the weighing material (Coins were used for weight) and multi-meter is connected on the rods to measure the resistance at different pressure.

For comparison of the pressure sensing capability, the developed conductive cotton sample was compared with the market sample. The market sample was brought from Adafruit, it was a nonwoven fabric filled with conductive material and the specifications are 170 GSM, resistivity of 20 Ohm /sq., 0.6 mm thickness and polyester/ nylon 6 filament blend ratio of 70:30 [10].

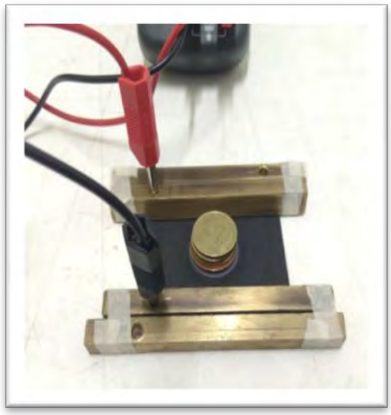

Figure 2. An image of the force sensitive resistor setup.

The force sensitive resistor test results are shown in figure 3 and 4 for standard nonwoven fabric and PPy coated cotton woven fabric respectively. The pressure sensing ability is measured in resistance with respect to varying weights. Linear regression analysis is used to compare the test results by graphically. The machine direction (MD) is showing very good correlation than Cross direction (CD) in nonwoven standard sample. PPy coated cotton fabric shows that warp direction has better sensing ability than weft direction with help of correlation value.

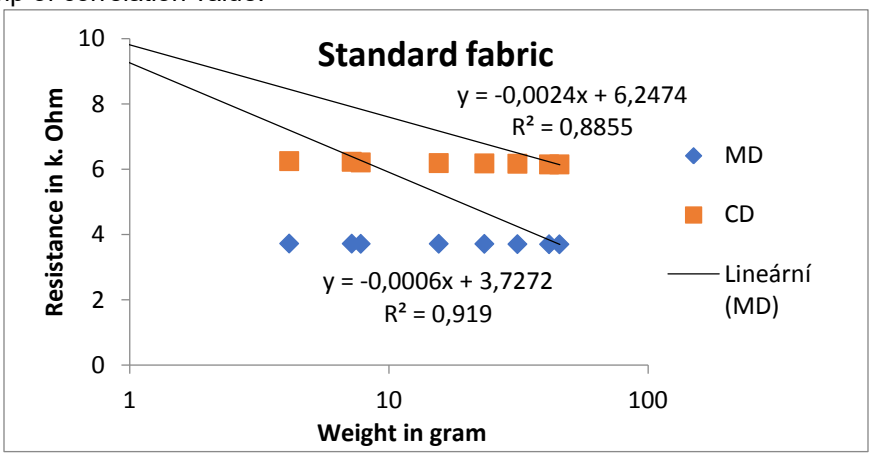

Figure 3. Graph of resistance [Ω] versus weight [gram] of standard nonwoven fabric with linear regression analysis.

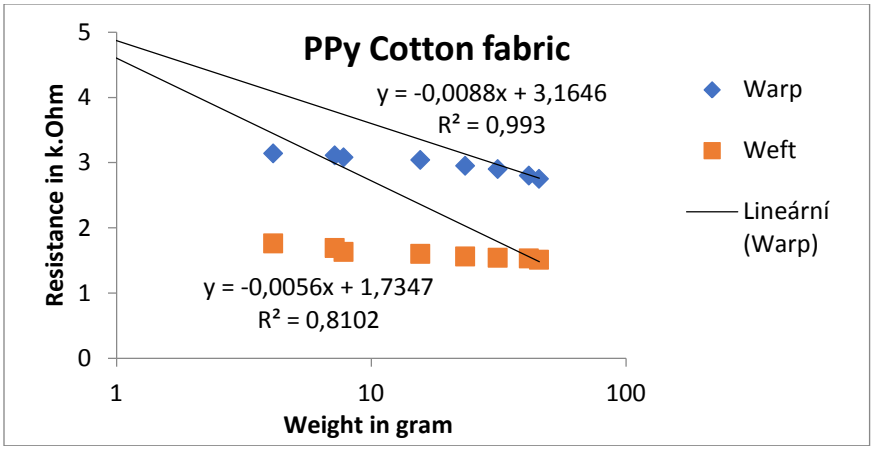

Figure 4. Graph of resistance [Ω] versus weight [gram] of PPy cotton coated fabric with linear regression analysis.

The coefficient of determination R^2=0.99 for PPy coated cotton fabric in warp direction and R^2=0.92 for standard nonwoven fabric in machine direction (MD). The coefficient of determination shows that the PPy coated cotton fabric is more sensitive with respect to force applied on sample.

4. CONCLUSIONS

The optimized pyrrole monomer concentration of 0.4M is used to coat the cotton woven fabric and the coating of polypyrrole looks evenly coated on the surface of the fabric (Figure 1.). The eight different weights were used to measure the resistivity change on the samples. For standard nonwoven fabric, the change in resistance with respect to weight is good in both MD and CD but MD shows the very good sensitivity and the coefficient of determination R^2=0.92 in MD compare with R^2=0.88 in CD shows there is no significance. PPy cotton fabric has coefficient of determination R^2=0.99 in warp direction and R^2=0.81 in weft direction. Hence, the warp direction is having more sensitive to applied pressure than weft. Overall, the PPy cotton fabric is having very good sensitivity to pressure that the standard fabric.

ACKNOWLEDGEMENTS

This project was funded through the 'Student Grant Competition' (SGS 2018) and its internal numbers are 21238 and 21243.

References

[1] M Lu, R Xie, Z Liu, Z Zhao, H Xu and Z Mao, 'Enhancement in electrical conductive property of polypyrrole-coated cotton fabrics using cationic surfactant', Journal of Applied Polymer Science, 2016.

[2] Y Liu, X Zhao and X Tuo, 'Preparation of polypyrrole coated cotton conductive fabrics', The Journal of The Textile Institute, 108, pp 829-834, 2017.

[3] Onno, A., Mitch, S., Theo, K. Fred, O., Ketie, S., Jos, A.,et al. (2016). Application of electrodeposited piezo-sensitivite bruxism sensor. Physica Status Solidi A, 6, 1505-1509.

[4] Rana, N. K., IEEE Computer Society. (2009). Application of force sensing resistor (FRS) in design of pressure scanning system for plantar measurement. IEEE, 678-685.

[5] Butler Technologies. (2018). Force sensing resistors and their applications. November 8, 2018. http://www.butlertechnologies.com/force-sensing-applications.

[6] Thomas, H., Alex, R., Holger, H., Gerhard, T., (2010).Textile pressure sensors for sports applications. IEEE sensors 2010 conference, 73 -737.

[7] Sumitra, R., Mohamad, S., Ebrahim, G. Z.,et al. (2008). A polypyrrole-based strain sensor dedicated to measure bladder volume in patients with urinary dysfunction.Sensors, 8, 5081-5095.

[8] Claudia, M., Rosemeire, D. S. A., Marcos, A. D., et al. (2014). Development of a novel pressure sensing material based on polypyrrole coated electrospun poly(vinylidene fluoride) fibers. Materials Science and Engineering B, 179, 52-59.

[9] Yuanjun, L., Xiaoming, Zhao., Xiao, T. (2017). Preparation of polypyrrole coated cotton conductive fabrics. The Journal of the Textile Institute, 108(5), 829-834.

[10] EeonTex high-conductive heater fabric. Downloaded on https://www.adafruit.com/product/3670. 12th November 2018.

VISIBILITY OF SELECTED SAMPLES AT LOW LUMINANCE

Marcela Pechová[1], Michal Vik, Martina Viková

[1]Technical University of Liberec, Faculty of Textile Engineering, Department of Material Engineering, Laboratory color and appearance measurement, Liberec, Czech Republic
marcela.pechova@tul.cz

Abstract

The visibility at low luminance levels is a very discussed topic which is solved across the whole industry. The warning elements that increase the visibility of people or things are very necessary and desirable at low luminance levels caused by an unexpected situation (for example accidents, power failure, natural disaster). Contrary to these experimental works that are focused on adaptive luminance of color lights, the proposed work is focused on the perception of the color surface contrast on the mesopic and photopic of luminance level, where differences from Purkinje shift and the pseudotritanopic defect have occurred. Selected steel plates were measured with a spectrophotometer to determine their color coordinates in the CIELAB color space. Various luminescence plates were included in the visual assessments. A suitable combination of colors with the high color purity, the black and white contrast strip and the phosphorescent pigments appear as the potentially beneficial solution that will increase visibility.

Key words

colorimetry, mesopic luminance level, visibility, warning elements, gloss, luminescence

1. INTRODUCTION

The visibility of people at low light conditions such as a road traffic, natural disasters, a blackout of electricity, or evacuation are very discussed topics across various disciplines [1]. The discrimination of safety elements for people orientation and the visibility of elements is therefore very important and care must be taken to ensure their easy distinguishable and visible. Visual function decreases at an earlier age and to a greater extent for low contrast targets and mesopic conditions compared to high contrast targets and photopic conditions [2]. It is known that conditions at night are particularly difficult for older adults due to age-related deteriorations in vision, particularly under the mesopic and glare conditions of the nighttime. Additionally, it is necessary to care people with low vision or color deficiency. Subsidiary development of automatic driving system that are actually tested in some cities also need for improvement of navigation ability simple recognizable signs.

The spectral sensitivity of the human eye is different at different luminance levels. While cones are responsible for daytime vision, rods play an important role in nighttime vision. As cones and rods are not equally distributed across the retina, foveal vision and off-axis vision have to be dealt with separately. Considering the spatial distribution of the different receptors in the human retina and their different spectral sensitivity, both the luminance level and the viewing angle will influence the sensitivity of the eye to a given visual target. Between night-time and daytime vision, there is a transition luminance range called mesopic vision, roughly above 10^{-3} cd.m^{-2} and under 3 cd.m^{-2}. It was claimed [3] that several component mechanisms are working in parallel in a complex way and the mechanisms of foveal vision can be classified by sensitivity of L, M and S cones. Based on Purkinje shift phenomenon it is expected that sensitivity of L cones decrease more rapidly than S cones, which caused hypsochromic sensitivity shift. This idea was nevertheless discussed by some of authors [4-6]

as obsolete because it should cause slight pseudoprotanopic effect, which wasn't observed. Because some of researchers found more near to mesopic level slight tritanopic effect [7-9] it's appear as more complex problem. Therefore, the objective of the observer assessments was to find out how the luminance level affects the visibility of the set selected red and white painted samples.

2. EXPERIMENTAL

2.1. Materials

11 steel plates (next samples) produced by SYNPO, a.s. company were used for visual assessments. Various RAL (RAL 3024, RAL 3000 fiery red, RAL 9003 signal white) and newly developed paint shades called as OS (OS3117 red and OS 9118 white) were applied to surface of these plates and luminescence shades (OS9118 with different amount of this phosphorescent pigment) were also included. Visual assessments were carried out in the AT color light box with a daylight fluorescent lamp F7 (6500 K) under 5 different luminance level, 3 photopic (481, 76,5 a 14,5 cd/m^2) and 2 mesopic levels (2,21 and 0,59 cd/m^2). Luminance levels were controlled by neutral grey filters based on polymethylmethacrylate board equipped by with car solar protective foil. Division of luminance levels was chosen to involve both types of photoreceptors into vision. Each observer assessed the samples 5 times under each luminance level. Samples were assessed by pairwise comparison method. Thus, observers compared two samples to evaluate which sample is more visible. Observers did not evaluate the color difference between two samples.

Samples OS9118 that are luminescent (in figure 2 - samples 11, 12 a 13) were UV-illuminated for 10 minutes before each luminance level.

Before a start of visual experiments, each individual observer assessed a Farnsworth Munsell 100 Hue test to determine a color deficiency under 5 different luminance levels. Any observer did not have a color deficiency.

2.2. Methods

To determinate color coordinates of samples, a remission spectrophotometer HunterLab MiniScan XE Plus with measuring geometry 45°a:0° was used [10]. The positions of the samples in the CIELAB color space for geometry 45°a:0° are in figure 1.

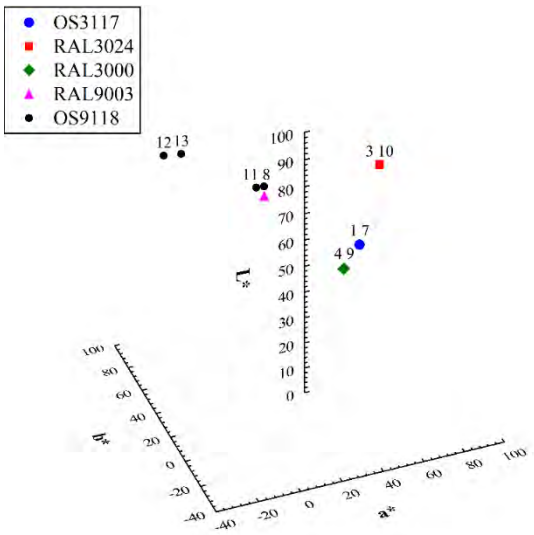

Figure 1. Samples in the color space CIELAB

Among the samples were included the same samples for the false evaluation. These are seen in the figure 2 (samples OS3117 red, RAL3000 red and RAL3024 red with luminescence).

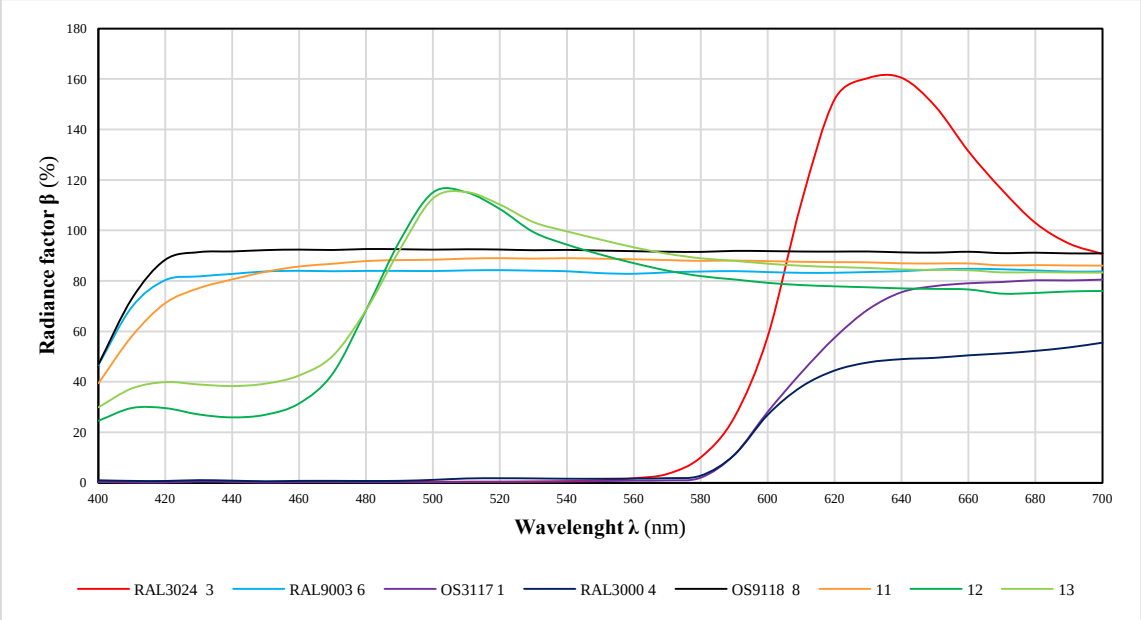

Figure 2. Radiance factor for the selected samples from RAL and OS shades

Figure 3 shows the radiance factor of selected samples from each group of samples. For evaluation of visual assessments were used the z-score and T-score. z-score determines the order of the samples with respect to their visibility at the various luminance level. z-score is normal random variable from the normal distribution. z-score achieves in 95% of cases value from -2 to +2. z-score is calculated using the following formula [11].

$$z = \frac{x - \bar{x}}{s}$$

where x_i is the value of sample, $\bar{x}$ is mean, s is standard deviation.

T-score is then used to compare the assessment of individual samples across various luminance levels. Understands the appearance, the preference one sample before other. T-score achieves only positive values. The values it can be compared to the normal distribution. T-score is calculated using the following formula.

$$T = (z + 10) + 50$$

where z is z-score.

3. RESULTS AND DISCUSSION

All used samples had a high lightness value, except for the samples RAL3000 and OS3117. During the evaluation, the samples with significantly higher lightness were given preference before samples with lower lightness. Samples RAL3000 were assessed from red shade (on the luminance level 481 cd/m^2) to dark brown or black due to decreased luminance level (2,21 or 0,12 cd/m^2). Figure 4 shows average results T-score for the individual group of samples. A great role in the preferences of white shades OS9118 and red shades RAL3024 was the fact that they were luminescence. However, this higher preference (visibility) was valid with higher luminance level. With the decreasing luminance level, their preferences have decreased. For example, samples RAL3024 had the approximately same value of T-score as the sample RAL9003 on the lowest luminance level (0,12 cd/m2). For sample RAL9003 (signal white), the visibility (the preference) increased slightly at low luminance level compared to higher luminance level. Samples RAL3117 (red) were assessed regardless of luminance level. Their order didn't change.

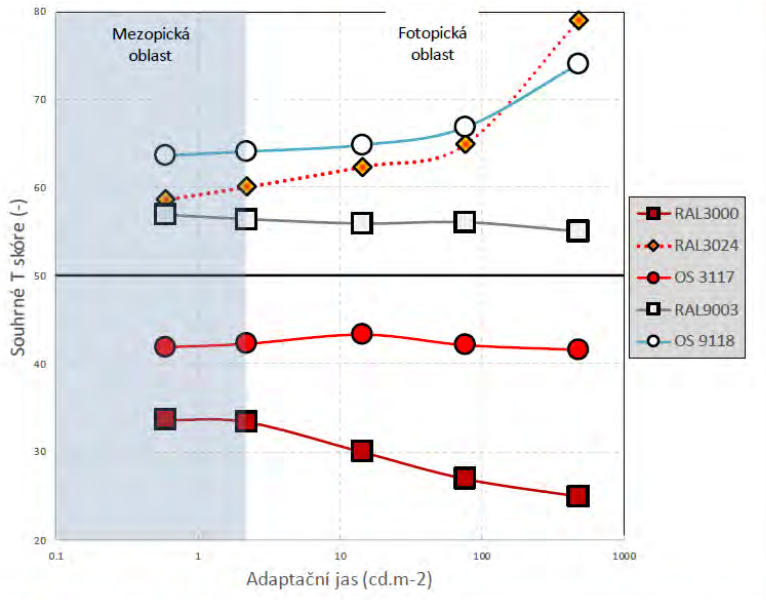

Figure 3. Results for average T-score

If we assessed the samples with high gloss, it is also necessary to keep the viewing angle at which the samples are assessed. It is also important that the unwanted effects must be removed. These effects are thought the reflection of illuminance or fingerprints as a remnant of samples handling [12].

4. CONCLUSIONS

During the assessments of these samples must take into account not only their shade, luminescence but also the type of illuminance. Under low visibility conditions, the samples with luminescence were not strongly preferred over samples without it (figure 4). This leads to the conclusion that only the presence of luminescence does not lead to increased visibility under low luminance level. It is necessary for an appropriate combination with other elements.

ACKNOWLEDGEMENTS

This work was supported by Students grant competition project number 21242 Visibility at low luminance, Technical University of Liberec and Department of Education of Czech Republic.

References

[1] Vik, M., Zelová, K., Kuzmová, M., Viková, M., Havelka, A. Influence of retroreflective sign on pedestrian visibility (in Czech), Book of proceedings of KOTXXXIV, 8.-10. October 2018, Kouty nad Desnou, CZ, pp. 82-85

[2] Thurman, S. M.; Davey, P. G.; McCray, K. L.; Paronian, V.; Seitz, A. R. Predicting Individual Contrast Sensitivity Functions From Acuity and Letter Contrast Sensitivity Measurements. J Vis 2016, 16 (15), 15–15.

[3] Wyszecki, G. and Stiles, W. S. (1982) Color Science. Wiley & Sons (New York).

[4] Pugh E. N. Jr and Kirk, D. B. (1986) The pi mechanisms of W S Stiles: an historical review. Perception 15, 705–728.

[5] Stockman, A.; Sharpe, L. T.; Fach, C. The Spectral Sensitivity of the Human Short-Wavelength Sensitive Cones Derived From Thresholds and Color Matches. Vision Res. 1999, 39 (17), 2901–2927.

*[6] Várady, G.; Bodrogi, P. Mesopic Spectral Sensitivity Functions Based on Visibility and Recognition Contrast Thresholds. Ophthalmic Physiol Opt **2006**, 26 (3), 246–253.*

[7] Foster, D.H., Amano, K., Nascimento, S.M. Tritanopic colour constancy under daylight changes, In Normal & Defective Colour Vision (ed. J.D. Mollon, J. Pokorny & K. Knoblauch), pp 218-224 Oxford University Press 2003

[8] Vik, M., Viková, M. a Pechová, M. Color discrimination on the border of photopic/mesopic vision. In: Proceedings of the 21st International Conference IGH V online . Vy ok u en technick v Brn , akulta elektrotechniky a komunika n ch technologi , 2015, s. 97-100

[9] Pechová, M., Kašparová, M., Vik, M., Viková, M. a Štefl, J. Influence of luminance level of illumination d65 on evaluation of high chromatic colour, PROCEEDINGS of the 4th CIE Expert Symposium on Colour and Visual Appearance, 6–7 September 2016, Prague, Czech Republic, pp. 269-277

[10] Vik, M. (2017). Colorimetry in Textile Industry (1. ed.). VÚ , a. . (Liberec)

[11] Meloun, M., Militký, J. ( ). Kompendium tati tick h o zpracován dat. Metody a řešen úlohy v etn CD. Academia (Prague).

[12] Fairchild, M. (2005). Color appearance models (2. ed.). John Wiley (Barcelona)

PHOTOCHROMIC POLYPROPYLENE FILAMENTS: INFLUENCE OF DRAW RATIO ON THERMAL PROPERTIES

Periyasamy. A.P, Vikova. M, Vik, M
LCAM, DMI, Faculty of Textile Engineering, Technical University of Liberec, Czech Republic.
aravinprince@gmail.com

Abstract
The metallocene isotactic polypropylene (miPP) filaments was produced with different concentration of spiro [2H-indole-2,3'-[3H] naphtho[2,1-b] [1,4]oxazine],1,3-dihydro-1,3,3-trimethyl-6'-(1-piperidinyl) via mass coloration. After production, miPP filaments was applied different drawing ratios (DR) and then analyzed optical, structural and mechanical properties. In overall the results are significantly depending on the DR. The photochromic color build was found maximum with the highest concentration of pigment as well as the lowest DR. Thermal properties were improved with increasing the draw ratio, which directly influenced on the crystallinity of produced filaments. In this experimental work, the impact of draw ratio on optical, structural, thermal and mechanical properties of photochromic miPP filaments was investigated.

Keywords
Crystallinity, Drawing process, Photochromism, Polypropylene.

1. INTRODUCTION
One flourishing field in photochemistry is photochromism and the photochromic behavior of both organic and inorganic materials [1]. Innovation in the textile industry has been increased day by day and there is no limit in the field of functional textiles, photochromism in textiles are one among them. Recent research manuscripts were rapidly increased with the interest on the application of photochromic compounds in textile materials, though comparatively few reports are there in this specified area. Polypropylene (PP) was chosen since it is most versatile polymer available currently with huge potential applications, such as plastics, filaments, textile fabrics, medical devices and etc. For mass coloration, commercial photochromic pigment is used for this study, the pigment is formulated with many additives which include, hindered amine light stabilizer (HALS). However, these additives are not only impaired the tensile strength but also show some significant changes in optical and physical properties of final product. Our research studies are focusing on the application of photochromic materials on the textile materials to develop functional textile such as flexible UV sensors, camouflage and other smart applications with enhanced properties. In these regards, we conduct many research studies and wrote several scientific papers [1–4]. The main aim of this paper is to investigate the effect of drawing process on the optical, structural, thermal and mechanical properties of photochromic miPP filaments.

2. EXPERIMENTAL PROCEDURE

2.1 Materials
Metallocene catalyst isotactic polypropylene: Metocene HM 562R (miPP) with melting flow rate (MFR) 26.6 g/10 min was procured from Lyondell Basell, Italy. Photochromic pigment: Spiro [2H-indole-2,3'-[3H]naphtho[2,1-b][1,4]oxazine],1,3-dihydro-1,3,3-trimethyl-6'-(1-piperidinyl); it is available commercially under Matsui Photopia Purple (denoted as MPP). MPP pigment is available in ink form with 50% concentration of pure pigment and rest are formulated by the tetrakis(1,2,2,6,6-pentamethyl-1-4-piperdyl)-1,2,3,4-butanetetra carboxylate and other additives, the formulated pigment was purchased from Matsui Shikiso Chemical Co., Ltd, Japan.

2.2 Incorporation and production of photochromic filaments

Two varieties of miPP filaments were produced (i.e. with and without MPP), during the production, miPP dried chips were used with standard conditions which could be specified by the manufacturer. For the production of colored filaments, first 100% colored miPP was produced like a tape/ ribbon form, therefore, MPP pigments and miPP dried chips (uncolored) were mechanically mixed before it melted, finally, it can dry and converted into chips form. The single-screw tape extruder was used to produce the tape, however, it having the three temperature zones, but in this case, the same temperature was maintained in all the zones (i.e. MPP pigment is sensitivity towards temperature if more than 230 °C), after extruding the colored tapes, passed through water bath immediately and then dried to make chips. Later, these air-dried colored chips were vacuum dried for 2 hours at 105°C, then these chips (colored chips) were mixed to colorless chips with four different concentrations (0.25; 0.50; 1.50 and 2.50 on weight % of the filament (owf)) to produce colored photochromic filament. The filament was produced by laboratory scale single-screw melt extruder (melt spinning) with the diameter of 16mm, L/D ratio of 30. The spinneret has 13 orifices and each having the diameter of 0.5 mm. The temperature of 220°C was maintained in the spinning zone and the rate of dope solution was fed with 1.56 grams per min. In this work, we used six different drawing ratios (DR-1.0; DR-2.0; DR-2.5; DR-3.0; D-3.5 and DR-4.0) was applied under 120°C to analyze the mechanical and kinetic properties.

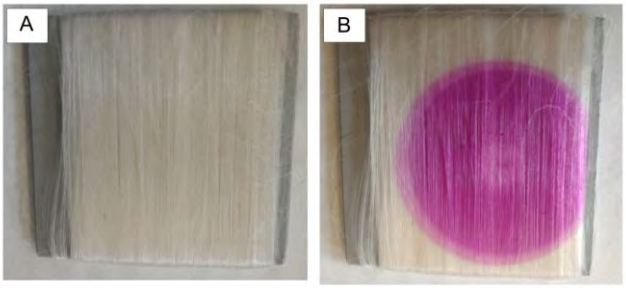

Figure 1. miPP photochromic filaments (A) under the UV irradiance (B).

2.3 Analysis of thermal properties

The thermal behavior of a material which undergoes the physical and chemical changes with absorption or emission of heat as a function of the temperature is studied by differential scanning calorimetry (DSC). In this work, the DSC tests were performed on a Perkin Elmer based on ASTM standard D3418-08. The miPP filaments were heated at a rate of 10 °C min^{-1} from 25 °C to 200 °C (melting) and 200 °C to 25°C (cooling), under the nitrogen atmosphere (20 mL/min). After the DSC measurements, the various properties can be calculated such as melting temperature (T_m) and melting enthalpy (H_m), change in melting enthalpy (ΔH_m) and change in entropy (ΔS_m) can be calculated through Eq. 1;

$$\Delta S_m = \frac{\Delta H_m}{T_m} \quad (1)$$

The crystallinity (Xc%) of the produced filament was computed from the Eq. 2; where $\Delta H_m°$ is 209 J/g [5],

$$Xc(\%) = \frac{\Delta H_m}{\Delta H_m^o} \times 100 \quad (2)$$

3. RESULTS AND DISCUSSION

3.1 Thermal properties of miPP filaments

DSC is one of the most widely accepted techniques to study the thermal properties of polymeric materials. It helps to analyze the crystallization exotherm of photochromic miPP filaments, the results were shown in

Figure 2. However, the miPP belongs to semi-crystalline polymer and it forms the structure during the higher temperature, particularly close to their melting temperature when relaxation of polymer chain in amorphous phase is prevented mechanically, keeping fibers under tension, therefore, it significantly changes the thermal characteristics namely melting temperature, melting enthalpy and entropy, it is sure that these changes further influencing on their mechanical properties. The quantities structural characterization of isotactic polypropylene was studied very first by Samuel [6] and concluded as follows; isotactic polypropylene fibers are providing the higher melting temperature and enthalpy, the orientation of crystalline phase will not affected by the melting temperature of the filaments, whereas the linear dependence of melting temperature on the factor of amorphous phase, which means that melting temperature of the constrained PP fibers drawn for gradually higher draw ratio is fully controlled by orientation of the non-crystalline phase of the filaments. The melting temperature of the polymer is known to the function of crystallization temperature, generally, it is dependence on the crystal lamella thickness of polymeric materials. From the results, melting temperature was increased with the increasing the draw ratio, also the heat of fusion is increased continuously with increasing the draw ratio, this is due to the thickness of lamella can be reduced as well as the increased molecular orientation of the filaments with respect to the draw ratio. The increasing the heat of fusion can be seen in the entropy with respect to the draw ratio, results confirm that change in entropy can lead to increase the melting temperature along with draw ratio was increased. The results reveal the difference in the melting peak temperature dependence on the draw ratio. The melting temperature (T_m) of undrawn filament shows 146.65 °C, whereas the draw ratio 4 shows 150.28 °C.

Table 1. Thermal and crystallinity properties of miPP filaments with respect to various draw ratio (i.e. without the addition of photochromic pigment).

Sample	T_m (°C)	Xc (%)	ΔH_m (J.g^{-1})	ΔS_m (J.g^{-1})
DR1	146.65	27.11	56.16	0.38
DR2	147.20	28.63	59.30	0.40
DR2.5	147.97	29.50	61.10	0.41
DR3	148.60	35.78	74.11	0.49
DR3.5	149.45	37.73	78.15	0.52
DR4	150.28	40.65	84.20	0.56

The changing of melting enthalpy is increased with increasing the draw ratio, from 56.16 to 84.20 for draw ratio 1 and 4 respectively (Table 1), this is due to the thermal demonstration of the components during the crystallization of the polymer which may create the supermolecular structure of the polymer. In general, the liquid phase may reduce the distance between adjacent chains and therefore it increases the fraction of lower energy trans conformation. The melting temperature miPP filaments with MPP pigments remains practically constant with little change, this result confirms that there is no influence of MPP pigment on the thermal properties of miPP filaments. However, it is desired and expected effects on the photochromic filaments. The crystallinity of photochromic miPP filament is increased with increasing the draw ratio, therefore, the higher rate of crystallization makes many modifications in the filament, mainly the α,β modification of morphological structure. From the results (Table 2), pigment concentration on crystallinity can be changed 13% on the draw ratio of 1, however, this effects purely depend on the draw ratio and not on the pigment concentration. The variation in the crystallinity can be found is higher when the draw ratio is less and difference can be reduced in case of higher draw ratio. Similarly, the changing in melting enthalpy and entropy was observed there is a variation with respect to the pigment concentration, however, it is due to the draw process and not influencing of pigment.

Table 2. Thermal and crystallinity properties of miPP filaments with respect to their photochromic pigments (i.e. DR-1)

Pigment Concentration (%)	T_m (°C)	Xc (%)	ΔH_m (J.g^{-1})	ΔS_m (J.g^{-1})
0	146.47	26.24	54.34	0.37
0.25	146.30	27.30	56.54	0.38
0.5	146.31	28.63	59.29	0.40
1.5	146.64	29.02	60.10	0.40
2.5	145.79	30.18	62.51	0.42

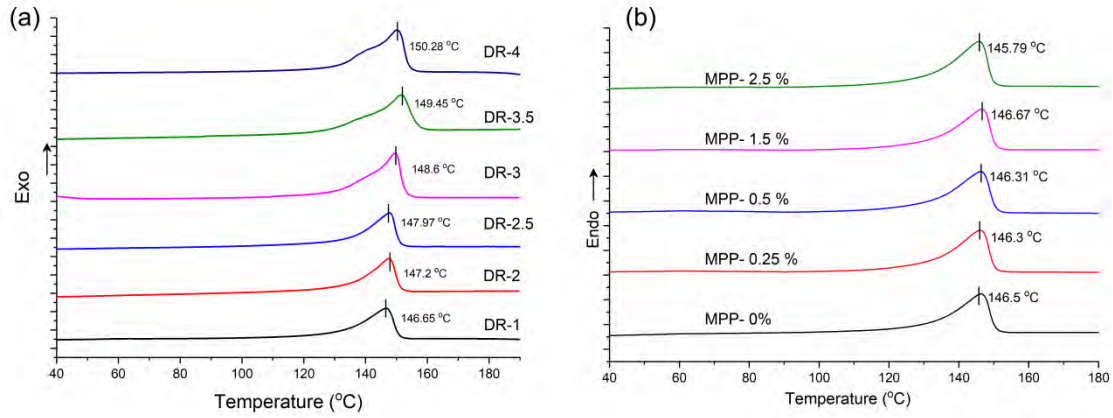

Figure 2. Normalized DSC curves for miPP filaments with different draw ratios (a); as well as different concentration of photochromic pigment (MPP) (b).

4. CONCLUSION

The photochromic colored filaments were produced and analyzed thermal properties via, results indicates that the drawing ratio has a strong influence on the melting enthalpy, melting temperature which was increase with increasing the drawing ratios. The changing of melting enthalpy is increased with increasing the drawing ratio, from 56.16 to 84.20 *J.g*$^{-1}$ for drawing ratio 1 and 4 respectively (i.e. without pigmentation), this is due to the thermal demonstration of the components during the crystallization of the polymer which may create the supermolecular structure of the miPP filament. The crystallinity of photochromic miPP filaments were increased with increasing the drawing ratio, therefore, the higher rate of crystallization makes many modifications in the filament, mainly the *α, β* modification of morphological structure, pigment concentration on crystallinity can be changed 13% on the drawing ratio of one, in case of drawing ratio four does show much influence, however, this effects purely depend on the drawing ratio and not on the pigment concentration. Addition of pigment shows that there no much influence on the melting temperature of the filaments, however, it varies the changing in enthalpy as well as the crystallinity%.

References

[1] Periyasamy AP, Vikova M, Vik M (2017) A review of photochromism in textiles and its measurement. Text Prog 49:53–136 . doi: 10.1080/00405167.2017.1305833

[2] Seipel S, Yu J, Periyasamy AP, et al (2018) Inkjet printing and UV-LED curing of photochromic dyes for functional and smart textile applications. RSC Adv 8:28395–28404 . doi: 10.1039/C8RA05856C

[3] Viková M, Periyasamy AP, Vik M, Ujhelyiová A (2017) Effect of drawing ratio on difference in optical density and mechanical properties of mass colored photochromic polypropylene filaments. J Text Inst 108:1365–1370 . doi: 10.1080/00405000.2016.1251290

[4] Periyasamy AP, Viková M, Vik M (2016) Optical properties of photochromic pigment incorporated into polypropylene filaments. Vlakna a Text 23:171–178

[5] Kong Y, Hay YN (2002) The measurement of cristalinity of polymers by DSC. Polymer (Guildf) 43:3873–3878 . doi: https://doi.org/10.1016/S0032-3861(02)00235-5

[6] Samuels RJ (1975) Quantitative structural characterization of the melting behavior of isotactic polypropylene. J Polym Sci Polym Phys Ed 13:1417–1446 . doi: 10.1002/pol.1975.180130713

IMPACT OF THE PLASTER MEDIUM ON FIBRES DEGRADATION

Alžbeta Samková, Petr Kulhavý, Radek Jirkovec

Technical university of Liberec, department of Textile engineering, Liberec, Czech Republic,
alzbeta.samkova@tul.cz

Abstract

The current trend in plaster materials is to improve their physical properties and thus way increase also their lifetime. The aim of this article is to determine possible mutual influencing or changes in the main mechanical properties of the tested fibers used as the reinforcement in the studied plasters. The used filaments were exposed to an environment simulating an environment in the real plasters and subsequently were examined by scanning electron microscopy (SEM). The images has shown that the mutual chemical reactions appeared and caused local disruptions on top surfaces of the fibers and also in their covering chemical treatments.

Key words

Plaster, leno wave, fiber, SEM.

1. INTRODUCTION

Plasters are generally one of the basic technologies and materials used in the construction industry. Due to its availability, low price, the fast setting and the lightness is suitable for many applications, people have been using it since an ancient times. Brittleness and low tensile strength have a negative impact on lifetime and its possible usability [1, 2]. One of the possibilities eliminating these unwanted properties could be addition of fibers in order to obtain fiber-reinforced composites [3, 4]. High performance filaments such as carbon, glass or ceramic fibers are often used because of their strength and rigidity into the diametrically weaker matrix [5]. In the author previous works it has been shown than cement-based fibrous composites have significantly better mechanical properties than plaster itself [6]. One of the aspects influencing the final composites is the durability of used fibers and their behavior in critical environments. For this reason, it is very important to study and understand the behavior of those materials for long-term applications [7, 8]. Many authors whose were dealing with the degradation of the reinforcement in chemical environments, predominantly studied just the materials where the fibers are covered by the matrix. Some work shows that the fiber resistance depends on the matrix corrosion-resistance [9, 10]. It is known that prolonged exposure to the critical environment could cause damage on the fiber surface. The glass fibers are more sensitive to corrosion under the stress [11]. The basalt and carbon fibers have high chemical stability which makes them suitable for use in corrosion-resistant materials [12]. The corrosion rate is affected by several parameters such as temperature, aging time, composition and size of the fibers [13]. The aim of this work was to find out whether using of the chosen fibres as reinforcement in plaster composites could demonstrably cause their degradation.

2. EXPERIMENTAL

In the author previous work, the basic types of fibres were used as the reinforcement in commonly used plasters (cement, lime, gypsum, lime-cement). In all kind of those plasters the pH was measured using the 209 R Bench Top HANNA instruments when results of this measurement can be seen in Tab. 1. Because the pH values of the individual plasters were almost the same, for the further

experiments the average value 12.14 [-] has been used. Subsequently a solution of NaOH and water into which the fibers were submerged was prepared. For further evaluation, the fibers were removed from the solution after 24 hours, 3 days, 1 week, 1 month, 3 months and 6 months, and every time their images were taken using the SEM - TESCAN Vega 3SB.

Table 1. PH of plasters

	pH
Cement	12.09
Lime	12.52
Gypsum	12.27
Lime-cement	12.03
Used pH	**12.14**

2.1. Materials

Alkali-resistant glass fibres 12 mm long were used for the carried experiment. The fibres are in the form of integral strands each made up of 100 monofilaments and connected by special abrasion-resistant lubrication. The fibre diameter was 14 μm. When compared glass and basalt fibres, the basalt ones are more stable in a strongly alkaline environment. At the other hand, basalt fibres have lower stability in strongly acidic environment [14]. The used basalt fibres were 7.7 mm long and their diameter was 13 μm. Last of the used, carbon fibres have the widest range of the required properties. They are characterised by high strength and modulus, good thermal and chemical resistance with a low density. The carbon fibres with a diameter of 1.76 μm and length of 8 mm were used for the experiment. To asses also the various formations of the dispersion basalt leno weave with dimensions of the grid 6 x 4 mm and glass leno wave with dimensions of 4 x 4 mm were used.

3. RESULTS AND DISCUSSION

The chosen fiber dispersion has been tested for 6 months. The first images of the fibrous material were taken before testing. Fig. 1 shows the glass fibers before and during the experiment. In the Fig. 1c could be seen that after one week of testing, some chemical reactions occurred on the fibers.

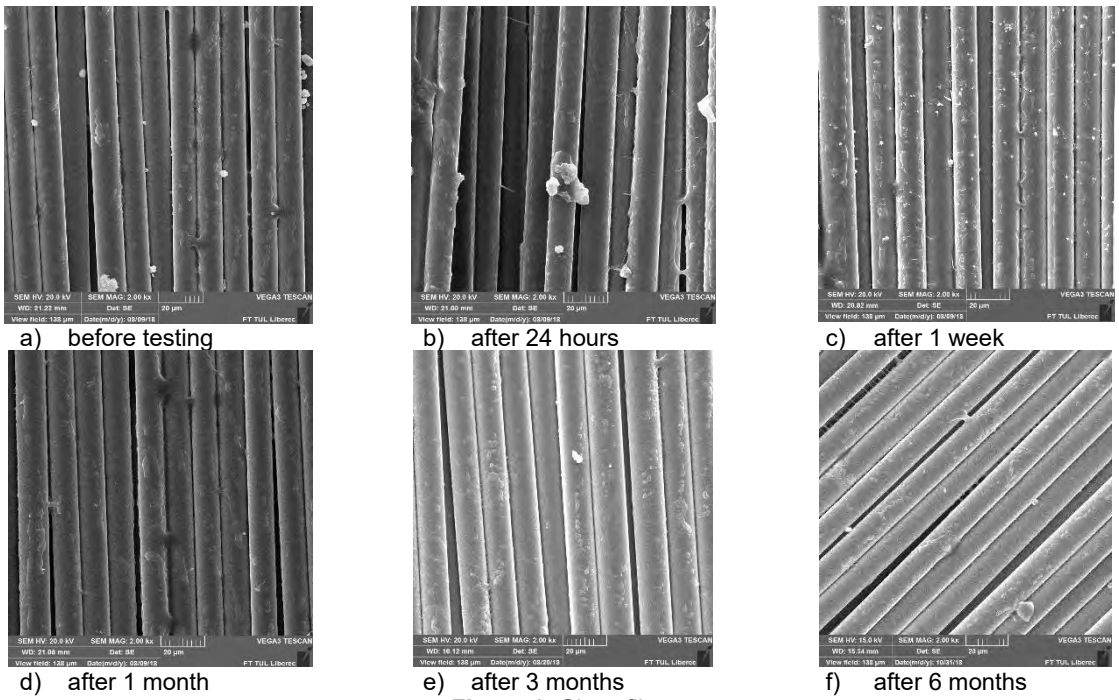

a) before testing b) after 24 hours c) after 1 week

d) after 1 month e) after 3 months f) after 6 months

Figure 1. Glass fiber

However, in the picture taken after 1 month of running tests no chemical reactions are visible. No damage can be seen on the fibers after 3 and 6 months of testing. The same behavior was recorded for basalt fibers. The images with carbon fibers showed small dark spots after 24 hours. However, any spots or defects were no more seen after 1 week of testing. As has been already mentioned, also the glass and basalt leno weave were also studied. From the pictures taken before the experiment it is obvious that the leno weave have a surface treatment. This sizing protects not only the fibers but is also fixing the weave itself. In Fig. 2a it is possible to see the glass leno weave. The surface treatment was for the solved application better, but there were a lot of bubbles. In addition, the layers itself were not uniform. These deficiencies make it difficult to assess the real changes arising during the experiment. Some of the pictures show defects caused by the manipulation however, it was not possible to say whether the defects occurred also due to the effects of the acting solution. It is possible to claim that these defects were related mainly to the surface treatment.

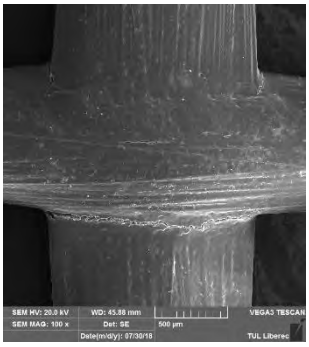

a) before testing

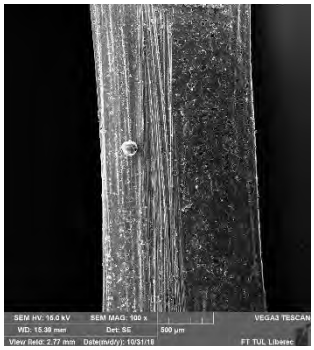

b) after 6 months (100x zvětšeno)

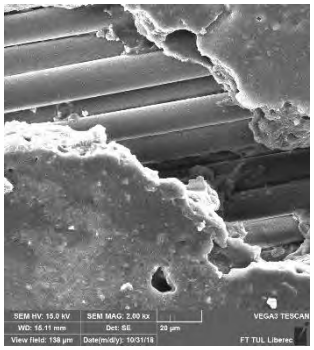

c) after 6 months (2000 x zvětšeno)

Figure 2. Glass leno wave

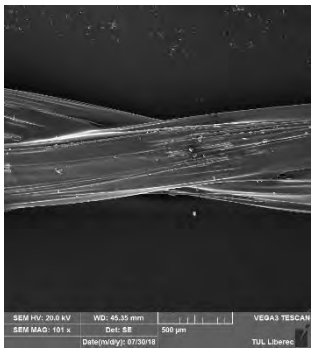

a) before testing

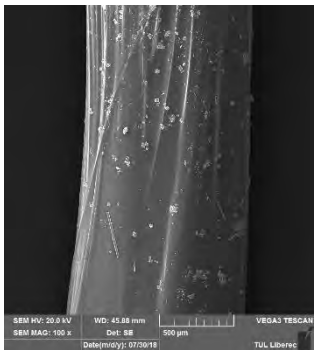

b) after 24 hours

c) after 1 week

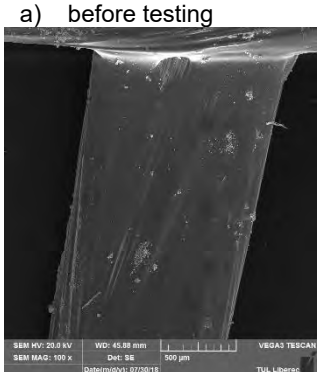

d) after 1 month

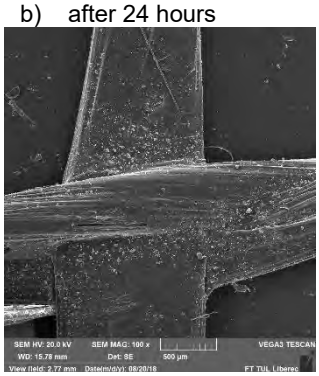

e) after 3 months

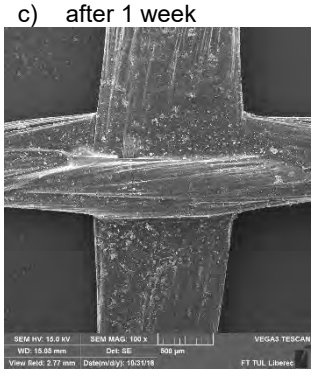

f) after 6 months

Figure 3. Basalt leno wave

On the other hand, the basalt leno weave has a smoother surface and there were no bubbles on it. The images (Fig. 3) show that some chemical reactions occurred here. This could be obvious just with the naked eye. After insertion into the solution, the leno weave become covered a milky (white) film.

However, after drying of the structure the white film and fragility disappeared. The images show that there was no significant damage on the top surface neither the fibers themselves.

4. CONCLUSIONS

This study investigated the chemical effects of various plaster environments on the used short-fiber and leno weave dispersion. Based on the carried experiment, it can be concluded that there was no damage or degradation of the fibers caused by this environment, even though some chemical reactions between the fiber treatment (sizing) and the matrix environment were obvious.

ACKNOWLEDGEMENTS

This publication was written at the Technical University of Liberec as part of the project Assessment of change physical behavior of plaster reinforced by fibre material, 21 252 with the support of the Specific University Research Grant, as provided by the Ministry of Education, Youth and Sports of the Czech Republic in the year 2018.

References

[1] Karni J, Karni EY. (1995). Gypsum in construction: origin and properties. Mater Struct.;28(2):92 - 100.
[2] Arikan M, Sobolev K. (2002). The optimization of a gypsum-based composite material. Cem Concr Res;32(11):1725–8
[3] Iucolano F, Liguori B, Colella C. (2013). Fibre-reinforced lime-based mortars: a possible resource for ancient masonry restoration. Constr Build Mater; 38:785–9
[4] Hamzaoui R, Guessasma S, Mecheri B, Eshtiaghi AM, Bennabi A. (2014). Microstructure and mechanical performance of modified mortar using hemp fibres and carbon nanotubes. Mat Des;56:60–8.
[5] Sim Jongsung, Park Cheolwoo, Moon Do Young. (2005). Characteristics of basalt fiber as a strengthening material for concrete structures. Compos: Part B Eng;36:504–12.
[6] Samková A., Kulhavý P., Pechočiaková M. M. (2015). Fibre reinforcement effect on plaster composite properties. NART Conference Proceeding, p. 189-195.
[7] Shan Y, Liao K. (2001) Environmental fatigue of unidirectional glass-carbon fiber reinforced hybrid composite. Compos: Part B;32:355–63.
[8] Tsotsis Thomas K, Keller Scott, Le Kyejune, Bardisc Jason, Bishd Jack. (2001) Aging of polymeric composite specimens for 5000 h at elevated pressure and temperature. Compos Sci Technol;61:75–86.
[9] Mertiny P, Ursinus K. (2007). A methodology for assessing fatigue degradation of joined fiber-reinforced polymer composite tubes. Polym Test;26:751–60.
[10] Amiruddin AK, Sapuan SM, Jaafarb AA. (2007). Analysis of glass fiber reinforced epoxy composite hovercraft hull base. Mater Des 2007.
[11] Myers TJ, Kytomaaa HK, Smith TR. (2007). Environmental stress-corrosion cracking of fiberglass: lessons learned from failures in the chemical industry. J Hazard Mater;142:695–704.
[12] Berozashvili M. (2001). Continuous reinforcing fibers are being offered for construction, civil engineering and other composites applications. Adv Mater Com News Compos Worldwide;21(6):5–6.
[13] Scheffler C, Forster T, Mader E, Heinrich G, Hempel S, Mechtcherine V. (2009). Aging of alkali-resistant glass and basalt fibers in alkaline solutions: evaluation of the failure stress by Weibull distribution function. J Non-Cryst Solids;355:2588–95.
[14] Wei B., Cao H., Song S. (2010). Enviromental resistance and mechanical performance of basalt and glass fiber. Material Science and Engineering, 2010.

THERMAL PERFORMANCE OF AEROGEL-EMBEDDED FIBROUS MATERIALS UNDER CONVECTION

Xiaoman Xiong[1*], Mohanapriya Venkataraman[1], Darina Jašíková[2], Tao Yang[1], Rajesh Mishra[1], and Jiří Militký[1]

[1]Department of Material Engineering, Faculty of Textile Engineering, Technical University of Liberec, Liberec 46117, Czech Republic

[2] Center for Nanomaterials, Advanced Technologies and Innovations, Liberec 46117, Czech Republic

[*] corresponding author e-mail: xiaoman.xiong@tul.cz

Abstract

This study presents an experimental investigation on the thermal performance of aerogel-embedded nonwoven fabrics under convection. Experiments were performed on a laboratory-made dynamic heat transfer measuring device. The real-time temperature curves of different materials with varying airflow velocities and heating conditions were compared and discussed. Results showed that under preheated conditions the aerogel-embedded nonwoven fabrics had very small temperature drops, fabrics with higher thickness and aerogel content required longer time to approach steady state and behaved better under convection. As for the continuous heating conditions, the heat transfer rate of each material showed an increasing trend with the increasing of airflow velocity. The aerogel-treated nonwoven, with lower fabric thickness and aerogel content, delivered significantly increased heat transfer rate at higher Reynolds number. Thicker fabrics with higher aerogel content can provide better insulation ability under convection.

Key words

nonwoven fabrics, silica aerogel, heating, airflow velocity, heat transfer rate

1. INTRODUCTION

Silica aerogel has been well acknowledged as one of the most attractive thermal insulating materials. Aerogels are usually incorporated with lightweight fibrous material to improve thermal insulation ability. The fibrous structure density and the aerogel present in the fibrous nonwovens with silica aerogel impregnation have significant effect on thermal properties of the overall structures.[1-3] However, there is sparse information available regarding convection through aerogel-embedded nonwoven. The aim of this present work is to study thermal behavior of aerogel-embedded polyester nonwovens when subjected to wind-induced cross airflow. A laboratory-made dynamic heat transfer device was used to figure out convective thermal behavior of the selected materials under different airflow velocities and heating conditions. Real-time temperature values from different fabrics were collected and compared. The convective heat transfer coefficients under continuous heating condition were calculated and investigated.

2. EXPERIMENTAL

2.1. Materials

In this study, three types of 50:50 ratio compositions of polyester/polyethylene nonwoven fabrics embedded with aerogel were selected to measure thermal performance under convection heat transfer with air. The aerogel used was hydrophobic amorphous silica aerogel, which is mesoporous and has nearly 98% of air and 2% solid. The aerogel particles were added during thermal bonding of

the nonwoven web. High resolution images for the aerogel/polymer nonwoven fabrics are shown in Figure 1. All these fabrics have high porosity over 90%.

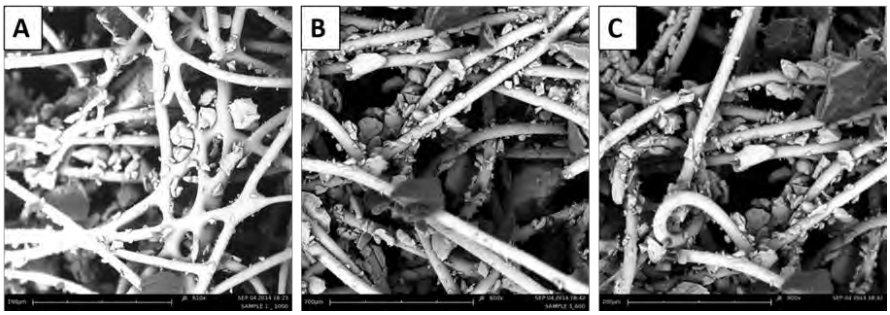

Figure 1. Scanning electron microscope (SEM) images of aerogel/polymer nonwovens.

2.2 Experimental setup

The tests were carried out in a laboratory made device, the experimental section is presented in Figure 2. The experiments involve measurements of real-time temperatures of the heating rod as well as the fabric insulator, wind velocity, wind pressure and the temperature of airflow before entering the testing section. Temperatures of the heating rod and fabric were measured by T-type copper constantan thermocouples. A thermoanemometricl sensor FVAD35TH4 was mounted in the upstream to monitor the velocity, pressure and temperature of the free stream.

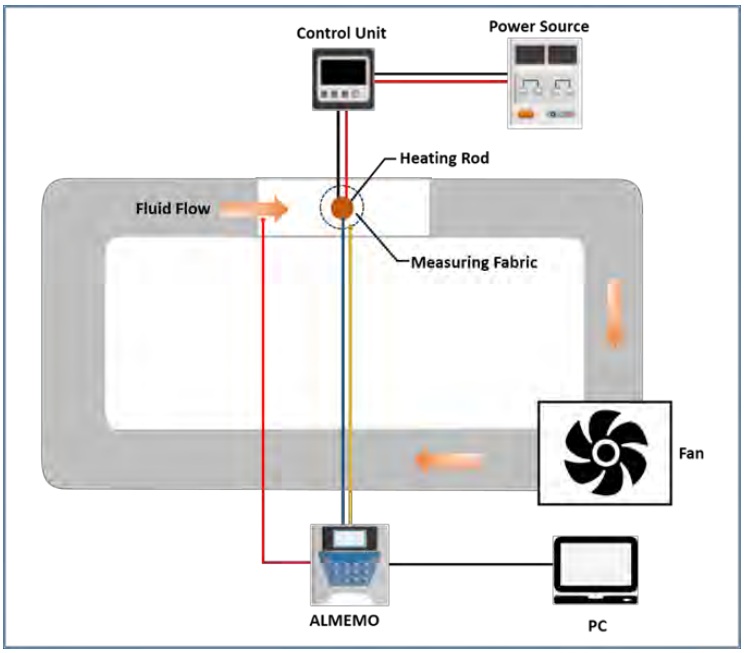

Figure 2. Schematic diagram of the measurement device

The selected aerogel-embedded nonwoven fabric was wrapped on the heating rod by using insulating rubber tape to seal the lateral gap. Any gaps between the measuring fabric and the heating rod were eliminated. The tests were carried out at different levels of air velocity under two different heating conditions, preheated and continuous heating conditions. The preheated condition refers to preheat the heating rod to a specific temperature value and then switch off the heating power to let the system cools down with a selected air velocity. The continuous heating condition involves non-stop heating during the whole measuring process.

3. RESULTS AND DISCUSSION

3.1 Thermal behavior under preheated condition

The real-time temperature curves from different fabrics are compared in Figure 3. Apparently, a low airflow velocity gives a gentle downslope of the heating rod and fabric temperature, a high velocity leads to rapid temperature declines and higher heat loss rates of the system. The real-time temperatures of the heating rod and fibrous insulator are both exponentially related with the time duration. Fabrics with higher aerogel content and higher thickness demonstrate better ability to prevent against heat loss under airflow-induced convection.

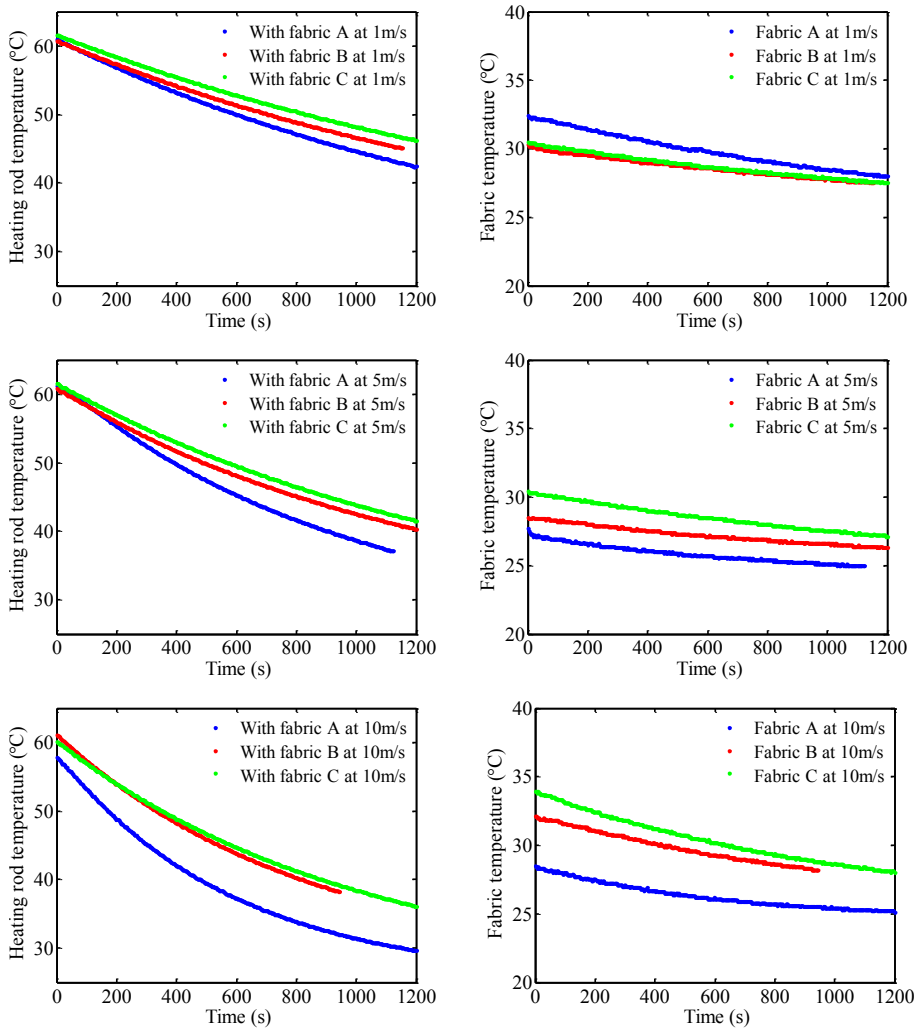

Figure 3. Comparison of temperature curves under preheated condition

3.1 Thermal behavior under continuous heating condition

The real-time temperature curves of the heating rod and different fabrics under continuous heating are presented in Figure 4. Generally, the fabrics maintain quite stable temperature values under continuous heating condition, while the heating rod temperature curves demonstrate slight fluctuations at low airflow speed (1 m/s and 5 m/s) and gently increasing at higher airflow speed (10 m/s). Similar to the results from the preheated condition, samples B and C, with higher fabric thickness and aerogel content, exhibit better ability to prevent against heat loss from the heating rod. Especially at high airflow speed (10 m/s) the heating rod is able to achieve quite high temperature values, meaning better thermal protection given by these fabrics.

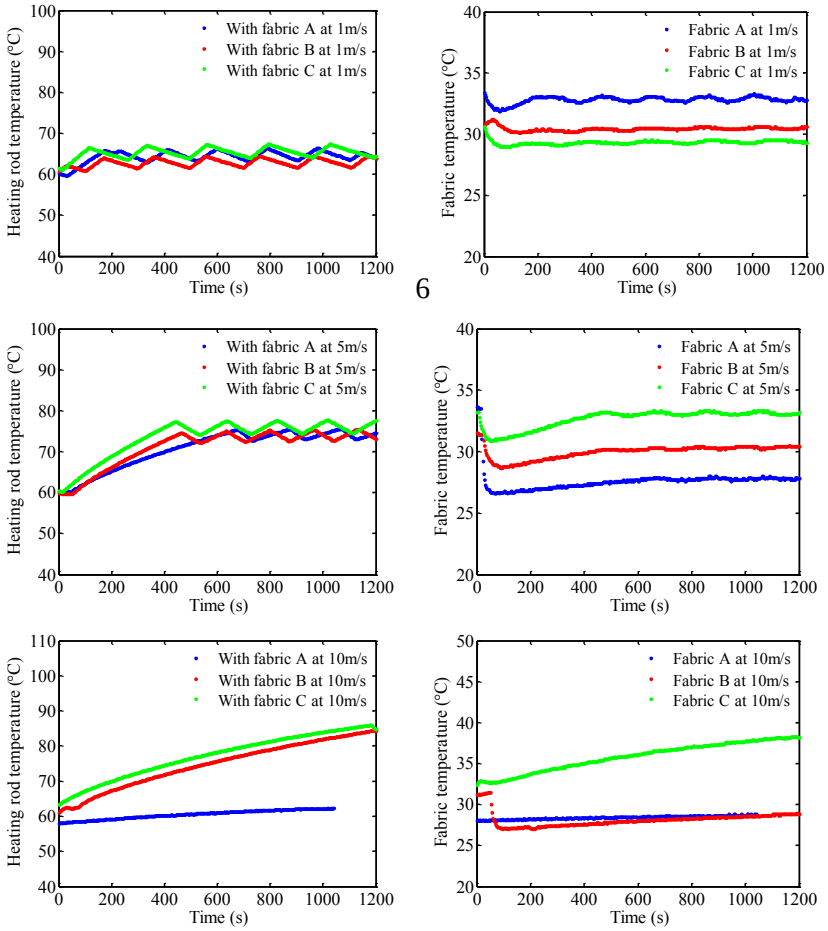

6

Figure 4. Comparison of real-time temperature curves under continuous heating condition

4. CONCLUSIONS

Three aerogel-embedded nonwoven fabrics were selected to investigate their thermal behavior by convection with varying airflow velocities and heating conditions. It was concluded that thicker fabrics with higher aerogel content demonstrated lower heat transfer rate especially under high airflow velocities.

ACKNOWLEDGEMENTS

This work was supported by the research project of the Student Grant Competition of Technical University of Liberec no. 21244/115 granted by the Ministry of Education Youth and Sports of the Czech Republic.

References

[1] Venkataraman, M., Mishra, R., Militky, J. and Hes, L. (2014). Aerogel based nanoporous fibrous materials for thermal insulation. Fibers and Ploymers, 15(7), 1444-1449.

[2] Venkataraman, M., Mishra, R., Kotresh, T.M., Sakoi, T. and Militky, J. (2015). Effect of compressibility on heat transport phenomena in aerogel-treated nonwoven fabrics. The Journal of The Textile Institute, 107(9), 1150-1158.

[3] Hoseini, A., Malekian, A.,Bahrami, M. (2016). Deformation and thermal resistance study of aerogel blanket insulation material under uniaxial compression. Energy and Buildings, 130, 228-237.

EVALUATION ON THE ACOUSTIC PROPERTIES OF MULTI-COMPONENT POLYESTER NONWOVENS

Tao Yang[1*], Xiaoman Xiong[1], Ferina Saati[2], Kai Yang[1], Yuanfeng Wang[1], Rajesh Mishra[1], Jan Novák[3] and Jiří Militký[1]

[1]Department of Material Engineering, Faculty of Textile Engineering, Technical University of Liberec, Liberec 46117, Czech Republic

[2]Vibroacoustics of Vehicles and Machines, Technical University of Munich, Boltzmannstrasse 15, 85748 Garching, Germany

[3]Department of Vehicles and Engines, Faculty of Mechanical Engineering, Technical University of Liberec, Liberec 46117, Czech Republic

* corresponding author e-mail: tao.yang@tul.cz

Abstract

This study presents an investigation on the acoustical properties of multi-component polyester nonwovens by using experimental and numerical methods. 15 types of nonwoven samples made by staple, hollow and bi-component polyester fibers were chosen to carry out this study. The AFD300 AcoustiFlow device was employed to measure airflow resistivity. Several models were applied to conduct the prediction of airflow resistivity. The surface impedance and sound absorption coefficient were determined by using 45mm Materiacustica impedance tube. Some widely used impedance models were used to predict acoustical properties. Comparison between measured and predicted values has been performed to get the most acceptable model. The power-fitted empirical model exhibits very small error of 6.8%. It is shown that Delany-Bazley and Miki models can accurately predict surface impedance of multi-component polyester nonwovens, but Komatsu model has inaccuracy in prediction especially at low-frequency band. The results indicate that Miki model is the most acceptable method to predict the sound absorption coefficient with mean error 8.39% from all the samples.

Key words

polyester, nonwoven, airflow resistivity, impedance, sound absorption, models

1. INTRODUCTION

Porous sound absorbers are widely used to treat acoustic problems in the way of noise and reverberation reduction. Energy loss caused by viscous effects and thermal losses are primarily the mechanism involved in sound absorption by porous materials [1]. Fibrous materials are typical porous materials, playing an important role in building and automotive industries for noise reduction and control. Due to high porosity, no pollution, light weight, low cost and highly efficient absorbing ability, fibrous materials are considered to be ideal sounds absorbers [2]. The noise reduction application of inorganic fibrous materials, such as glass fiber and mineral wool, attracted a lot of attention due to their large specific surface area and high acoustical performance. Compared to glass fiber and mineral wool, natural fibers as sound-absorbing materials have relatively high thermal and acoustic performances and are more environmentally friendly. Reviews of acoustic properties of natural fibers can be found in literature [3-4]. Beside inorganic and natural fibers, synthetic fibers presently play an important role on the application for noise reduction.

The aim of the current study is to investigate the airflow resistivity, impedance and sound absorption of multi-component polyester nonwovens by using practical measurements and existing prediction methods.

2. EXPERIMENTAL

2.1. Materials

In this study, three samples were selected. First, a polyester nonwoven sample was produced using vibrating perpendicular technology. In addition, two commercially available types of polyester nonwoven materials that were made separately rotation-vibration perpendicular technology [5-6]. The fiber content in all of the samples in this study is the same. Cross sectional and longitudinal microscopic images were also captured (see in Figure 1) at the Technical University of Liberec using JENAPOL microscope and NIS-elements software.

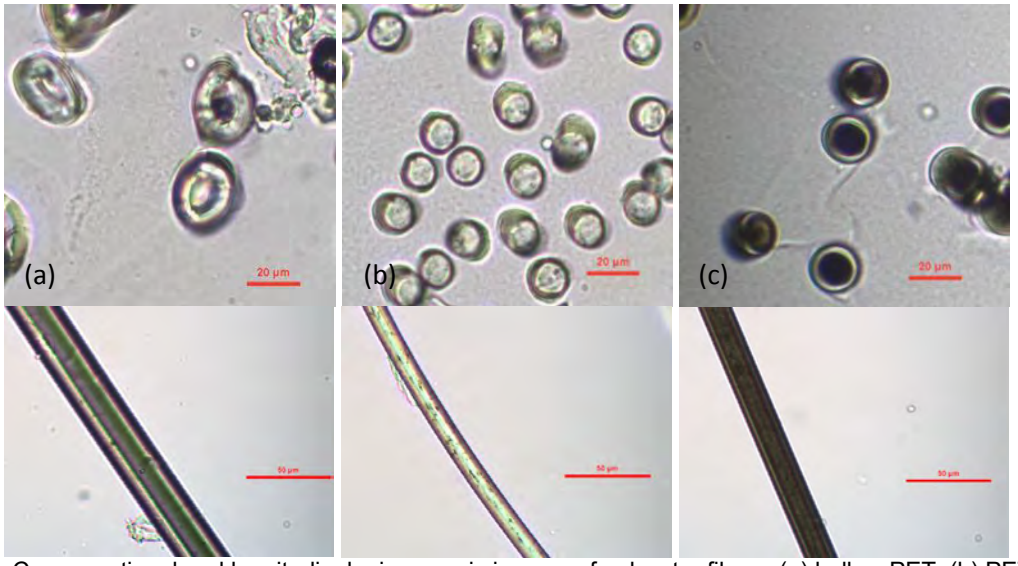

Figure 1. Cross-sectional and longitudinal microscopic images of polyester fibers: (a) hollow PET; (b) PET; (c) bi-component PET.

2.2 Impedance tube measurement

Acoustic properties of materials can be evaluated by steady-state methods, reverberant chamber methods, impedance tube methods, etc. In this study, the impedance tube was used to obtain normal incidence impedance. The surface impedance of polyester nonwovens was determined according to ISO 10534-2[7].

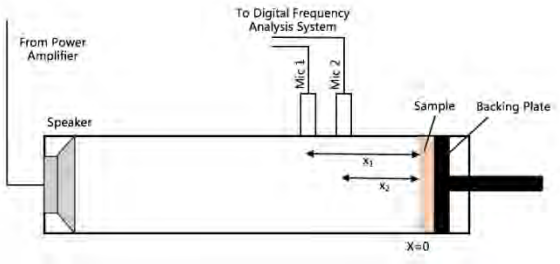

Figure 2. Two-microphone impedance tube schematic

The 45 mm impedance tube manufactured by Materiacustica was applied to carry out the impedance measurements. The measurement frequency range starts from 200 and goes up to 4200 Hz. The lower boundary was chosen higher than the tube limit in order to avoid inaccuracies caused by structural vibrations or phase mismatch [8].

2.3 Impedance models

When modeling the acoustical behavior of porous materials, non-acoustic parameters are tiring and time consuming to determine. Therefore, usage of empirical models that are developed by regression method is more common, in which such parameters are not necessary. It is essential to obtain the characteristic impedance and complex wave number to predict the surface characteristic impedance and sound absorption coefficient. The widely used impedance models such as Delany-Bazley, Miki, Garai-Pompoli and Komatsu models were used to predict acoustical properties [9-12].

3. RESULTS AND DISCUSSION

3.1 Airflow resistivity

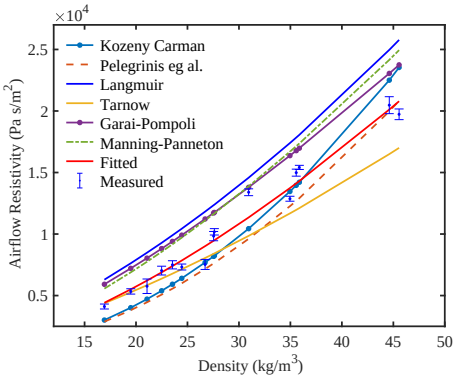

Figure 3. Predicted airflow resistivity and fitted model

Figure 3 shows that the model developed by Langmuir significantly overestimates the resistivity. The most accurate model for the airflow resistivity of multi component polyester nonwovens is the Tarnow model that is accurate within 12%. Furthermore, when materials are of relatively lower density, the Tarnow model gives higher accuracy, whereas this model exhibits higher variation compared to measured values at high density range. Although one drag force theory model exhibits acceptable prediction for multi-component polyester nonwovens, the two empirical models are not reliable which overestimate the airflow resistivity by 24%. One simple empirical model was developed by power-fitting the values of measured resistivity, the model presented in Eq. (1). The fitted empirical model is show in Figure 5. The relative prediction error of the model is 6.8%.

$$\sigma = \frac{.3395\times10^{-8}\times\rho^{1.565}}{d^2} \tag{1}$$

3.1 Surface impedance and absorption coefficient

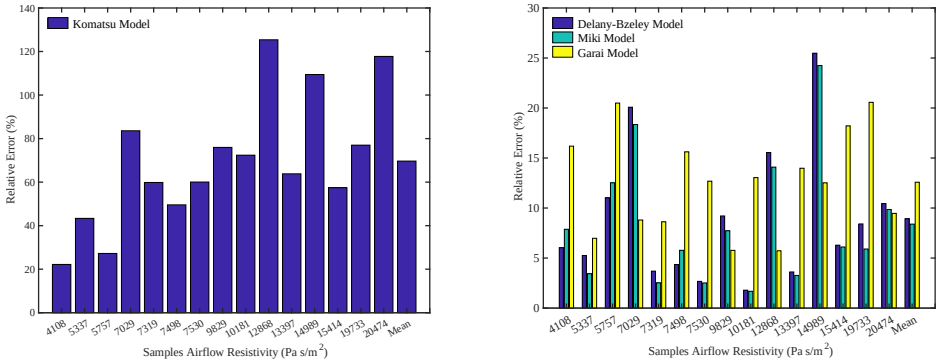

Figure 4. Relative prediction error based on Komatsu model (left), relative prediction error based on Delany–Bazley model, Miki model and Garai-Pompoli model (right)

The errors based on Komatsu, Delany-Bazley model, Miki model and Garai-Pompoli model were shown in Figure 4. The Komatsu model exhibits the highest error of 125% for the sample with 12868 Pa·s/m² airflow resistivity. It is found that Delany–Bazley model and Miki model have similar results. The difference on their mean errors is less than 0.6% which is 8.92% and 8.39%, respectively. The maximum error of 25.48% is found between the absorption coefficient predicted by the Delany-Bazley model and that measured for the sample with 14989 Pa·s/m² airflow resistivity. The maximum error of Garai-Pompoli model is 20.57% for the sample with 19733 Pa·s/m² airlow resistivity. The minimum values of error based on Delany-Bazley and Miki methods are 1.79% and 1.67%, respectively.

4. CONCLUSIONS

This work studied the airflow resistivity, impedance and sound absorption properties of multi-component polyester nonwoven materials by using experimental and numerical methods. Impedance and sound absorption coefficient measurements on some samples were conducted by using Materiacustica impedance tube. The proposed empirical model demonstrates an error of 6.8%. Some impedance models were applied to predict the acoustic properties. Subsequently, the measured and predicted values of the acoustical properties were compared to study their prediction accuracy. It was found that the Komatsu model is the least accurately predict the surface impedance, especially in the low-frequency range. It was also observed that the Delany-Bazley and Miki models can accurately predict absorption coefficient for multi-component polyester nonwoven materials. Miki model exhibits the lowest mean relative error of 8.39%.

ACKNOWLEDGEMENTS

This work was supported by the research project of the Student Grant Competition of Technical University of Liberec no. 21239 granted by the Ministry of Education Youth and Sports of the Czech Republic, DENORMS Cost Action Short Term Scientific Mission funding scheme.

References

[1] Acoustic Absorbers and Diffusers: Theory, Design and Application, editors: Cox TJ and D'Antonio P. (2nd ed). (2009). Taylor & Francis (New York).

[2] Nonwoven fabrics, editor: Albrecht W. (2003). Fuchs H and Kittelmann W.

[3] Mamtaz H, Fouladi MH, Al-Atabi M and Namasivayam SN. Acoustic Absorption of Natural Fiber Composites. Journal of Engineering 2016; 2016: 1-11.

[4] Tang X and Yan X. Acoustic energy absorption properties of fibrous materials: A review. Composites Part A 2017; 101: 360-380.

[5] an T ion i a o J i it J. Sound absorption and compression properties of perpendicular-laid nonwovens. Text Res J 2018. doi: 10. 1177/0040517517753634.

[6] Nonwoven Textiles, editors: Jirsak O and Wadsworth L. (1998) , NC: Carolina Academic Pr (Durham).

[7] ISO10534-2:1998. Determination of sound absorption coefficient and impedance in impedance tubes, Part 2: Transfer-function method international organization for standardization.

[8] Hurrell AI, Horoshenkov KV and Pelegrinis MT. The Accuracy of Some Models for the Airflow Resistivity of Nonwoven Materials. Appl Acoust 2018; 130: 230-237.

[9] Delany ME and Bazley EN. Acoustical Properties of Fibrous Absorbent Materials. Appl Acoust 1970; 3: 105–116.

[10] Miki Y. Acoustical Properties of Porous Materials-Modifications of Delany-Bazley Models. Journal of the Acoustical Society of Japan (E) 1990; 11: 19–24.

[11] Garai M and Pompoli F. A Simple Empirical Model of Polyester Fibre Materials for Acoustical Applications. Appl Acoust 2005; 66: 1383–1398.

[12] Komatsu T. Improvement of the Delany-Bazley and Miki Models for Fibrous Sound-Absorbing Materials. Acoust Sci & Tech 2008; 29: 121-129.